Electrochemical Energy Reviews (2023) 6:16
https://doi.org/10.1007/s41918-023-00180-y

REVIEW ARTICLE

Overcoming the Electrode Challenges of High-Temperature Proton Exchange Membrane Fuel Cells

Quentin Meyer[1] · Chujie Yang[2] · Yi Cheng[2] · Chuan Zhao[1]

Received: 15 February 2022 / Revised: 31 May 2022 / Accepted: 17 January 2023 / Published online: 3 April 2023

Abstract

Proton exchange membrane fuel cells (PEMFCs) are becoming a major part of a greener and more sustainable future. However, the costs of high-purity hydrogen and noble metal catalysts alongside the complexity of the PEMFC system severely hamper their commercialization. Operating PEMFCs at high temperatures (HT-PEMFCs, above 120 °C) brings several advantages, such as increased tolerance to contaminants, more affordable catalysts, and operations without liquid water, hence considerably simplifying the system. While recent progresses in proton exchange membranes for HT-PEMFCs have made this technology more viable, the HT-PEMFC viscous acid electrolyte lowers the active site utilization by unevenly diffusing into the catalyst layer while it acutely poisons the catalytic sites. In recent years, the synthesis of platinum group metal (PGM) and PGM-free catalysts with higher acid tolerance and phosphate-promoted oxygen reduction reaction, in conjunction with the design of catalyst layers with improved acid distribution and more triple-phase boundaries, has provided great opportunities for more efficient HT-PEMFCs. The progress in these two interconnected fields is reviewed here, with recommendations for the most promising routes worthy of further investigation. Using these approaches, the performance and durability of HT-PEMFCs will be significantly improved.

Keyword High-temperature proton exchange membrane fuel cells · Platinum catalysts · Platinum-group metal-free catalysts · Phosphate-tolerant electrode

1 Introduction

With increasing global warming concerns and on-going depletion of fossil fuels, the need for clean and renewable energy sources is greater than ever [1]. However, their storage and redistribution remain a challenge. As a result, the development of non-polluting electrochemical energy conversion technologies, such as lithium-ion batteries and hydrogen fuel cells, has intensified in recent years [2, 3]. Hydrogen fuel cells are broadly acknowledged to be better suited to heavy-duty and high-power applications, whereas lithium-ion batteries are more suitable for light-duty and lower-power applications [4]. Based on the ions (anions/cations) and/or nature (liquid/solid) of the electrolyte, fuel cells can be divided into alkaline polymer electrolyte fuel cells (APEFCs), proton exchange membrane fuel cells (PEMFCs), phosphoric acid fuel cells (PAFCs), molten carbonate fuel cells (MCFCs), and solid oxide fuel cells (SOFCs). Low-temperature (LT)-PEMFCs (< 120 °C, optimum ~ 80 °C) use Nafion as the solid electrolyte membrane and water as the proton carrier, while high-temperature (HT)-PEMFCs (120–200 °C) typically use phosphoric acid (PA) as the proton conductor. APEFCs with different cationic groups to conduct OH^- groups are attracting attention due to their high power density and potential to use platinum-group metal (PGM)-free catalysts [5]. MCFCs, operating at approximately 600–700 °C, use a mixture of a molten carbonate salt suspended in a chemically inert porous ceramic as an electrolyte. SOFCs,

✉ Yi Cheng
yi.cheng@csu.edu.cn

✉ Chuan Zhao
chuan.zhao@unsw.edu.au

[1] School of Chemistry, The University of New South Wales, Sydney, NSW 2052, Australia

[2] Hunan Provincial Key Laboratory of Nonferrous Value-Added Metallurgy, Central South University, Changsha 410083, Hunan, China

solid-state electrochemical devices that convert chemical energy into electrical energy, are operated at even higher temperatures (700–1 000 °C) [6]. Compared to other types of fuel cells, PEMFCs have distinct advantages, such as (i) easy start-up without gas preheating, (ii) broad selectivity of construction materials, including elastomers, for sealing, and (iii) slow degradation processes due to the low temperatures [7, 8].

Following decades of development, LT-PEMFCs are in the early stages of commercialization, with Japan, the UK, the US, China, and the Republic of Korea aiming to deploy large volumes of fuel cell electric vehicles within the next decade, with 200,000 by 2025 and 1 million by 2030 [9, 10]. Despite these recent developments, major roadblocks still lie ahead. As LT-PEMFCs operate optimally at approximately 80 °C with water as a mixture of liquid and vapor, their heat and water balance requires a complex and costly management system [3, 11, 12]. In addition, LT-PEMFCs are sensitive to contaminants and therefore require high-purity and costly hydrogen (US$10 kg^{-1} by electrolysis) [13–15]. More importantly, the lack of an infrastructure for hydrogen transport and refueling is one of the major roadblocks hindering commercialization of hydrogen fuel cell vehicles and other applications [16, 17]. While methanol is a far less expensive alternative to hydrogen (US$0.3 kg^{-1}) and is significantly easier to store and transport than hydrogen, its utilization in LT-PEMFCs through reformed hydrogen is challenging, as its carbon monoxide content needs to be below 10 ppm (1 ppm = 1 μmol mol^{-1}) to avoid substantial poisoning of the active sites [18–23]. Furthermore, its temperature needs to be lowered from its reforming temperature (> 200 °C) to the operating temperature of LT-PEMFCs (~ 80 °C) (Fig. 1a) [24–26]. The reformate gas is first cooled by a condenser (cooling I), with the methanol in the reformate gas separated from the gas by the first cold trap (cold trap I) and washed in a scrubbing bottle. Then, the reformate gas flows into the methanation chamber to carry out CO clean-up by lowering the CO concentration. Downstream from the methanation chamber, the reformate gas with a significantly reduced CO concentration is further cooled down by the second condenser (cooling II), with vapor separation in the second cold trap (cold trap II). Due to the complexity of these components with cooling, vapor formation, and CO cleaning necessary, there is an urgent demand for fuel cells operating at higher temperatures with better carbon monoxide tolerance, without the need for CO clean-up and heat utilization for evaporation [27]. Fuel cells operating at elevated temperatures typically offer higher energy efficiency with more fuel options and can use low-PGM and PGM-free catalysts. Operating a PEMFC between 100 and 300 °C allows (i) increased oxygen reduction reaction (ORR) and hydrogen oxidation reaction (HOR) kinetics with opportunities for low-PGM and PGM-free catalysts, (ii) higher tolerance to catalyst poisoning from carbon monoxide, sulfur oxide, nitrogen oxide, and hydrogen sulfide with opportunities for low-purity hydrogen, (iii) easier heat dissipation without liquid water issues, and (iv) better thermodynamic quality of the produced heat [28–35]. In HT-PEMFCs, the fuel can consist of a methanol and water mixture, which is pumped into an evaporator before it is directed to the reformer (Fig. 2b). The steam reforming process then converts this fuel mix to a hydrogen-rich gas with a higher CO content than LT-PEMFC, due to the superior CO tolerance of HT-PEMFCs. Finally, this system allows the use of the heat of the HT-PEMFC to heat up the evaporator [36]. To meet these requirements, liquid water-free HT-PEMFCs have been developed by using proton-conducting acids with high boiling points (e.g., PA, phosphates) within a proton-conducting polymer membrane that is thermally stable up to 400 °C [37].

High-temperature proton exchange membranes (HT-PEMs) have tremendously improved, with major progress achieved in their stability, durability, and proton conductivity. The proton conductivity of different classes of HT-PEMs are summarized in Table 1 [37–40]. While progresses in membrane technologies are crucial, they must occur in conjunction with progresses in electrodes. For instance, to perform well in HT-PEMFCs, a membrane with an extremely high PA retention will require an electrode doped with a high PA content and overall outstanding proton-conducting compounds and fillers to efficiently conduct protons from the membrane to the electrode. Furthermore, while operating HT-PEMFCs above 200 °C is under acute scrutiny, this will likely result in hydration/dehydration issues for PA, causing its decomposition and reduction in its proton conductivity within the membrane and the electrode [41]. While membrane advancements have been investigated in depth and are under active development, significantly less effort has been dedicated to the design of highly efficient catalysts and catalyst layers in highly concentrated and HT acidic environments. Although PGM catalysts are currently the most efficient catalysts for HT-PEMFCs, their low active site utilization and unsatisfactory stability need to be addressed, as these make the assessment of new membranes in real devices inherently challenging and reduce the durability of HT-PEMFCs. Aiming to bring the opportunities of HT-PEMFCs into the spotlight, this review first outlines the advantages of PA-doped membranes for HT-PEMFCs from a durability and stability standpoint and then focuses on the most promising strategies to develop both efficient catalysts and catalyst layers to meet the requirements of the harsh HT-PEMFC environment and therefore overcome the electrode challenges of HT-PEMFCs.

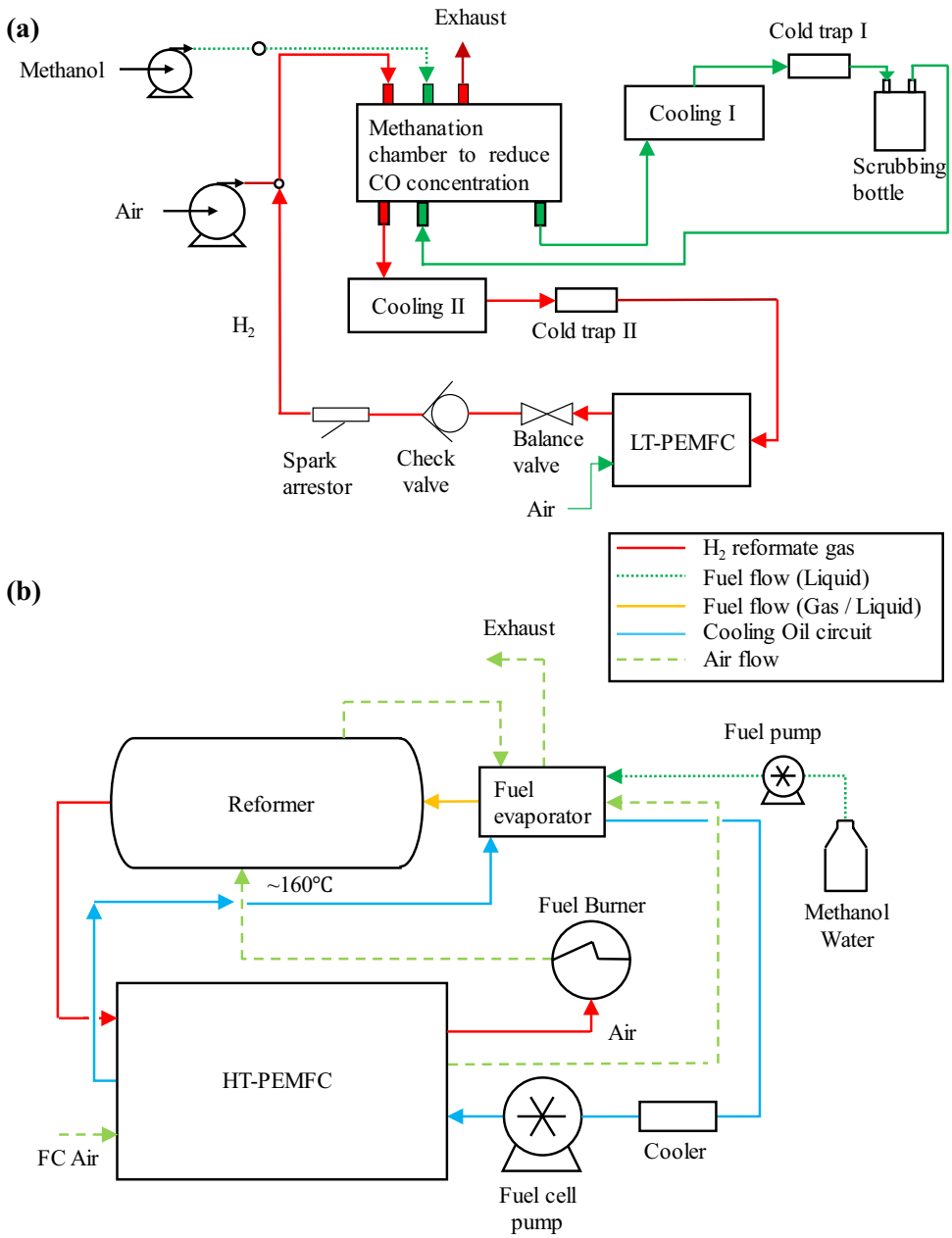

Fig. 1 **a** Operation of LT-PEMFC system with a methanol reformer. Adapted with permission from Ref. [27]. Copyright 2020, Elsevier. **b** Operation of liquid-cooled HT-PEMFC systems with a methanol reformer. Adapted with permission from Ref. [36]. Copyright 2016, Elsevier

2 Proton Conductors in HT-PEMFC Membranes

The core component of a PEMFC is the membrane electrode assembly, which is composed of a proton exchange membrane sandwiched between two catalyst layers, a microporous layer (MPL) and a gas diffusion layer (GDL), with a typical HT-PEMFC scheme shown in Fig. 2. The proton exchange membrane (PEM) determines the working mode and performance of the PEMFC. A wide range of electrolytes and membranes has been proposed for operation in HT-PEMFCs. For a high-performance polymer electrolyte, stable mechanical properties and high proton conductivity ($> 10^{-2}$ S cm^{-1}) at low humidity (or under anhydrous conditions) and at high temperature are ultimately necessary [42]. Following these principles, three main types of proton carriers have emerged: (i) water/hydrated protons, (ii) solid acids, and (iii) PA as the proton conductor, with a variety of polymer matrices proposed to host these proton carriers.

2.1 Water-Based Proton Conductors

The perfluorosulfonic acid (PFSA)-based membrane (Nafion, DuPont) is one of the most broadly used membranes using hydrated protons as the proton conductor and is ideal for

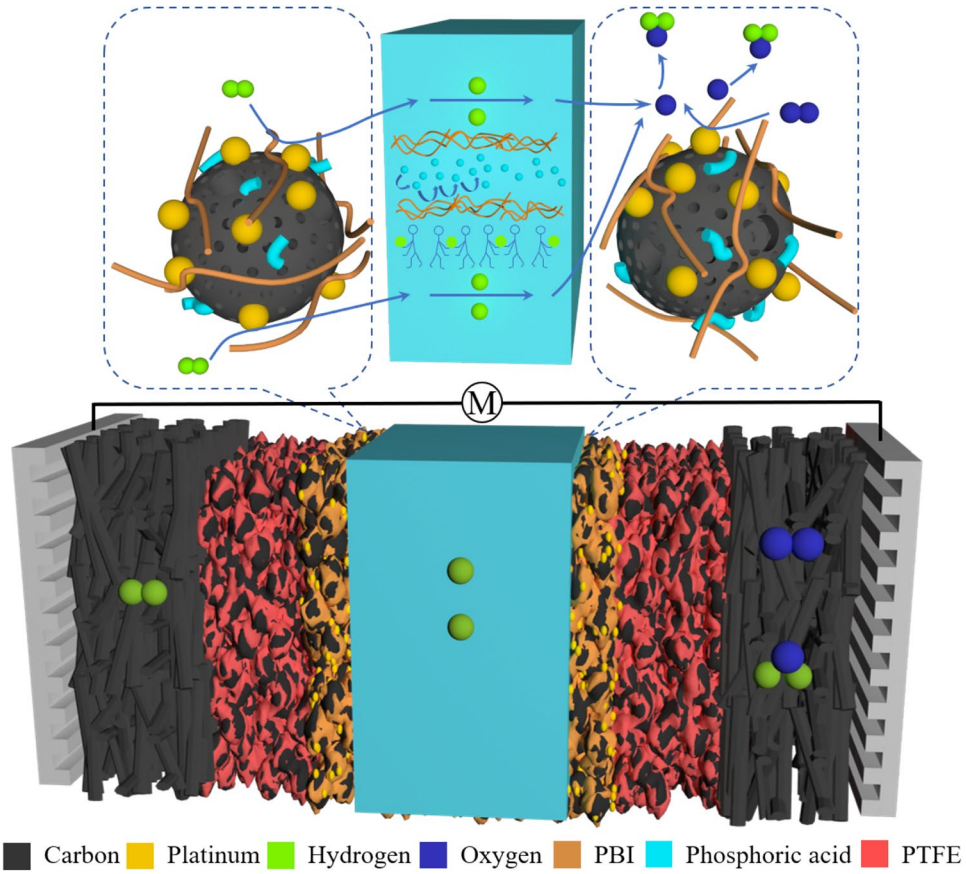

Fig. 2 Schematic representation of the structure of HT-PEMFCs. The relative sizes and distances are not to scale, and the catalyst layer, binder, filler, MPL, and carbon fibers possess significantly different porosities and sizes

Table 1 Membrane proton conductivity for HT-PEMs

Membrane type	Proton conductivity /(mS cm^{-1})	References
Caesium dihydrogen phosphate solid acid	410	[49, 50]
Ionic liquid-doped membrane composites	59–148	[43]
Pyridine-based PBI	200	[75]
$Sn_{0.9}In_{0.1}P_2O_7$	195	[101]
Nanocomposite membranes (based on PBI and porous SiO_2 NPs)	244	[86]
Ionically cross-linked PBI-blend membranes mixed with PBI and sulfonated or phosphonated acidic polymers	100	[74]
3,5-Pyridine-PBI	279.38	[102]
Protic ionic liquid-modified silica	238.17	[103]
Functionalized PBI	152.41	[104]
H_3PO_4-PBI (20.4 mol per repeating unit)	200	[75]
H_3PO_4-PTFE/PBI (300% mol)	300	[105]
Polybenzimidazole (PBI-OO)	98	[58]
c-PBI-30	198	[106]
Anhydrous m-PBI composite membrane using Al-substituted mesoporous silica (Al-MCM-41)	356	[85]
Polytetrafluoroethylene–poly(ethersulfone)–poly(vinyl pyrrolidone) (PES–PVP/PTFE)	260	[64]
PA/PBI/SiO_2	41	[100]

LT-PEMFCs below 120 °C. Modifications of the PFSA membrane have been explored to increase its operating temperature to 140 °C using ionic liquid or PA doping [43]. The progress in and limitations of these technologies have been recently outlined in high-quality reviews, with the key findings briefly summarized here [34, 37, 39, 44]. PA and proton ionic liquids experience leaching for PFSA membranes, a problem that needs to be resolved via either modification of the PFSA membrane or use of alternative materials [45]. Similar to PFSA-based membranes, sulfonated hydrocarbon polymers (SHPs) have attracted attention due to their outstanding mechanical and thermal properties and are potential PEM candidates for HT-PEMFCs. However, both the modified PFSA and SHP-based membranes suffer from dehydration under the harsh operating conditions and require a continuous water supply for membrane humidification, making the system impractical for most real-life applications. Sulfonated polymer and their composite-based membranes have also been explored in HT-PEMFCs (100–150 °C). These membranes include neutral polymer backbones of materials such as poly(ethylene-alt-tetrafluoroethylene) (ETFE) grafted with poly(4-vinyl pyridine), acrylic monomers, acrylic acid, and associated polymers due to their high thermal and chemical stability [46–48]. Inorganic membranes using solid acids or metal phosphates are promising for HT-PEMFCs and have been explored for the past two decades. Among others, caesium dihydrogen phosphate solid acid (CsH_2PO_4), for instance, has good conductivity (410 mS cm^{-1}) between 160 and 250 °C [49, 50]. Furthermore, metal pyrophosphates (MP_2O_7, M = Sn, Ti, Si, Ge, Ce, and Zr) exhibit relatively high proton conductivity between 100 and 400 °C under water-free conditions [51]. However, the synthesis of a dense, flexible, and heat-resistant electrolyte membrane remains a key requirement for practical application of these materials due to their poor film forming capability. Some progress has been made through the development of organic−inorganic structures using, for instance, $Sn_{0.95}Al_{0.05}P_2O_7$ and sulfonated polystyrene-b-poly(ethylene/butylene)-b-polystyrene (sSEBS) and inorganic membranes using SnP_2O_7–LaP_3O_9 [52, 53]. More recently, polybenzimidazole (PBI) with gadolinium-doped cerium pyrophosphate membranes has also shown promise, with higher performance than PBI membranes with reduced PA doping amount, while their peak power density decreases above 160 °C [54]. Altogether, although these approaches are interesting, the currently unsatisfactory stability and conductivity of these membranes have led to low performance in HT-PEMFCs compared to PA, and these membranes are therefore not further discussed in this review, with further information available elsewhere [39]. Therefore, this review focuses primarily on PA-doped membranes, as these are currently the most promising and commercially available membranes for HT-PEMFCs.

2.2 PA-Doped PBI Membranes

2.2.1 PA-Doped PBI Membranes

The strong and extensive hydrogen bonding network of PA causes its high viscosity and its Grotthuss mechanism with high intrinsic conductivity, which renders PA the most stable and most efficient proton carrier for HT-PEMFCs to date (Fig. 2) [55, 56]. While the proton conduction mechanism in HT-PEMFCs does not involve solely PA as the proton carrier, the PA/phosphate approach has thus far yielded superior performance and durability. PA needs to be immobilized within a polymer structure, which has directed scientific attention to phosphonic acid polyelectrolytes [57]. Therefore, polymers such as PBI, polysulfones, poly(phenylene oxide) (PPO), polyether ketones, poly(vinylpyrrolidone) (PVP), and their composites (e.g., polytetrafluoroethylene-poly(ethersulfone)-poly(vinyl pyrrolidone) (PES-PVP/PTFE)) have emerged as promising candidates for PA doping and operation in HT-PEMFCs [41, 58–64]. As an aromatic heterocyclic polymer, PBI possesses a glass transition temperature of 427 °C and excellent thermal and chemical stability [65]. PBI membranes with a molecular weight ranging from 40–65 kDa (1 kDa = 1 000 g mol^{-1}), following doping with PA (PA-PBI membranes), have been widely adopted for HT-PEMFCs [41, 57, 66, 67]. Recent advances in membrane technology have brought about HT-PEMFCs using PA-PBI that have achieved outstanding performance and stability of over 18 000 h at 160–180 °C [68]. While doping a high PA content within the PBI membrane is crucial to ensure the long-term stability and proton conductivity of the membrane electrode assembly, the mechanical stability of PBI membranes weakens when doped with an excessively high PA content [69–71]. Therefore, improvements in the PBI mechanical strength and the PA doping and retention ability are necessary to reach a higher proton conductivity. These topics have been recently discussed in an excellent review [72]. Modification of the PBI membrane, or membrane alternatives, has been investigated by using PBI blends and inorganic additives to improve its performance and proton conductivity and increase its operating temperature to beyond 200 °C.

2.2.2 PBI-Blend Membranes, Ionically Cross-Linked Membranes, and Silica-Based Composite Membranes

PBI blending and ionic cross-linking of proton-conducting membranes can improve their thermal, dimensional, and chemical stability and their PA retention [73]. Ionically cross-linked PBI-blend membranes mixed with sulfonated or phosphonated acidic polymers exhibit proton conductivities above 100 mS cm^{-1}, with excellent mechanical strength and low swelling [74]. In-depth investigation suggests that

the chemical and radical stability results from acid–base cross-linking. Aromatic polyether backbones attached to polar pyridine moieties create complexes with PA, which can enhance the PA uptake. Pyridine-based PBI, using PA as both a solvent and a polycondensation agent, can achieve a proton conductivity of 200 mS cm^{-1} at 200 °C [75]. Low-cost poly(arylene pyridine)s also demonstrate promise, with excellent durability at 160 °C for 100 h [76]. Furthermore, rigid polymeric backbones with high acid absorption through the interaction with the basic backbone create clusters of acid molecules for proton transport. Pyridine units as basic moieties in a rigid aromatic polymer were demonstrated to provide a basic polymer to adsorb PA. Phenyl phosphinoxide moieties included in the polymer structure improve the PA solubility and create more interaction with the doping agent [77]. Solubilizing side chain substituents can also improve the PA solubility and uptake ability [78]. Phosphonated mesoporous silica-based composite membranes have also been explored. These membranes benefit from a high density of ion exchange groups in the composite membrane and the mesoporous morphology of the fillers to conduct protons above 100 °C [79]. Furthermore, promising results have been achieved by using composite membranes based on a phosphotungstic acid (PWA)-doped polyethersulfone-PVP (PES-PVP) matrix for HT-PEMFCs [80]. The addition of PWA (5%) to PA could improve the performance of the HT-PEMFC from 250 to 400 mW cm^{-2} [80].

2.2.3 Additives to Enhance the Stability and Conductivity of PBI-Based Membranes

The PA retention and proton conductivity properties of PBI membranes have been further improved by adding additives, such as carbon materials (carbon nanotubes (CNTs), graphene), heteropoly acids (HPAs), and oxides (silica, TiO_2, Al_2O_3, ZrO_2, SnO_2) [62, 81, 82]. Organic/inorganic hybrid nanocomposites (OPBI) have been prepared with surface functionalized silica nanoparticles (NPs) to improve the thermal and mechanical stability of the PBI membrane [83]. PBI and mesoporous silica composite membranes (APBI-DIL4.5-MDA1.5) have a high proton conductivity (220 mS cm^{-1}) and good mechanical stability at 180 °C [84, 85]. Nanocomposite membranes (based on PBI and porous SiO_2 NPs) in particular have a 329 wt% (wt% means the weight percentage) PA uptake with a 244 mS cm^{-1} proton conductivity at 200 °C [86]. The incorporation of PWA-functionalized mesoporous silica into a PA-PBI membrane substantially enhances its durability in HT-PEMFCs at 200 °C [87]. Composite membranes with 15 wt% PWA-meso-silica have high proton conductivity and exceptional durability, with reduced PA uptake and good mechanical strength. PA stabilization by the PWA-meso-SiO_2 filler enables an ultrahigh stability over 2 700 h in HT-PEMFCs (< 30 mV h^{-1}) at 200 °C and 0.2 A cm^{-2} [88]. The dispersion of micro-sized anatase titanium dioxide into a PBI membrane can increase its acid absorption capability and ionic conductivity in HT-PEMFCs [89]. Furthermore, the incorporation of hydrophilic and acidophilic NPs into a soluble PBI solution enhances its PA absorption ability at 120 °C [90].

2.3 Proton Conductors above 200 °C

Operating HT-PEMFCs above 200 °C could improve their carbon monoxide tolerance even further. However, operations at these temperatures require a new class of membranes, as the stability of the PA/PBI membrane decreases above 180 °C due to the loss of water content and formation of pyrophosphoric acid ($H_4P_2O_7$) produced by the condensation of PA [91]. Pyridine units containing copolymers and terpolymers have been explored via cross-linking with carboxylic acid side groups and hydrophobic methyl groups to create more robust and stabler polymer electrolyte membranes for HT-PEMFCs. This approach was demonstrated in HT-PEMFCs, achieving outstanding stability for over 350 h [92]. These membranes exhibit outstanding properties compared to PBI polymer membranes in terms of proton conductivity, mechanical strength, and manufacturing properties. A high-performance SnP_2O_7–polymer composite ceramic membrane, with closely packed P_2O_7 creating proton bonding sites and transport pathways, was also investigated, achieving 0.87 W cm^{-2} at 240 °C with minimal performance loss in 25% carbon monoxide [93, 94]. Other membrane breakthroughs used poly(2,3,5,6-tetrafluorostyrene-4-phosphonic acid) and phosphonated polymers to reach peak power densities of 1.13 W cm^{-2} at 160 °C and 1.74 W cm^{-2} at 240 °C under H_2/O_2 conditions. Recently, Atanasov revealed the properties of several state-of-the-art HT-PEMFC phosphonated polymers as proton conductors, such as poly(2,3,5,6-tetrafluorostyrene-4-phosphonic acid) (PWN) with a 70% degree of phosphonation (PWN70), ion-pair coordinated polymer (PA-QAPOH), and PA-doped tin pyrophosphate (TPP/Nafion) composite membranes, and compared their properties with those of PA-PBI (Fig. 3a) [95]. The PWN membranes based on phosphonated poly(pentafluorostyrene) (PPFS) benefit from an efficient and versatile polymer phosphonation method, have high resistance to heat and radicals, and achieve high proton conductivity and performance in hydrogen fuel cells [96]. Tin pyrophosphate (TPP) has received significant interest in the last decade due to its potential as a proton conductor for ionomer electrolytes in HT-PEMFCs [97]. The ion-pair coordinated membranes (PA-QAPOH) use the strong interaction between bisphosphate–ammonium ionic pairs to increase the water tolerance and reduce evaporation of PA at elevated temperatures [98]. The proton conductivity of

the ion-pair coordinated polymer (PA-QAPOH) is higher than that of PA-PBI and keeps increasing before decreasing above 220 °C. The maximum conductivity at a higher temperature for the ion-pair polymer could be caused by the higher interaction of the ion pair. The PA-doped tin pyrophosphate (TPP/Nafion) composite membrane shows lower conductivity than the PA-PBI and PA-QAPOH membranes in the temperature range of 120–200 °C, with no decrease in conductivity up to 300 °C. The proton conductivity of PWN70 increases from 10^{-4} to 0.2 mS cm^{-1} as the temperature increases from 120 °C to 220 °C, but the proton conductivity is two orders of magnitude lower than that of TPP/Nafion, PA-PBI and PA-QAPOH (Fig. 3b, c). Overall, TPP/Nafion, PA-PBI and PA-QAPOH electrolytes are unimpacted by changes in relative humidity (RH) as they do not require liquid water to conduct protons, unlike PWN70 which conductivity increases by several orders of magnitude from with higher RH [95].

Despite substantially outperforming PBI- and metal phosphate-based HT-PEMFCs, the poor stability of the PWN70 ionomer electrolyte above 160 °C must be addressed [95]. HT-PEMs has tremendously improved their performance and stability, the most practical membranes rely on PA/phosphates as proton conductors. These environments significantly impact the selection of catalyst materials and the design of the membrane electrode assembly.

3 Catalysts in HT-PEMFCs

Over the past decades, considerable improvements in HT-PEMs have increased their viability. Figure 4 compares the typically reported peak power densities of LT-PEMFCs and HT-PEMFCs as a function of their operating temperature [95, 107, 108]. HT-PEMFCs have achieved impressive progress, with values of 1.2 W cm^{-2} at 160 °C and 1.5–1.7 W cm^{-2} in the 200–240 °C range in H_2/O_2 and 0.6–0.9 W cm^{-2} in H_2/air [95]. These studies thus far have predominantly focused on the membrane, while the exploration of highly active catalysts and catalyst layers has received less attention. To design a high-performance membrane electrode assembly for HT-PEMFCs, one should consider not only the

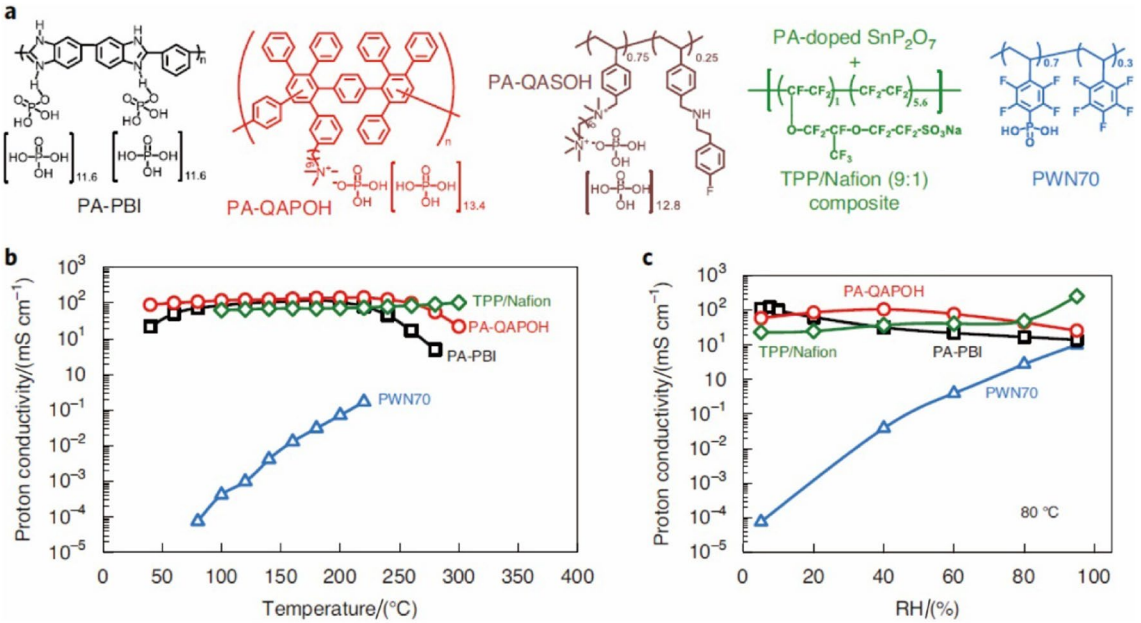

Fig. 3 **a** Chemical structures of PA-PBI, PA-QAPOH, PA-QASOH, PA-doped SnP_2O_7, and PWN70 proton conductors. **b** Anhydrous proton conductivity of proton conductors as a function of temperature. **c** Proton conductivity as a function of RH at 80 °C. Reproduced with permission from Ref. [95]. Copyright Springer Nature 2021

Recently, Cheng et al. developed a PA/PBI/SiO_2 composite membrane that can stably operate at temperatures of 210–250 °C [99, 100]. Altogether, these studies bring new opportunities for the practical application of HT-PEMFCs at higher performance and open new routes for commercialization of PEMFCs. Overall, while the development of catalyst activity and the coupling of protons, electrons, and reactants at the triple-phase boundaries but also the stability at high temperatures, resistivity to phosphate ion poisoning, and PA flooding. Therefore, developing catalysts and catalyst layers compatible with PA-doped membranes should tremendously promote HT-PEMFCs for practical applications.

3.1 PGM Catalysts for HT-PEMFCs

The synthesis of PGM catalysts has significantly progressed in recent years, with major achievements regarding the Pt utilization and interactions between the catalyst and its support. However, the HT-PEMFC challenges need to be mitigated, such as phosphate poisoning and accelerated carbon corrosion at elevated temperatures, alongside the opportunities this environment offers such as phosphate-promoted ORR.

3.1.1 Highly Active PGM Catalysts

HT-PEMFCs currently rely on PGM catalysts for both the ORR and HOR. As the cathodic ORR is approximately 4–6 times slower than the anodic HOR, great efforts in the past several decades have focused on developing efficient Pt catalysts using low amounts of Pt for the ORR. Several innovative strategies have successfully reduced the Pt utilization via engineering of effective and stable PGM catalysts (Fig. 5) [109]. These strategies include (i) controlling the size of the NPs to increase the mass activity (Fig. 5a), (ii) engineering strong support-particle interactions (Fig. 5b), (iii) controlling the composition to tune the electron structure and reduce the PGM loading (Fig. 5c), and (iv) engineering the shapes and facets to yield high-activity active sites (Fig. 5d).

Nanoscale particle size: reducing the size of noble metal particles, despite the specific activity following the order of polycrystalline Pt > unsupported Pt black particles (~30 nm) > high surface area (HSA) carbon-supported Pt NP catalysts, has been extensively explored to increase the mass activity (Fig. 6a, b) [111]. Decreasing the particle size exposes more Pt sites, thereby increasing the mass activity. The development of nanotechnologies has brought great opportunities to increase the ORR activity while reducing the Pt loading from 4.0 mg cm^{-2} to 0.2 mg cm^{-2} [112]. The influence of the particle size on the ORR kinetics was intensively investigated in the first decade of the twenty-first century, and one of the most active and stable catalysts for PEMFCs is now widely accepted to be carbon-supported Pt NPs with 2–3 nm particle sizes [111, 113]. Further decreasing the NP size (< 2 nm) may reduce both the stability and mass activity (Fig. 6a, b). However, pioneering work suggests that subnanometre Pt particles may follow a different trend due to the quantum size effect, with the ORR catalytic activity increasing by removing one atom from a 13 Pt atom cluster (Pt_{13}), in which the Pt_{12} cluster exhibits a twofold improvement in the catalytic activity [114]. The optimal performance in terms of the ORR electrochemical activity of clusters with between 12 and 20 atoms is reached for Pt_{19} (Fig. 6c, d) [114]. Further downsizing the particle size to the atomic scale, namely single-atom catalysts, has attracted extensive interest [115, 116]. Pt single atoms anchored on N-doped carbon show good carbon monoxide/methanol tolerance for the ORR. The acidic single cell with this cathode catalyst delivers a peak power density of 0.68 W cm^{-2} at 80 °C with 0.09 mg_{Pt} cm^{-2} for LT-PEMFCs, offering great potential opportunities [115].

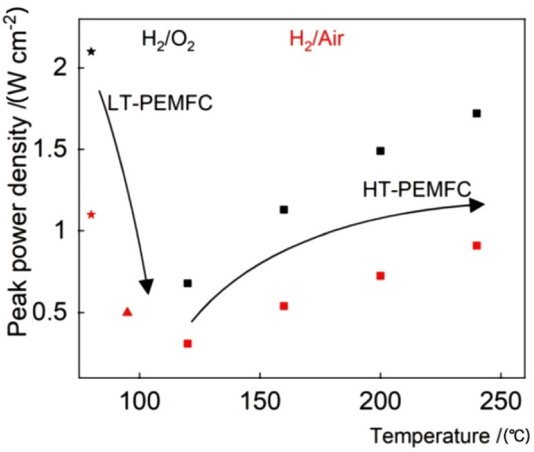

Fig. 4 Performance comparison of different types of fuel cells at different operating temperatures in H_2/O_2 (black) and H_2/air (red). Fuel cell data are reproduced with permission for LT-PEMFCs from Ref. [108] and △ [107] and for □ HT-PEMFCs from Ref. [95]

Pt NP interaction with the support: as the size of the Pt NPs decreases, their interaction with the support is enhanced, which allows improvement in the ORR performance by exploring the support-NP interaction to tune the catalytic activity and stability. Carbon materials, such as amorphous carbon, activated carbon, CNTs, carbon nanofibers, graphene, porous carbons, and heteroatom-doped carbon materials, have been intensively studied due to their high surface area, high electronic conductivity, and good stability [119]. PGM NP sintering requires a strong interaction between the NPs and the graphitized carbon supports to prevent carbon corrosion. Thus, CNTs are particularly promising supports for HT-PEMFCs [120, 121]. Functionalization of CNTs with poly(2,2-(2,6-pyridine)-5,5-bibenzimidazole) (PyPBI) or with PVP, pyridine or hydroxypyridine moieties could provide a strong π–π interaction and Pt–N bonding that improve the power density output and stability [121–124]. Highly graphitized carbons are preferred due to their enhanced electronic conductivity and stability against corrosion [125]. Heteroatom-doped carbon materials, such as N-doped CNTs and iron–nitrogen codoped mesoporous CNFs, have good properties to promote Pt catalysts [126, 127]. Pt NPs loaded on N-doped mesoporous carbon (Pt/NMC) have a mass activity of 0.384 A mg_{Pt}^{-1} at 0.9 V versus the reversible hydrogen electrode (RHE) in acidic media, which is 8.1 times higher than that of Pt NPs on Vulcan XC-72R and 5.9 times higher than that of commercialized Pt/C

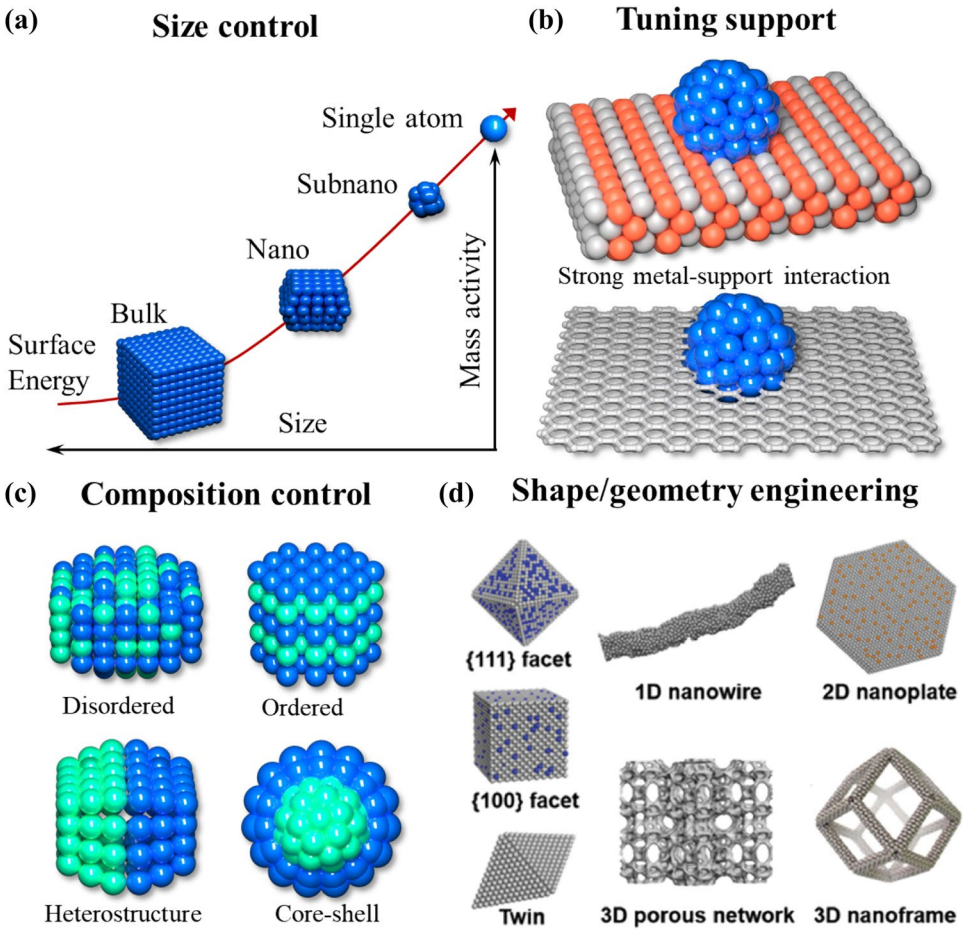

Fig. 5 **a** Size control. **b** Tuning the support. **c** Composition control. **d** Shape/geometry engineering, with (**d**) reproduced with permission from Ref. [110]. Copyright 2018, Wiley

[128]. Metal oxides (e.g., TiO_2, ruthenium-titanium mixed oxide, Ta_2O_5), metal nitrides, oxynitrides, carbide and carbonitrides (TiC, WC, Mo_2C, VC, NbC, Fe_2C, $Co_6Mo_6C_2$) have attracted enormous interest due to the strong interaction of Pt NPs with these supports to tune both the activity and stability [129–137]. However, the reaction of metal oxides with PA at high temperatures to form phosphates could be an issue for catalysts due to their nonconductive properties. Among the materials, transition metal carbides are used as supports due to their chemical stability in acidic media, resistance to poisoning, excellent mechanical durability, and high electronic conductivity. Tungsten carbide-supported Pt NPs, for instance, have demonstrated, with their enhanced ORR activity, increased mass activity and specific activity approximately twofold (at 0.85 V vs. RHE) and sevenfold higher than those of Pt/C, respectively [138]. Pt NPs supported on MoO_x-modified CNTs exhibit higher performance in PBI membrane-based HT-PEMFCs at 140 °C [139]. Finally, graphitized carbon functionalized with metal oxides, metal nitrides, oxynitrides, carbides, and carbonitrides could offer new opportunities.

Pt alloys: the turnover frequency of Pt NPs can be increased by introducing other elements to tune the electronic structure of the Pt sites and optimize the adsorption energy of oxygen intermediates. Furthermore, the introduced metal can reduce the utilization of Pt atoms, especially in the inner core of the Pt NPs. This new class of ORR catalysts is commonly known as PGM alloys [140, 141]. PGM alloys with ORR activity orders of magnitude higher than that of commercial Pt/C have been developed after intensive screening of the optimum composition of PGM alloys. Some well-known systems include PtNi, PtCo, and PtPd [142–145]. The $Pt_3Ni(111)$ surface is 10 times more active for the ORR than the corresponding Pt(111) surface and 90-fold more active than the current state-of-the-art Pt/C catalysts for PEMFCs; Pt_3Ni is one of the most active ORR catalysts (Fig. 6e, f) [142]. Pt_3Co, Pt_3Ni, Pt_3Y, and Pt_3Sc have promising activity for the ORR, while Pt_3Y and Pt_3Sc can meet both the high activity and outstanding stability requirements [118]. The activity of polycrystalline Pt_3Sc and Pt_3Y electrodes is 1.5–1.8 and 6–10 higher than that of pure Pt, respectively [118]. Among different types of Pt alloys, ordered alloys, core–shell alloys, and Pt-skin alloys have attracted enormous interest due to their superior activity and stability and could be promising for HT-PEMFCs [146–156]. For instance, the use of ordered Pt_3Co

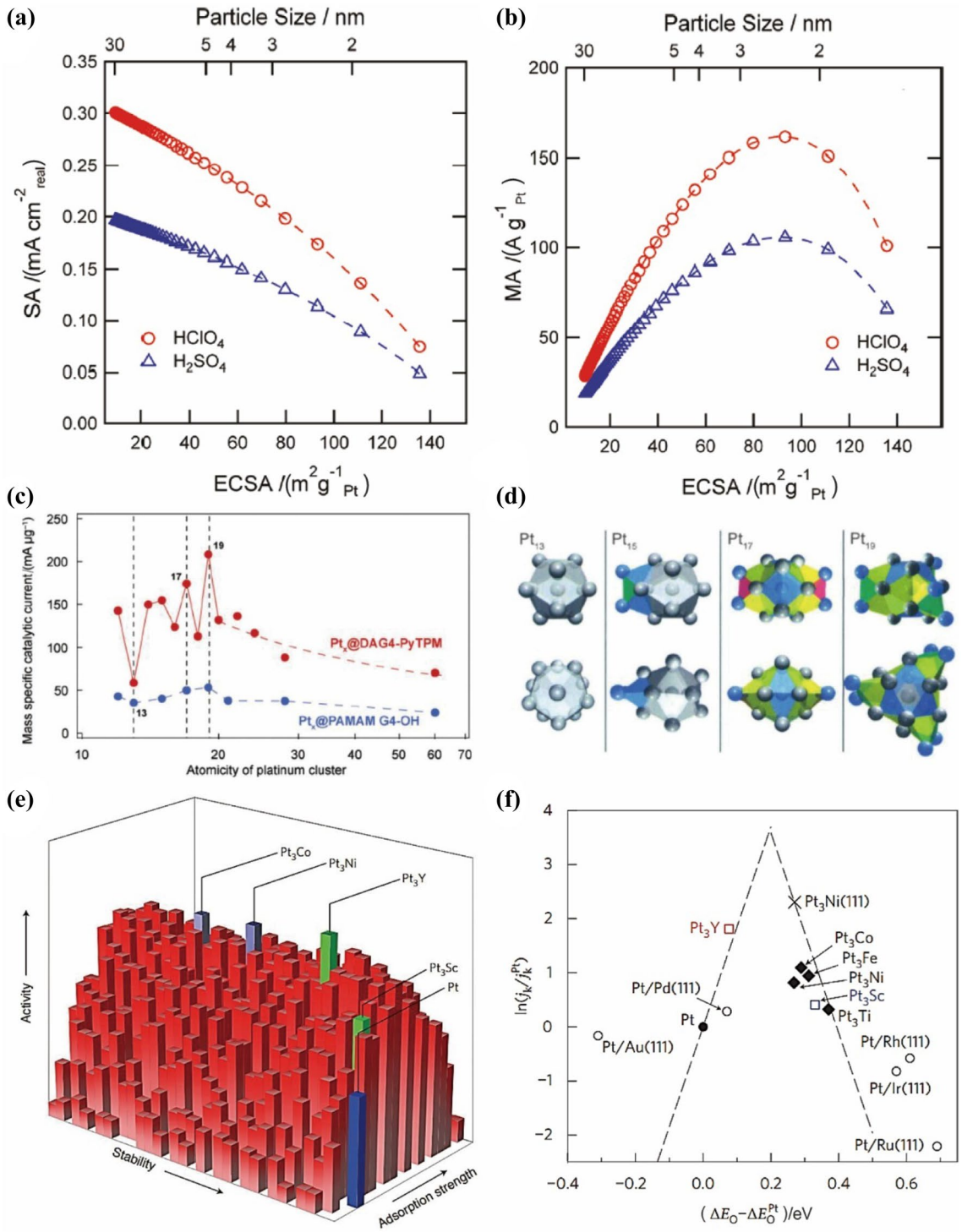

Fig. 6 **a** Specific activity (SA) and **b** mass activity (MA) at 0.9 V_{RHE} as a function of the electrochemical surface area (ECSA) for $HClO_4$ and H_2SO_4, with 100 active sites and 30% of the particle covered by the support. Reproduced with permission from Ref. [111]. Copyright 2011, American Chemistry Society. **c** Mass–specific activity as a function of the number of Pt atoms within Pt_x ($x = 12-24$) clusters, synthesized by using either triphenylpyridylmethane (Pt_xDPAG4-PyTPM) or polyamidoamine (Pt_xPAMAM G4-OH). **d** Atomic structure of Pt NPs (13–19 atoms). Reproduced with permission from Ref. [114]. Copyright 2015, Wiley. **e** Three-dimensional volcano plot of PGM metal alloy catalysts for the ORR. Reproduced with permission from Ref. [117]. Copyright 2009, Springer Nature. **f** Volcano plots and free-energy diagrams for the ORR on PGM transition metal alloys. Reproduced with permission from Ref. [118]. Copyright 2009, Springer Nature

intermetallic cores with a 2–3-atomic-layer-thick Pt shell increases the mass activity and specific activity by 200% and 300%, respectively, compared to disordered Pt_3Co alloy NPs and Pt/C. A minimal loss of catalytic activity occurs after 5,000 potential cycles, while the ordered core–shell structure remains virtually intact. The Pt-rich shell and stable intermetallic Pt_3Co core arrangement improves the activity and stability [143]. N-doped carbon-encapsulated ordered PtFe intermetallic compounds have a 1.3-fold enhancement in the peak power density and high stability due to effective prevention of agglomeration, coalescence, and Oswald ripening of the particles [157]. Alternatively, Pd-based core–shell alloys can replace Pt catalysts in HT-PEMFCs. The performance of the PdNiCu@PdIr/C catalyst is higher than that of PdNi@PdIr/C and PdCu@PdIr/C catalysts and reaches 95% of the performance of the commercial PtCo/C catalyst [158]. With improvements in PGM ORR catalysts, new catalysts have been developed by controlling the size, alloy composition, crystalline structure, and morphology to achieve the ORR activity goal set by the US Department of Energy (0.44 A mg_{PGM}^{-1} for 0.1 mg_{PGM} cm^{-2}) [159]. One-dimensional (1-D) nanostructures (such as nanowires, nanorods and nanotubes), two-dimensional nanosheets and nanoplates, and three-dimensional nanostructures (such as nanoframes and nanoporous structures) have attracted great attention due to their unique anisotropic structure, which is beneficial to many catalytic reactions [160–170]. Pt_3Ni nanoframes, prepared by erosion of crystalline $PtNi_3$ polyhedra with surface and three-dimensional molecular accessibility, enhance the mass activity and specific activity 36- and 22-fold, respectively [171].

Overall, readers should keep in mind that while insightful, some of these pioneering demonstrations have been either purely theoretical or only investigated by using aqueous model systems with 3-electrode cells and a rotating disk electrode (RDE) suppressing mass transport at ambient temperature. As the HT-PEMFC environment is far harsher than diluted perchloric acid or that in LT-PEMFCs, the performance of these materials needs to be further elucidated with concentrated PA, at elevated temperatures and finally in HT-PEMFCs.

3.1.2 PGM Catalysts for HT-PEMFCs

To further the research in this direction, PGM catalysts have been synthesized with the unique challenges of HT-PEMFCs in mind, such as increased phosphate poisoning resistance, phosphate-promoted ORR, and higher carbon corrosion resistance at elevated temperatures.

Phosphate poisoning challenges of PGM catalysts: PGM catalysts for the ORR have been intensively studied in the past decades for LT-PEMFCs. However, the high temperature and PA environment of HT-PEMFCs cause severe underperformance of the most promising PGM catalysts. The impact of the concentrated PA electrolyte on the performance, durability, and gas diffusion cannot be assessed in an RDE configuration using diluted PA (0.1–1 M PA, 1 M = 1 mol L^{-1}). The differences between the RDE and HT-PEMFC environments have recently come under focus [172]. To summarize, in the RDE environment, the active sites are saturated with dissolved O_2 in a liquid acidic electrolyte at typically ambient temperature, whereas in the HT-PEMFC membrane electrode assembly, the reaction only occurs at the triple-phase interface between the gas, catalytic sites, and charge transfer species (protons and electrons) [172]. PA adsorption on the PGM active sites hinders the utilization of active sites for the ORR in the cathode and reduces the performance and durability [41, 66, 67, 173–176]. As a result, Pt catalysts usually exhibit poor performance and stability in PA environments and HT-PEMFCs even at high Pt loadings [176]. For instance, the ORR activity and kinetic current density of Pt(100), Pt(110), Pt(111), and PtSn(111) decrease even with small amounts of PA (1 mM to 100 mM) in the perchloric acid solution (Fig. 7a, b). Specifically, 100 mM PA in $HClO_4$ reduces the half-wave potential of Pt(100), Pt(110), Pt (111), and PtSn(111) in $HClO_4$ solution at ambient temperature by 38 mV to 93 mV [173]. As a result, the performance of most PA-PBI-based HT-PEMFCs is typically half that of LT-PEMFCs, despite a much higher Pt loading (1 mg_{Pt} cm^{-2} vs. 0.2–0.3 mg_{Pt} cm^{-2}) [41].

Increasing the phosphate tolerance: preventing the adsorption of PA on Pt surfaces can prevent phosphate poisoning-related limitations [179]. N-doped carbon-encapsulated Pt-Fe ordered intermetallic NPs (O-Pt-Fe@NC/C) exhibit higher activity and poisoning resistance than Pt/C in a PA environment, as the N-doped carbon creates a protective layer between the Pt-Fe surface and phosphate anions [157]. Surfactant organic molecules and oleylamine similarly enhance the ORR activity of Pt NPs while preventing the adsorption of phosphate anions (Fig. 7c) [179]. Similarly, the addition of small amounts of oleylamine-modified Pt NPs can triple the ORR activity by preventing PA adsorption [177]. Modifying the support can improve the performance of PGM catalysts in HT-PEMFCs. For instance, polymers, such as PVP and poly[2,2-(2,5-pyridine)-5,5-bibenzimidazole] (para-PyPBI), have been used to functionalize the carbon supports of Pt NPs and improve the power density [178]. Protic ionic liquid modifications have been explored for a new class of CNT Pt NP catalysts, as the strong affinity of the ionic liquid with PA avoids active site poisoning and improves the HT-PEMFC performance and durability (Fig. 7d) [178]. Phosphate poisoning of PGM electrocatalysts can be reduced by altering the crystallinity and alloy composition. Modifying the electronic structure of Pt_2Ni_1 by argon heat treatment following specific anion adsorption has seen promising developments, improving the PA

poisoning resistance and enhancing the ORR activity and stability [180]. As the ORR is a proton-coupled electron process with sluggish kinetics, improving the proton transport mechanism could greatly improve its activity. Despite PA adsorption poisoning the Pt sites and reducing the activity of PGM catalysts, PA conducts protons and could also be used to facilitate the ORR. Therefore, using phosphates to promote the ORR activity of PGM catalysts has been explored to improve the performance of HT-PEMFCs.

Silica-promoted ORR: silica (SiO_2), while inactive to the ORR, strongly bonds to acids such as PA and can both prevent acid leaching and improve the proton conductivity. The introduction of SiO_2 reduces the loss of PA from both the membrane and catalyst layers and prevents phosphate poisoning of Pt. Most recently, Cheng and Wang's group prepared a CNT@*x*-SiO_2-Pt cathode catalyst by modifying CNTs with SiO_2 nanoclusters (Fig. 8) [181]. This catalyst achieves a record power density of 0.765 W cm^{-2} in H_2/O_2 and 0.486 W cm^{-2} in H_2/air without back pressure at 160 °C. Furthermore, this catalyst achieves 1.061 W cm^{-2} in H_2/O_2 at 240 °C (with 4 wt% SiO_2 loading). At 160 °C, the strong adsorption of phosphate on SiO_2 hinders phosphate poisoning of Pt, enhances the distribution of PA in the catalyst layer, and supplies local protons for the ORR (Fig. 8c). Most importantly, above 200 °C, the SiO_2 nanoclusters transform into phosphate silicate and supply a stable proton chain, which enables much higher HT-PEMFC performance than previously reported under similar conditions. Furthermore, the enhanced proton conductivity is also consistent with the smaller ohmic resistance and faster charge transfer of CNT@*x*-SiO_2-Pt catalysts than commercial Pt/C and CNT-Pt at 0.6 V. Therefore, introducing SiO_2 next to the Pt NPs can maintain stable operation and power density of HT-PEMFCs. This new discovery provides a new pathway to develop efficient HT-PEMFC catalysts and resolves the phosphate poisoning issues for commercialization of HT-PEMFCs [181].

PGM catalyst stability at high temperature: the chemical and structural stability of PGM catalysts in PEMFCs is impacted by (i) metal dissolution, including the dissolution of Pt and its alloys (e.g., Ni, Co), (ii) Ostwald ripening and agglomeration and (iii) support corrosion and particle detachment (Fig. 9). These degradations can often occur

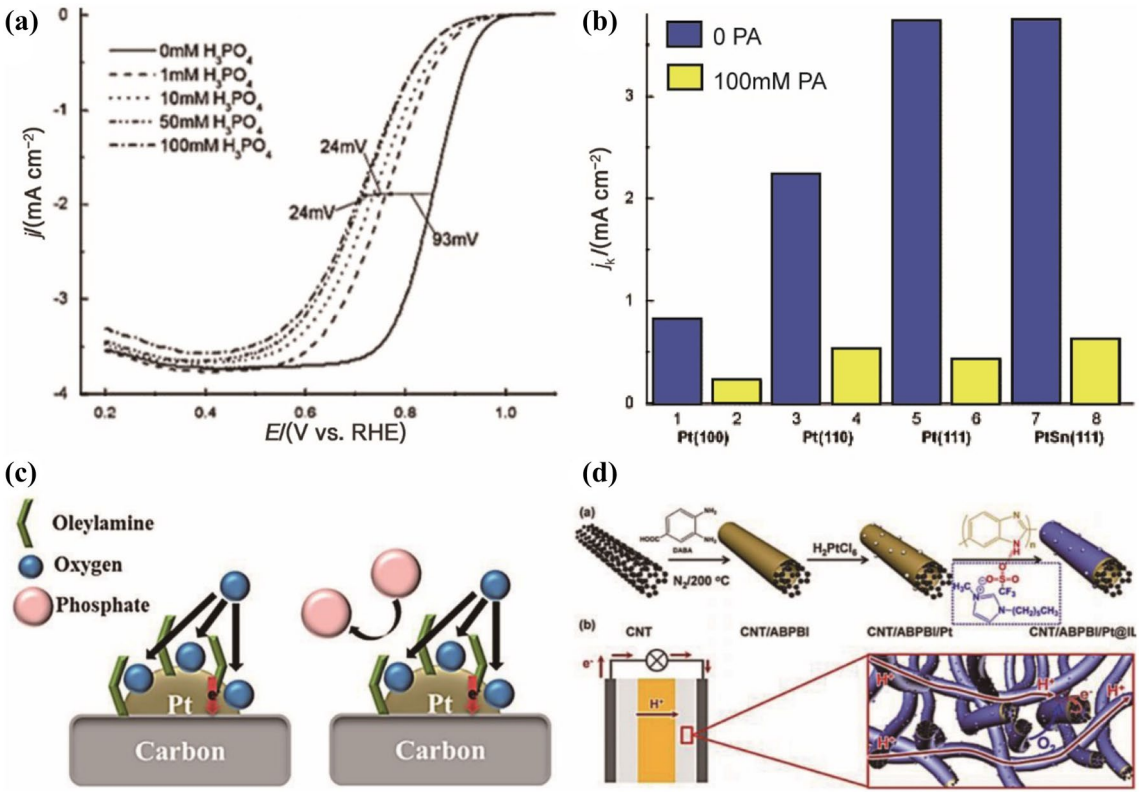

Fig. 7 PA poisoning and mitigation strategies of PGM catalysts. **a** Performance of Pt(111) in 0.1 M $HClO_4$ with 0, 1, 10, 50 and 100 mM PA. **b** ORR kinetic current density of Pt(100), Pt(110), Pt(111), and PtSn(111) in 0.1 M $HClO_4$ with/without 100 mM PA (recolorized for this review). Reproduced with permission from Ref. [173]. Copyright 2010, Royal Society of Chemistry. **c** Phosphate-ion adsorption on oleylamine-doped Pt/C. Reproduced with permission from Ref. [177]. Copyright 2013, American Chemistry Society. **d** CNT/ABPBI/Pt@IL synthesis and H^+ and ORR pathways. Reproduced with permission from Ref. [178]. Copyright 2018, Wiley

simultaneously, as the dissolved metal forms nanoclusters can promote carbon corrosion and weaken the interaction of the metal particles with the supports, which has been well studied for LT-PEMFCs [182]. However, operations at elevated temperatures (100–250 °C) accelerate the chemical and structural degradation, with an increase in Pt NP size after operations in HT-PEMFCs [32]. Therefore, catalysts with higher stability must be designed for successful application of HT-PEMFCs, with a few promising approaches. The addition of PWA-meso-silica into PBI membranes has been reported to increase the stability of the Pt catalyst in the electrodes due to the formation of phosphosilicate preventing PA leaching. In these configurations, Pt NPs confined by SiO_2 nanoclusters have a higher stability due to the strong interaction between Pt and SiO_2, the Pt nanoconfinement hindering aggregation, and the graphitized CNTs offering a stable support at high temperatures (Fig. 8). This paves the way for further catalyst development. Therefore, a combination of spatial nanoconfinement within nanopores enhancing the interactions between particles and the carbon support, stable core shells/Pt skin and engineered intermetallic structures could improve the Pt stability issue in HT-PEMFCs [183]. These approaches offer new opportunities to improve the stability of PGM catalysts in HT-PEMFCs (Fig. 9).

3.2 PGM-Free Catalysts

Currently, high PGM catalyst loadings are needed to improve the viability of HT-PEMFCs for practical applications due to the phosphate chemisorption of PGM cathode catalysts. The high cost of PGM catalysts and poor expression of catalytic sites in the PA environment drive the development of PGM-free catalysts for HT-PEMFCs [174].

3.2.1 Highly Active PGM-Free Catalysts

PGM-free catalysts: extensive efforts have been dedicated to developing low-cost PGM-free cathode catalysts for PEMFCs over the past two decades. Their performance and efficiency have been significantly improved, narrowing the half-wave potential gap from 100 to 12 mV [184, 185]. As cathode potentials below 0.7 V are typically used to generate high

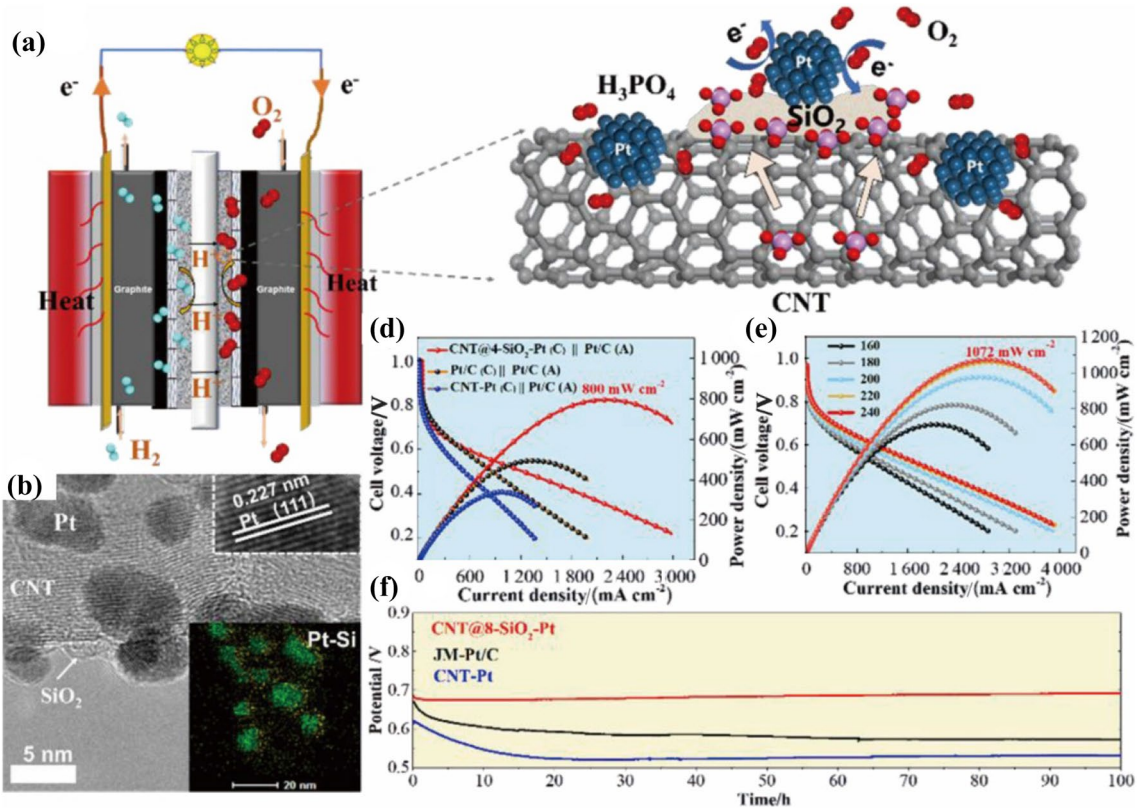

Fig. 8 **a** Pt-SiO_2 structure and **b** transmission electron microscopy (TEM) image of Pt-SiO_2. **c** to **e** Performance of cathode catalysts in HT-PEMFCs. **c** Pt/C, CNT-Pt and Pt-SiO_2 at 160 °C, and **d** Pt-SiO_2 from 160 °C to 240 °C. **e** Stability of Pt-SiO_2Pt/C, CNT-Pt, and commercial Pt/C at 160 °C without back pressure (H_2/O_2). Reproduced with permission from Ref. [181]. Copyright 2021, Springer Nature

power densities, the synthesis of metal–nitrogen–carbon (M–N–C) catalysts free of reduced metal, metal carbide, or metal oxide particles is preferred due to the poor activity and stability of these compounds under acidic conditions. Single-atom M–N–C catalysts have emerged as one of the most promising alternatives due to their high intrinsic activity for the ORR [185]. Therefore, there has been a focus on the synthesis of single atom-based catalysts for LT-PEMFCs [186–189]. Specifically, nitrogen-coordinated Fe/Co/Mn/Sn single-atom catalysts have been generally recognized as the most promising alternatives to Pt catalysts [187–190].

A number of good reviews have been published to summarize the advancements and challenges in PGM-free catalysts for LT-PEMFCs, with the main findings summarized here [184, 189, 191, 192]. The major active center of these catalysts under acidic conditions is the nitrogen-coordinated Fe/Co/Mn/Sn atom embedded in the carbon matrix (M–N_x) [187–190, 193, 194]. Among Fe/Co/Mn/Sn–N_x-based catalysts, Fe–N_x single-atom catalysts outperform Co–N_x, Sn–N_x and Mn–N_x single-atom catalysts [195–197]. The half-wave potential of Fe–N_x single-atom catalysts has been enhanced by 100 mV in recent years, narrowly reaching that of Pt in acidic environments [188, 190, 198, 199]. Ballard Power Systems recently demonstrated and commercialized a 30 W stack using solely PGM-free catalysts for the cathode [200]. Dual Fe–Co–N_x sites have even recently displayed outstanding onset potential and half-wave potential (1.06 and 0.863 V, respectively) [201]. Figure 10 highlights the latest advances in these single-atom or single-atom configuration PGM-free catalysts to replace Pt/C.

Despite impressive improvements in performance, the stability of Fe–N–C catalysts in LT-PEMFCs is quite poor. These catalysts suffer from (i) flooding of the porous structure in the catalyst layer due to the liquid water, (ii) high mass transfer resistance due to the thicker catalyst layer resulting from the high catalyst loading, (iii) demetallation of Fe-based active sites via oxidation of atomically dispersed Fe by H_2O_2 radicals in active FeN_x moieties (< 1.0 V vs. RHE) and leaching of Fe NPs (> 0.3 V vs. RHE), and (iv) electrochemical carbon oxidation reaction and corrosion caused by starts-stops (> 0.207 V vs. RHE) and H_2O_2 or H_2O_2-derived radicals (e.g., hydroperoxyl). Carbon oxidation at high potential (> 0.9 V) destroys atomically dispersed active site Fe–N_x–C_y species. Stable operando potential windows below 0.7 V and operational strategies are suggested to avoid degradation of Fe–N–C catalysts in acidic media [186].

3.2.2 PGM-Free Catalysts for HT-PEMFCs

The HT-PEMFC environment presents interesting opportunities to utilize the active sites of PGM-free catalysts potentially better than in LT-PEMFCs. First, M–N_x single-atom catalysts have high tolerance for phosphate poisoning, which renders them attractive for HT-PEMFCs using phosphate or PA as proton carriers (Fig. 11) [174, 218]. In addition, increasing the operating temperature avoids liquid water flooding within the nanopores of the single-atom catalysts [31–33]. Therefore, operating these catalysts in HT-PEMFCs may finally fully unlock their potential [192] (Table 2).

PGM-free catalysts were reported in HT-PEMFCs for the first time in 2015 [215]. Following this technological breakthrough, PGM-free catalysts have come under increasing investigation over the past six years for HT-PEMFCs, with improvements in performance, efficiency, and durability

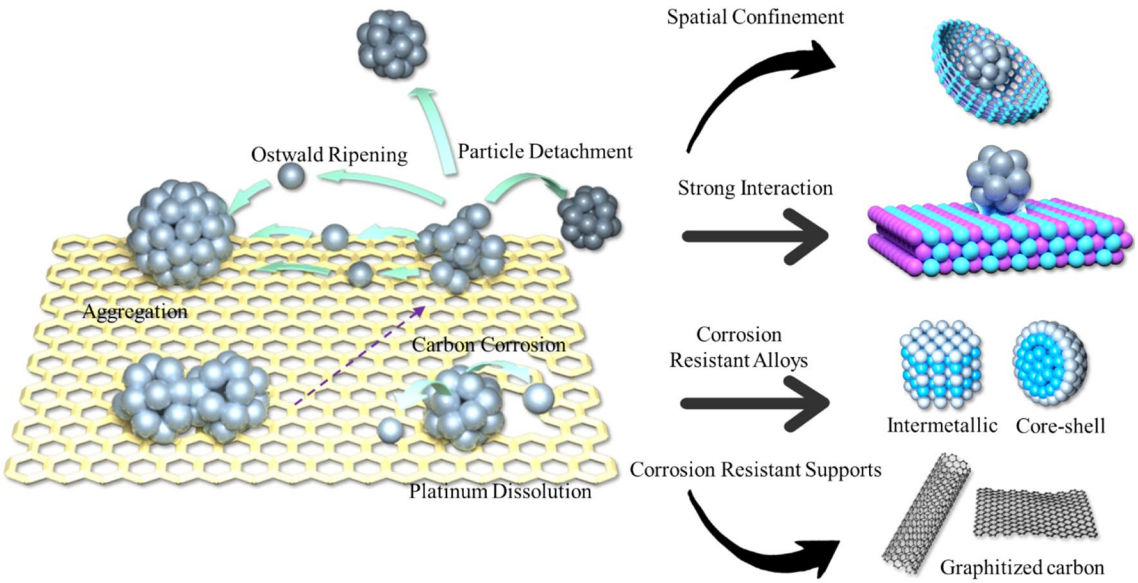

Fig. 9 Degradation mechanisms and mitigation strategies for PGM catalysts

(summarized in Table 3). Most importantly, the stability of PGM-free catalysts is far superior in HT-PEMFCs to that in LT-PEMFCs, as summarized in Fig. 12.

PGM-free catalysts were first reported in HT-PEMFCs using hollow microspheres with a graphitic layer of encapsulated Fe_3C NPs with a high surface area (374 m^2 g^{-1}) as the active sites (Fig. 13a, b) [215]. Most notably, this catalyst achieves a much higher stability in HT-PEMFCs than in LT-PEMFCs, confirming that the higher tolerance of PGM-free catalysts captured in low-concentration PA environments using a RDE (Fig. 11) occurs in real devices. Designing catalysts with etched silica templates can enhance oxygen and PA diffusion to the active sites in HT-PEMFCs (Fig. 13c, d) [216]. The durability of PGM-free catalysts in HT-PEMFCs was further increased by using a Fe–N–C catalyst (BP-FeNC) (Fig. 13e, f), with less than 32% performance degradation in 400 h [218]. The performance (0.06–0.18 W cm^{-2}) of these pioneering catalysts could be improved in HT-PEMFCs through increased active site density, reduced carbon corrosion, and phosphate-promoted ORR. Furthermore, more systematic investigations of the PA doping procedure, catalyst layer design, and membrane assembly procedure should be conducted.

Active site density and stability: iron-based single-atom catalysts suffer from a low surface-active site density, with active sites encapsulated within the carbon structure [217]. For instance, the ORR half-wave potential and onset potential of microporous carbon materials become more positive as the Fe content is increased from 0 to ~ 0.6 wt%, but a further increase in the Fe content does not improve the ORR activity due to the encapsulation of the active sites inside the structure [226]. The active site loading is generally limited in the range of 1–3 wt%(Fe) due to the undesired aggregation at high loading. Due to strong Fe clustering at high Fe content, the utilization efficiency of the Fe–N–C catalysts drops from ~ 0.4 to ~ 0.1 when the Fe loading increases from

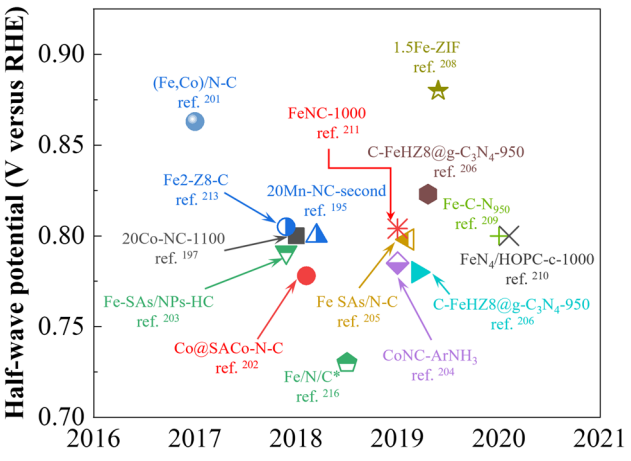

Fig. 10 Half-wave potential of various M–N–C catalysts evaluated in acidic electrolytes

0.3 to 2.8 wt% [199]. Enhancing the loading and utilization is one of the main solutions to further boost the performance of these noble metal-free catalysts. To enhance the Fe–N_4 site utilization, a chemical vapor deposition approach was developed by using transmetallation of Zn–N_4 sites into Fe–N_4 sites, achieving an active site density of 1.92×10^{20} sites per gram with 100% site utilization even with a Fe loading of 2.0 wt% [227]. Most recent research shows that strong interactions between active sites can alter the intrinsic ORR activity when the intersite distance is smaller than approximately 1.2 nm, while synergistic effects continuously boost the performance until the distance between adjacent Fe sites becomes smaller than 0.7 nm [228]. A new synthesis strategy successfully reduced the catalyst loading to 0.3 mg_{Fe} cm^{-2} by increasing the active site density (Fe loading of (7.7 ± 1.3) wt%) [221]. This procedure synthesizes two-dimensional thin graphene with a thickness of 0.4–0.6 nm (Fig. 14a, c). The iron single-atom catalysts embedded in nitrogen-coordinated graphene (FeSA-G) have a surface atomic Fe density of 3.5 sites nm^{-2}, which is among the highest for iron single-atom catalysts. These catalysts are highly active and stable for the ORR with high phosphate tolerance, which is particularly appealing for HT-PEMFCs. The FeSA-G catalyst in combination with the SiO_2 NP-doped PA-PBI (PA/PBI/SiO_2) membrane developed by Cheng's group achieves outstanding performance and stability in HT-PEMFCs, which is attributed to its high resistance to phosphate poisoning and enhanced ORR kinetics (Fig. 14d, f) [221]. This is consistent with Li's group reporting negligible adsorption of PA on a Fe–N–C catalyst [218]. Most importantly, the increase in power density from 160 to 230 °C, reaching similar performance to that of Pt at 230 °C, demonstrates the potential of this catalyst for operation at even higher temperatures (Fig. 14d, e). Most recently, high loading of Fe–N–C with 7 wt% atomic iron sites using a sacrificial metal (Zn) in the initial synthesis step achieved an active site density of 7.8×10^{19} sites g^{-1} by using the ex situ CO chemisorption method [229].

Reduced carbon corrosion: carbon corrosion is more severe for high-loading iron single-atom and nitrogen defect catalysts within the carbon matrix in HT-PEMFCs due to their elevated temperature and concentrated PA environment (Table 2) [207, 213]. Therefore, supporting high-density single atoms on conductive and corrosion-resistant carbon substrates can fulfill the requirement of HT-PEMFCs. Among the carbon-based supports, CNTs are thermally stable and enhance the electrocatalytic activity of the supported electrocatalysts due to their good graphitization [230, 231]. Supporting a monolayer of iron single atoms on graphitized carbon could expose all the active sites and boost the electrochemical stability [232–234]. However, depositing iron single atoms homogenously on CNTs with high density is challenging, as metal atoms tend to agglomerate. The use of a silica-protective layer allows preferential formation of atomic iron active

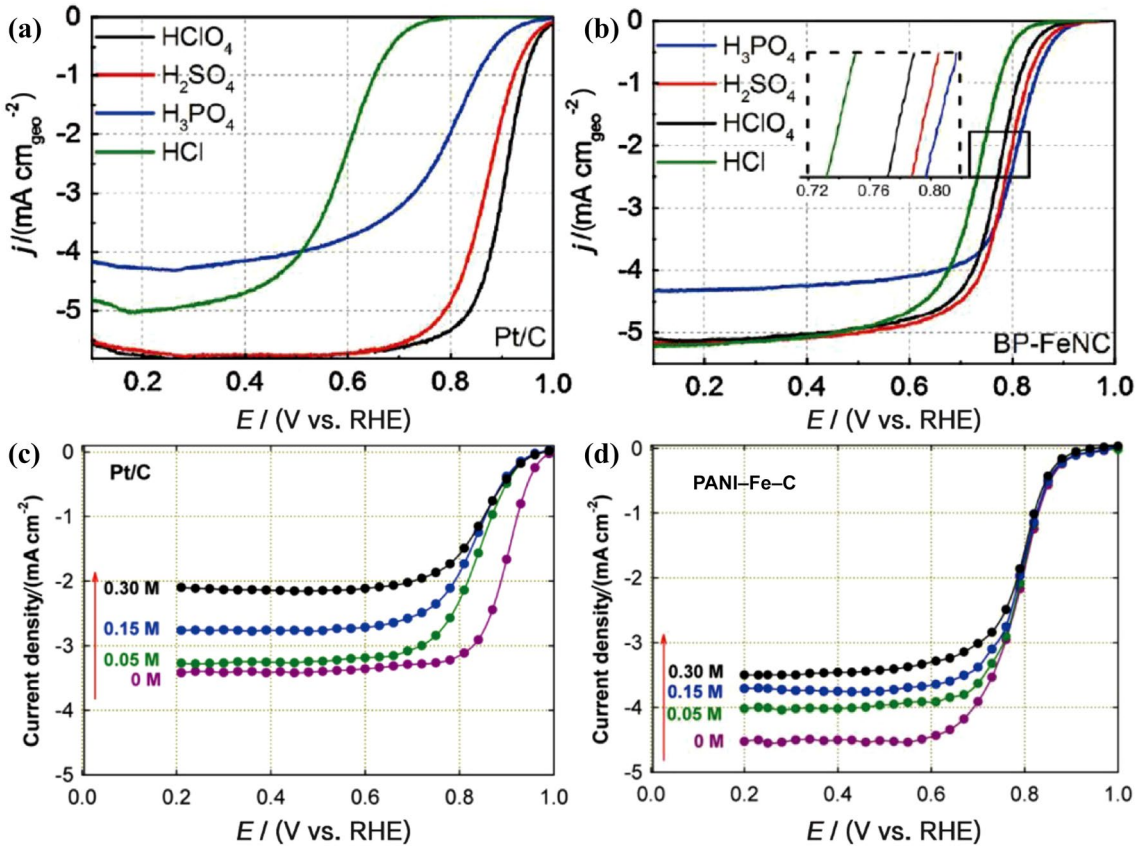

Fig. 11 Performance of Pt/C and Fe–N–C catalysts in different acidic environments. **a** Pt/C and **b** BP-FeNC in $HClO_4$, H_2SO_4, H_3PO_4 and HCl. Reproduced with permission from Ref. [218]. Copyright 2018, Elsevier. **c** Pt/C and **d** PANI–Fe–N–C in a 0.1 M $HClO_4$ electrolyte with 0, 0.05, 0.15 and 0.30 M H_3PO_4. Reproduced with permission from Ref. [174]. Copyright 2014, American Chemistry Society

sites instead of Fe NPs [235, 236]. The silicate template-based method involves multiple steps, while the loading of atomic Fe–N_x on the CNTs is less than 2.0 wt%. The active site density of PGM-free catalysts in HT-PEMFCs has been increased via a facile template-free method to prepare high-density iron single atoms supported on highly crystallized CNTs (Fig. 15a) [225]. Iron-based single-atom catalysts are synthesized through one-pot pyrolysis of well-ground hemin porcine with dicyandiamide and acid-oxidized CNTs. The surface of the CNTs (< an 8 nm diameter) supports a continuous layer of amorphous carbon, with a high density of isolated iron atoms on the CNT surface. The 3.5 wt% atomic iron loading single-atom catalyst has an onset potential of 0.95 V and a half-wave potential of 0.801 V for the ORR in O_2-saturated 0.1 M $HClO_4$ solution. This performance is comparable to that with 12.5 μg_{Pt} cm^{-2} and attributed to the high density of atomic sites and conductive CNT graphene networks. The as-synthesized iron single-atom catalyst has a 0.266 W cm^{-2} peak power density and excellent stability (negligible performance loss at 0.5 V over 100 h) at 240 °C in HT-PEMFC cathodes (Fig. 15c, e) due to the highly graphitized CNTs. This supplies a facile and practical route for efficient PGM-free catalysts for HT-PEMFCs. The Cheng group most recently demonstrated that the in situ growth of atomic layers of iron single atoms on carbon supports could boost the turnover frequency by using the sublayer to tune the activity of the top-layer atomic sites, enhancing the activity and durability for the ORR [237]. Interestingly, tuning the CO content (0–10%) within the hydrogen stream has also been reported to actually possibly reduce the carbon corrosion rate occurring during start-stop [238], while carbon corrosion can also be mitigated through careful control of HT-PEMFC operation [239].

PA-promoted ORR: in HT-PEMFCs, PA is the proton carrier in both the membrane and the catalyst layer. PA adsorption next to the active sites could locally supply protons to promote the ORR, leading to an enhanced performance of the HT-PEMFCs, rather than poisoning of the catalysts. Regulation of the proton transport mechanism could improve the ORR activity, as the ORR is a proton-coupled electron process [240–242]. Atomically dispersed bimetallic FeCu atoms anchored on nitrogen-doped CNTs (FeCu/N-CNTs) have been designed as a new electrocatalyst for the ORR in PA-based HT-PEMFCs [223]. The FeCu/N-CNT catalysts were synthesized through pyrolysis of dicyandiamide

Table 2 Overview of PGM-free catalysts in LT-PEMFCs. Data are extracted from different references so their significant digits are left unchanged

Catalysts	Configuration	Power density/(W cm^{-2})	Open-circuit voltage (O_2) /V	Half-wave potential/(V vs. RHE)	Onset potential /(V vs. RHE)	Performance loss over time	References
20Co–NC–1100	Co–N_4	0.560 (O_2)/0.280 (air)	0.95 (O_2)	0.80	0.93	55% over 100 h	[197]
Co@SACo–N–C	Co–N_x	0.42 (O_2)/0.23 (air)	0.91 (O_2)	0.778	0.925	16% over 100 h	[202]
20Mn–NC–second	Mn–N_4	0.46 (O_2)	0.95 (O_2)	0.800	–	22.5% over 100 h	[195]
Fe–SAs/NPs–HC	Fe–N_4	0.33 (air)	0.96 (air)	0.791	–	–	[203]
CoNC–$ArNH_3$	Co–N_4	0.44 (O_2)/0.21 (air)	0.88 (air)	0.785	0.890	65% over 20 h	[204]
Fe SAs/N–C	Fe–N_4	0.68 (O_2)/0.35 (air)	0.83 (O_2)	0.798	–	–	[205]
C–FeHZ8@g–C_3N_4–950	Fe–N_4	0.628 (O_2)	0.98 (O_2)	0.780	–	51.3% over 8 h	[206]
TPI@Z8(SiO_2)–650–C	Fe–N_4	1.180 (O_2)	0.91 (air)	0.823	–	80% over 50 h	[207]
1.5Fe–ZIF	Fe–N_4	0.66 (O_2)/0.36 (air)	0.98 (O_2)	0.88	–	40% over 100 h	[208]
(Fe,Co)/N–C	Fe–Co–N	–	–	0.863	1.060		[199]
Fe–C–N_{950}	–	0.680 (O_2)	0.80 (O_2)	0.800	–	–	[209]
FeN_4/HOPC–c–1000	Fe–N_4	0.660 (O_2)/0.420 (air)	0.99 (O_2)	0.800	0.900	47% over 100 h	[210]
FeNC–1000	Fe–N_4	1.01 (O_2)	0.98 (O_2)	0.804	0.894	–	[211]
Fe–N–C–Phen–PANI	Fe–N_4	1.06 (O_2)	0.92 (O_2)	–	–	–	[212]
Fe2–Z8–C	Fe–N_4	1.14 (O_2)	1.00	0.805	0.902	85% over 50 h	[213]
Fe/N/C(4mIm)–OAc–2 bar	Fe–N_4	1.33 (O_2)	1.00(O_2)	–	–	80.3% in 35 h	[214]
Fe/C–700 catalyst*	Fe_3C	0.18 (O_2)	0.80	0.700	0.85	80% over 50 h	[215]
Fe/N/C*	Fe–N_x	0.12 (O_2)	0.90	0.730	0.8	–	[216]
Sn–N–C	Sn–N_x	–	–	0.730	0.88		[217]

*These catalysts were evaluated in both LT-PEMFCs and HT-PEMFCs

Table 3 Overview of PGM-free catalysts in HT-PEMFCs. Data are extracted from different references so their significant digits are left unchanged

Catalysts	Configuration	Power density/(W cm^{-2})	Open-circuit voltage (O_2)/V	Half-wave potential/(V vs. RHE)	Onset potential/(V vs. RHE)	Performance loss over time	References
Fe/C–700 catalyst	Fe_3C	0.06	0.80	0.700	0.850	~20% over 120 h	[215]
Fe/N/C	Fe–N_x	0.02	0.85	0.730	0.800	–	[216]
BP-FeNC	Fe–N_x	0.18	0.97	0.770	0.900	~35% over 400 h	[218]
NCMI	Fe–N_x	~0.35	–	–	–	–	[219]
FePhen@MOF–$ArNH_3$	Fe–N_x	~0.4	0.93	0.750	0.900	–	[220]
FeSA–G	Fe–N_x	0.27 (160 °C)/0.32 (230 °C)	0.89	0.804	0.950	~37.5% over 100 h	[221]
LEDFe$_5$–NH_3	Fe–N_x	0.26	–	0.760	0.740	–	[222]
FeCu–N–CNTs	FeCu	0.25 (160 °C)/0.30 (230 °C)	0.87 – 0.89	0.811	0.900	~15% over 100 h	[223]
Fe–N–C	Fe–N_x	~0.14	1.0	–	–	120 h (from 0.22 to 0.42 V @ 0.25 A cm^{-2})	[224]
FeSA/HP	Fe–N_x	0.22 (160 °C)/0.26 (240 °C)	0.9	0.801	0.950	~12% over 100 h	[225]

~These values are not directly given in the papers and are obtained by estimating the peak power density from the *I–V* curve and the performance loss over the stability test.

in the presence of hemin porcine and copper(II) acetylacetonate after a subsequent acid treatment (FeCu(*X*:*Y*), with *X*:*Y* being the iron-to-copper atomic ratio) (Fig. 16a-b) [223]. The Fe–N and Cu–N sites with distances of 4–5 Å (1 Å = 1×10^{-10} m) synergistically promote the ORR activity under acidic conditions. In addition to high tolerance

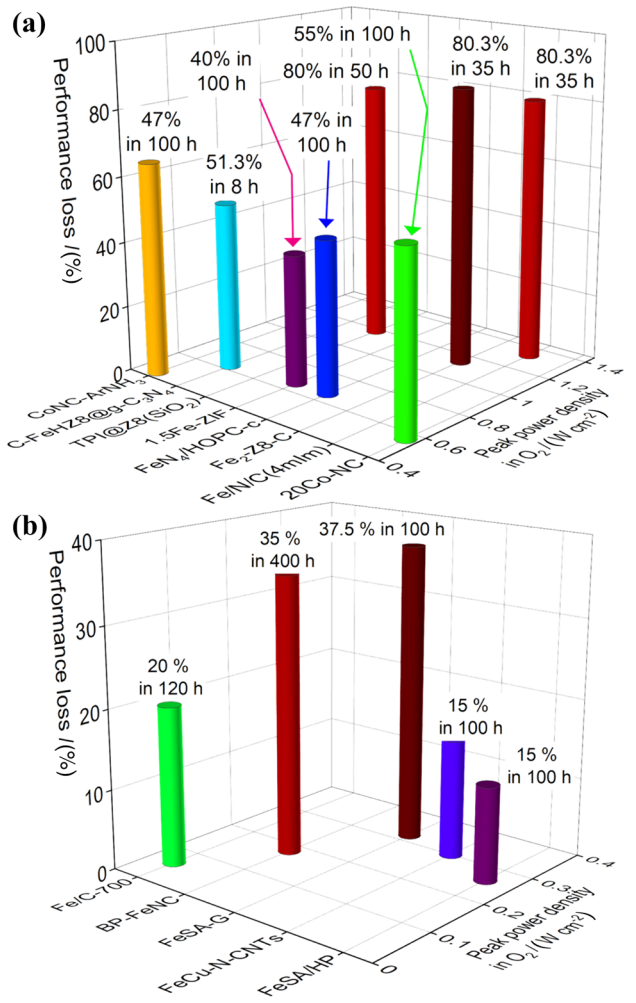

Fig. 12 Performance and durability of PGM-free catalysts in a LT-PEMFCs and b HT-PEMFCs. *Note*: this graph was produced by using the data from Tables 2 and 3

to phosphate, these FeCu/N-CNT catalysts have enhanced ORR activity in the presence of PA or so-called phosphate-promoted ORR activity. The ORR activity is closely correlated with the Fe:Cu ratio, with the best results obtained on FeCu(4:1), achieving an onset potential of 0.960 V versus RHE and a half-wave potential of 0.811 V versus RHE. The half-wave potential increases by 18 mV with increasing amount of PA (Fig. 16d). The Cu–N atomic site could strongly absorb the phosphate ions and local protons to assist the ORR at the adjacent Fe–N active site. The HT-PEMFCs with either the FeCu(1:0) or FeCu(4:1) cathode reach 0.24 and 0.30 W cm^{-2} peak power densities, with the latter identical to that with the Pt cathode (Fig. 16e). Furthermore, these catalysts achieve the highest stability to date for PGM-free catalysts for LT-PEMFCs and HT-PEMFCs, with retention for over 100 h (Fig. 16f). These new discoveries supply a new pathway to design phosphate-promoted ORR catalysts, offering new opportunities to overcome the PA poisoning in HT-PEMFCs.

Overall, the traditional synthesis of single-atom catalysts through pyrolysis of a mixture of carbon/nitrogen/metal sources, which encapsulates the active sites inside the carbon structure and poorly graphitizes the carbon, requires careful reconsideration to meet the challenges of M–N_x single-atom catalysts for the ORR in HT-PEMFCs. The development of novel methods based on supporting a single layer of high-density bimetallic or multimetallic atomically dispersed catalysts on conductive and corrosion-resistant carbon supports would be a promising approach to solve the challenges of poor intrinsic activity and stability and low active site density and utilization. In this sense, two-dimensional graphene could be a useful support because every carbon honeycomb is utilized in the conductive support, avoiding encapsulation. In addition, the graphene sheets supply a planar platform to build triple-phase boundaries on the surface and outperform microporous carbon structures. However, they are still unexplored at this stage. Furthermore, investigation of the best acid doping procedure and cell activation procedure, improvement in the membrane and GDL properties, and design of macropores in the catalyst should be explored, with a strong focus on the uniquely complex challenges of PGM-free catalysts.

4 Highly Efficient and Stable Catalyst Layers for HT-PEMFCs

While LT-PEMFCs and HT-PEMFCs may appear similar aside from the higher operating temperature, the proton transport mechanisms within the electrodes are fundamentally different. As a result, LT- and HT-PEMFC require catalyst layers with drastically different architectures and properties. Specifically, in LT-PEMFCs, proton transport occurs via the liquid water generated by the electrochemical reaction/provided by the humidified gas and via the proton-conducting ionomer in humidified conditions [243]. In contrast, HT-PEMFCs rely on the viscous acidic electrolyte, doped within the membrane electrode assembly prior to operation, to reliably and evenly conduct protons through their entire lifecycle [244]. While the requirements for the catalyst layer in LT-PEMFCs have been recently outlined in an excellent review by Suter et al., these requirements differ for HT-PEMFCs and should be investigated further [244]. In HT-PEMFCs, the catalyst layer structure must allow diffusion of the viscous acid to the active sites while also stabilizing it to avoid leaching and depletion. Figure 17 succinctly summarizes the differences in the electrode properties of LT- and HT-PEMFCs. The conventional RDE test system does not sufficiently

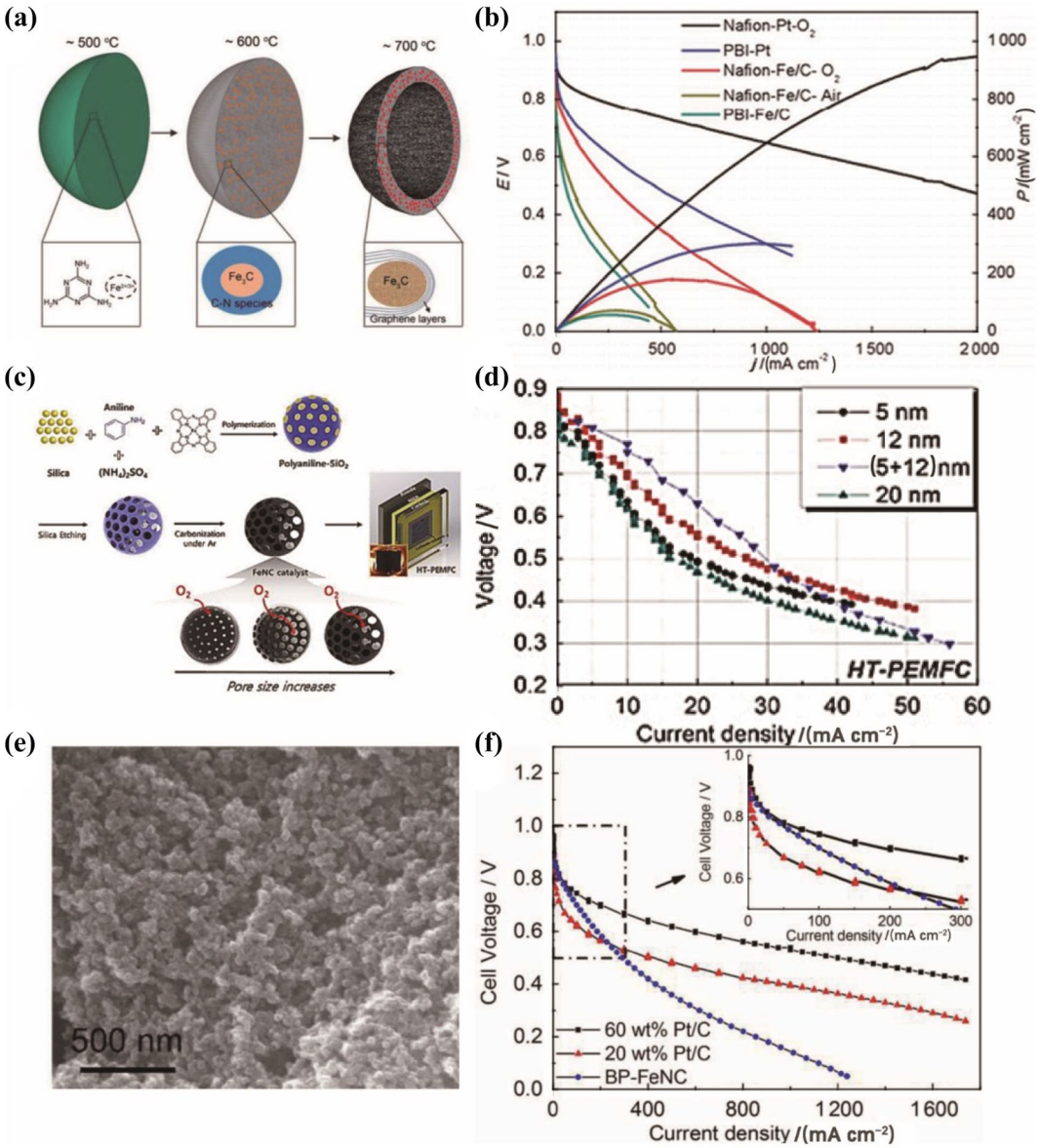

Fig. 13 PGM-free catalysts in HT-PEMFCs. **a** Synthesis of Fe/C and **b** polarization of Pt/C and Fe/C-700 cathodes in LT-PEMFCs (80 °C, Nafion membrane, 100% RH) and HT-PEMFCs (160 °C, PBI membrane, dry gases). Reproduced with permission from Ref. [215]. Copyright 2015, Royal Society of Chemistry. **c** Silicate-derived synthesis of Fe/N/C and **d** polarization at 150 °C, dry H_2/O_2. Reproduced with permission from Ref. [216]. Copyright 2018, Wiley. **e** BP-FeNC structure and **f** polarization of 60 wt% Pt/C (1.6 mg_{Pt} cm^{-2}), 20 wt% Pt/C (0.9 mg_{Pt} cm^{-2}), and BP-FeNC (7.8 mg_{cat} cm^{-2}) at 160 °C, dry H_2/O_2. Reproduced with permission from Ref. [218]. Copyright 2018, Elsevier

reflect the real conditions and the intrinsic activity in the PA environment for HT-PEMFCs (Fig. 17a, b). The liquid water-free PA environment of HT-PEMFCs makes establishing a robust triple-phase boundary at all active sites challenging and reduces the catalyst utilization (Fig. 17c, d).

As summarized in Fig. 17d, the viscous acid environment causes complex challenges for HT-PEMFCs, leading to higher catalytic loadings yet lower current densities than in LT-PEMFCs. This indicates that HT-PEMFCs currently suffer from a weaker ability to reflect the inherent catalytic activity and a poorer active site utilization than LT-PEMFC. A few groups have designed half-cells enabling high-loading gas diffusion electrodes (GDEs) at ambient temperature in liquid electrolytes [245–247] and in concentrated PA and HT environments [248–251] to assess catalysts at higher current densities. Such innovative configurations should be more heavily used by researchers working on catalysts for HT-PEMFCs to evaluate the catalyst performance at elevated temperatures in concentrated acids. Thus, the development

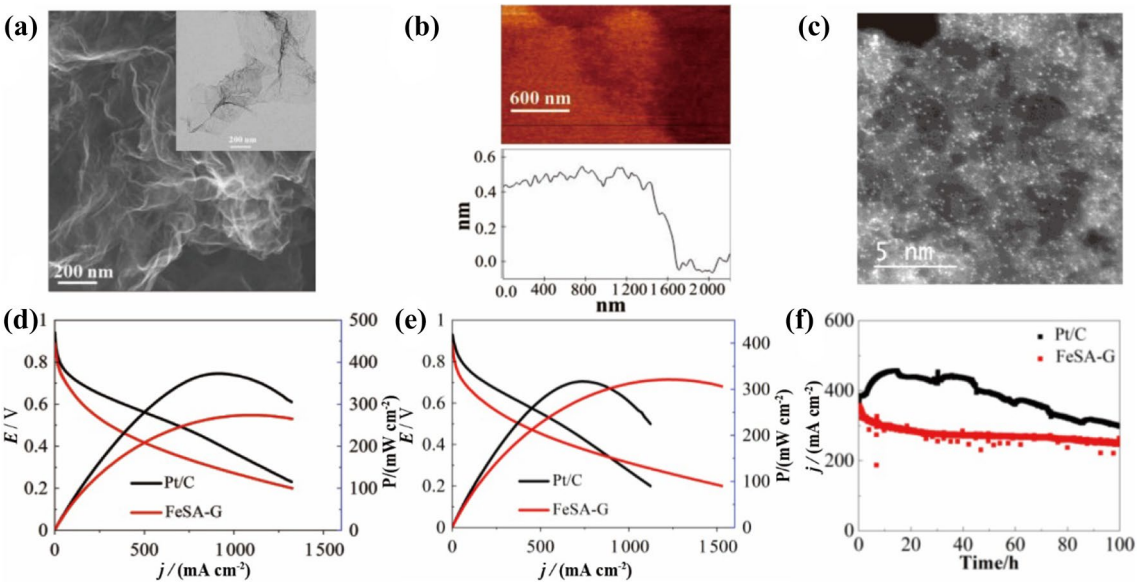

Fig. 14 **a** TEM, **b** atomic force microscopy (AFM), and **c** aberration corrected (AC)-scanning transmission electron microscopy (STEM) images of FeSA-G catalysts. Polarization and power density of HT-PEMFCs using 0.3 mg_{cat} cm^{-2} FeSA-G and 1 mg_{Pt} cm^{-2} cathodes **d** at 160 °C and **e** at 230 °C. **f** One-hundred-hour stability of the HT-PEMFC at 0.6 V for FeSA-G and 0.5 V for Pt. Reproduced with permission from Ref. [221]. Copyright 2019, Wiley

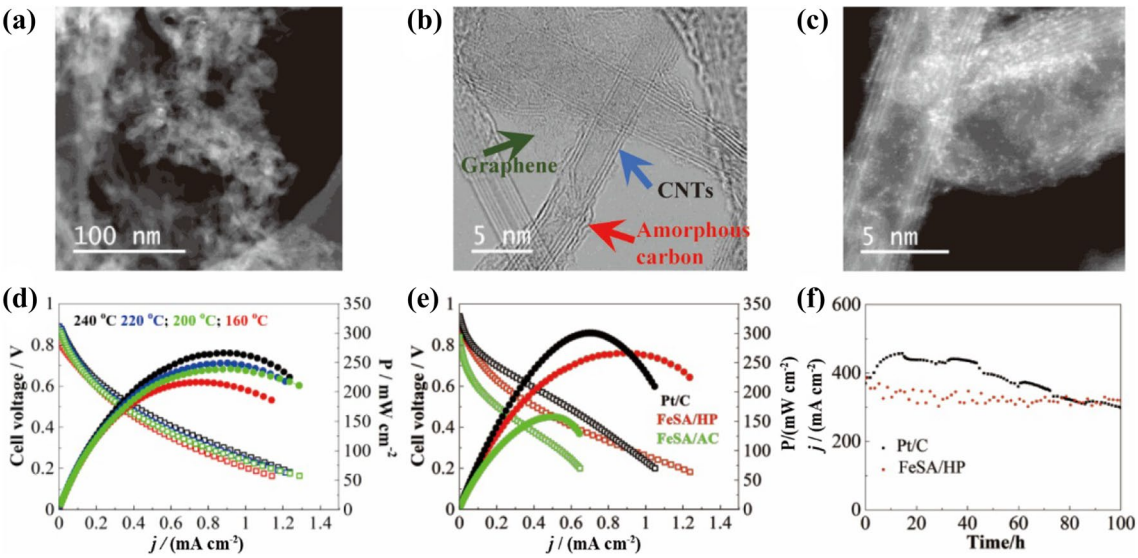

Fig. 15 **a** STEM, **b** high-resolution TEM and **c** AC-STEM images of FeSA/HP. **d** Polarization and power density of HT-PEMFCs with a 4 mg_{cat} cm^{-2} FeSA/HP cathode at 160, 200, 220 and 240 °C. **e** Performance of the HT-PEMFCs with Pt/C and FeSA/HP cathodes at 240 °C. **f** Stability of the HT-PEMFC using the Pt/C cathode at 0.6 V and the FeSA/HP cathode at 0.5 V and 240 °C. Reproduced with permission from Ref. [225]. Copyright 2021, Elsevier

of catalysts for HT-PEMFCs should be systematically evaluated in a practical HT-PEMFC to reflect the real conditions. Furthermore, the structure of the catalyst layer determines the catalytic site utilization. The following section discusses how to optimally design the membrane electrode assembly for HT-PEMFCs, with a special focus on optimizing the active site utilization and creating more efficient triple-phase boundaries to boost the expression of catalytic sites through improvement in the catalyst layer and MPL properties.

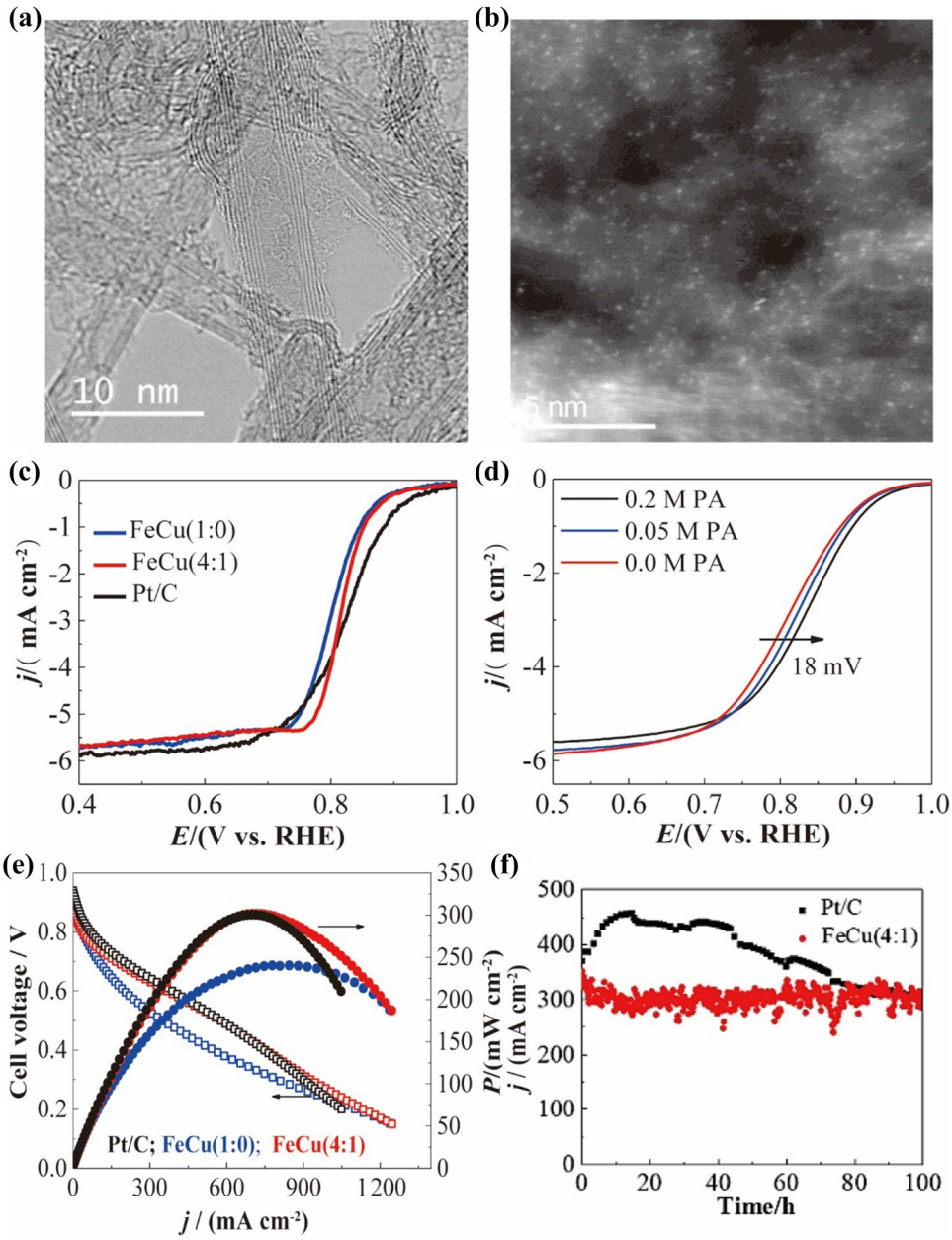

Fig. 16 **a** High-resolution TEM and **b** AC-STEM images of FeCu-N-CNTs. **c** Linear scan voltammetry curves of FeCu/N-CNTs with different Fe/Cu atomic ratios in 0.1 M O_2-saturated $HClO_4$. **d** FeCu(4:1) in O_2-saturated 0.1 M $HClO_4$ with the addition of PA. **e** Polarization and power density of PA/PBI composite membrane cells using 4 mg_{cat} cm^{-2} FeCu(1:0), FeCu(4:1) and 1 mg_{Pt} cm^{-2} cathodes at 230 °C. **f** Stability of the cells with a Pt/C cathode at 0.6 V and a FeSA/HP cathode at 0.5 V and 240 °C. Reproduced with permission from Ref. [223]. Copyright 2021, Elsevier

4.1 Preparation, Assembly, and Activation of HT-PEMFCs

4.1.1 Acid Doping

A high-quality membrane electrode assembly should have a high membrane conductivity, a high proton conductivity, and subsequently high performance. This can be achieved via an efficient PA doping process, optimized contact between the membrane and electrode to allow excellent proton conductivity, and optimized distribution of the electrolyte in both the membrane and electrode. Doping the viscous acid within the membrane electrode assembly constitutes a crucial step of HT-PEMFC preparation. The acid doping temperature and duration heavily impact the membrane proton conductivity and interactions [252, 253]. Careful consideration of the catalyst layer substrate and acid doping substrate is necessary, as both heavily impact the quality of the electrolyte/electrode interaction interface and performance. To date, doping PA on the membrane and depositing the catalyst layer on a GDL provide the highest power densities and current densities (Fig. 18) [254, 255]. Finally, physically removing the excess acid before operation (dabbing, wiping) improves the HT-PEMFC performance and stability by

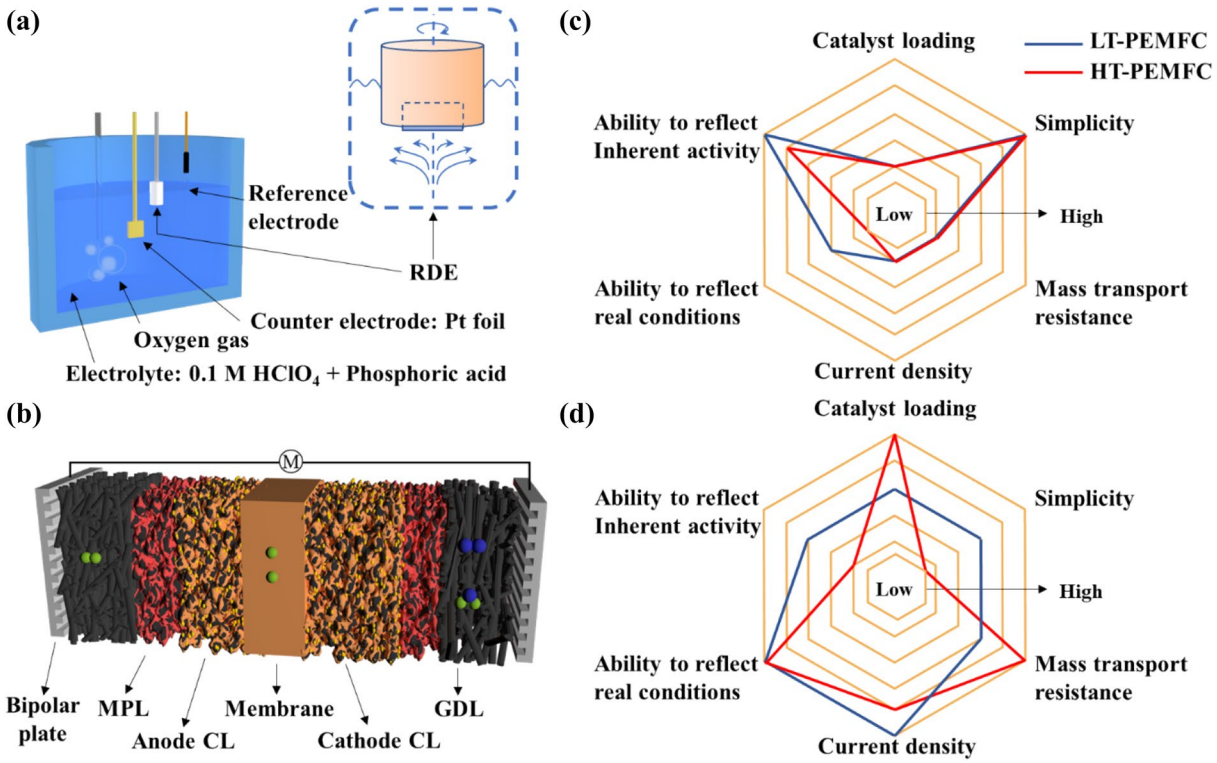

Fig. 17 **a** Typical three-electrode configuration and **b** single fuel cell to evaluate the ORR activity of PGM and PGM-free catalysts. Ability to reflect the conditions of the catalysts in three-electrode systems and fuel cells for **c** LT-PEMFC and **d** HT-PEMFC applications

mitigating the formation of phosphate compounds within the flow fields and endplates [256].

4.1.2 Membrane Electrode Assembly Fabrication

Once the PA is suitably doped within the membrane/electrode, binding the electrode to the membrane is necessary. LT-PEMFCs are typically hot-pressed at approximately the membrane glass transition temperature (127 °C) to bind the electrodes to the membrane and create a membrane electrode assembly [257]. However, this step may be redundant, as the heat of the LT-PEMFC during operation equally binds the materials together [258]. An important clarification is proposed here for the hot-pressing process of HT-PEMFCs. As PBI membranes are thermally stable up to 400 °C, hot pressing (130–200 °C) does not create a physical bond between the membrane and the electrode [259]. While heat and pressure might accelerate acid diffusion from the membrane to the electrode, this process might expel too much free-flowing acid and negatively affect the performance [260, 261]. Nevertheless, as the membrane mechanical strength can vary and decreases with increased doping amount, polysulfone sheets can strengthen the weakest edges of the membrane, in which case a hot-pressing step has been reported to bind these sheets to the membrane (200 °C) [262]. Recently, a new membrane electrode assembly fabrication method has been proposed by depositing a thin layer of PBI (35 µm) onto the GDE anode [263]. This approach doubles the power density and drastically reduces the ohmic resistance, highlighting that more innovative methods should be considered in the future.

4.2 PA Distribution in the Catalyst Layer

The structure and properties of the catalyst layer are crucial for diffusion of the protons from the membrane to the active sites and the gases from the GDL to the active sites. While the majority of the studies discussed here focus on PA as the viscous acid used, readers are encouraged to draw analogies for other viscous proton conductors, such as protic ionic liquids, while their properties may differ [43]. Although improvements in the catalyst utilization of HT-PEMFCs have been observed through better catalyst layer designs, the electrochemical performance and active site utilization remain lower than those in LT-PEMFCs, with only a minority of studies reporting reductions in catalyst loading and higher performance (Fig. 19) [264–266]. While both LT-PEMFCs and HT-PEMFCs have exhibited improvements in the volumetric

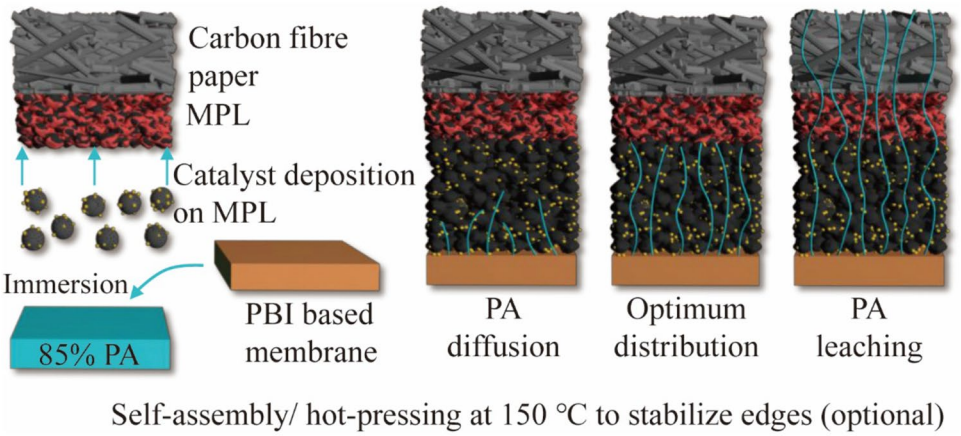

Fig. 18 Preparation and conditioning of HT-PEMFC membrane electrode assemblies with gradual acid diffusion. The relative sizes and distances are not to scale, and the catalyst layer, MPL, and carbon fibers possess significantly different porosities and sizes

power density with lower loadings, insufficient efforts have been dedicated to this area for HT-PEMFCs [264]. Advanced engineering catalyst deposition techniques have shown promise in reducing the catalyst loading and controlling the catalyst layer porosity. For instance, HT-PEMFCs prepared by electrospraying the Pt catalyst layer achieve good performance with loading lower than 0.1 mg_{Pt} cm^{-2} at the cathode, while the electrode suffers from a significantly slower conditioning time (500 h) due to its very high PA diffusion limitations [267]. Ultrasonic spraying allows reduction in the loading from 1.208 to 0.350 mg_{Pt} cm^{-2} and significantly improves the performance due to the enhanced catalyst ink distribution, causing a higher platinum utilization due to the efficient stirring and forced convection during the ultrasonic spraying process [265]. Reactive spray deposition technology, using a one-step jet-flame direct deposition process, also shows potential for loading reduction while suffering from proton and gas transport issues [268]. Although these advanced catalyst deposition techniques can reduce the catalyst loading and control the catalyst layer porosity, these methods are not widely applicable due to their high costs and limited availability [265, 267, 268]. Instead, dedicated approaches to improve the active site utilization via better membrane electrode assembly and GDE design should be investigated, with the main findings highlighted in the following sections.

4.2.1 PA Diffusion in the Electrode

The viscous acid slowly diffuses from the membrane to the catalyst layer to form triple-phase boundaries over the first 50–100 h, or activation period. After the activation, the performance usually stabilizes with a reduction and stabilization of the ohmic resistance [36, 215, 222, 224, 269–272]. Furthermore, more catalytic sites may become available in the electrodes during the activation period, as excess acid may evaporate/leach out [273]. As activation occurs under load (0.1–0.2 A cm^{-2}), faster activation procedures should be investigated to assess the catalytic activity before poisoning/degradation/corrosion occurs. While lowering the catalyst layer hydrophobicity activates the cell faster (low PTFE content/introduction of wetting agents) by enhancing PA diffusion, long-term durability studies are necessary, as this may accelerate acid leaching and reduce the number of triple-phase boundaries [260]. As these two challenges are inherently linked, they have been addressed simultaneously in the literature. Most studies use a viscous acid as the proton conductor. This can cause challenges in the establishment of triple-phase boundaries between the electrode, gas, and viscous electrolyte, as the gas diffusivity in viscous PA is low [274, 275]. Therefore, in this configuration, most triple-phase boundaries form when active sites are in close contact with the free-flowing viscous electrolyte. However, further electrode coverage/flooding will be detrimental to the electrochemical reactions, as gas diffusion limitations will occur. This has been partially mitigated via the addition of additives to the viscous acid to improve the oxygen permeability by increasing its solubility or diffusivity, as

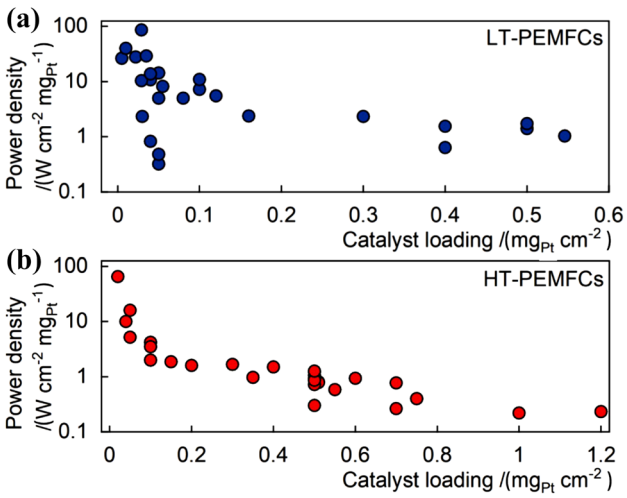

Fig. 19 Influence of the PGM catalyst loading on the performance of **a** LT-PEMFCs [264] and **b** HT-PEMFCs [265–268]

reviewed by Myles [276]. Localized PA accumulation within the catalyst layer pores can cause gas diffusion limitations by hindering gas diffusion to the active sites. This effect has been modeled by Kazdal, describing electrochemically active and inactive active sites depending on their PA coverage. To summarize, only partially covered particles create triple-phase boundaries, while fully immersed particles face gas diffusion limitations and may be inactive [277]. Furthermore, the pore size needs to be accurately controlled within both the catalyst and catalyst layers, as active sites within submicron-sized pores may not be reached by the viscous acid within the catalyst layer [224]. These challenges are summarized in Fig. 20a, highlighting viscous acid emerging from the membrane, diffusing through the catalyst layer, and eventually leaching through the MPL.

Hydrophobic binders: acid flooding issues have been mitigated via introduction of hydrophobic binders such as polyvinylidene fluoride (PVDF) and polytetrafluoroethylene (PTFE) and accurate control of the pore sizes within the catalyst layer (Fig. 20b) [254, 260, 275, 278–281]. A more uniform binder distribution using hydrophilic surfactants and a well-controlled ink sintering process (temperature, duration) is crucial, as binder clustering creates hydrophobic cavities with reduced PA content, reducing the active site utilization in these areas [267, 280, 282–288]. Innovative approaches have been proposed to improve the triple-phase boundary quality throughout the electrode, from relatively crude approaches (hydrophobicity gradients) to more complex approaches (in situ combination of hydrophobicity and electron/proton conductivity). A gradual increase in the hydrophobic binder content (deposition of a catalyst ink with increasing hydrophobicity) from the MPL to the membrane surface improves the electronic conductivity and acid diffusion while increasing the catalyst utilization and alleviating mass transfer issues [289–292]. More complex approaches involve (i) depositing hydrophobic NPs on carbon black to locally combine electronic conductivity with hydrophobicity, (ii) functionalizing hydrophobic nanospheres (200 nm PVDF) for interaction with PA and conduction of protons, and (iii) increasing the Pt hydrophobicity using pulse deposition [293–295].

Proton-conducting fillers: proton-conducting ionomers/metal fillers have been introduced into the catalyst layer to stabilize the electrolyte in solid form and create a better electrode/gas/solid electrolyte triple-phase boundary [88, 296–300]. A PBI dispersion was added to the catalyst ink to create a solid, acid-saturated and proton-conducting ionomer with easy binding and proton transfer between the acid-doped PBI membrane and the catalyst layer (Fig. Figure 20c) [218, 225, 278, 301]. The PBI content impacts the quality of the triple-phase boundary within the catalyst layer. Specifically, high PBI contents reduce the electrocatalytic activity and worsen gas diffusion by covering the catalyst particle, leading to increased oxygen diffusion resistance. In contrast, low PBI contents increase the ohmic resistance and reduce the electrocatalytic activity by reducing the proton pathways to the active sites [302, 303]. PBI swelling during PA doping (up to 200%) can block active site accessibility by causing mass transport limitations, which can be mitigated by the introduction of an inorganic filler (TiO_2) [300]. Conductive polymer binders composed of phosphate groups with methyl phosphonic acid (PPO-MPA)/6-oxohexyl phosphonic acid (PPO-HPA) have been introduced to HT-PEMFC catalyst layers. PA has been replaced with polymeric acids such as poly(vinylphosphonic acid) (PVPA) in the catalyst layer and the membrane, as this compound easily binds to PBI via acid–base reactions and provides impressive performance and durability [304]. Quaternary ammonium (QA) bisphosphate has been used as a solid polymer electrolyte within electrodes [94]. Other fillers have been introduced to create proton-conducting pathways through phosphate formation. Proton-conducting fillers using $CsHSO_4$, metal pyrophosphates such as zirconium hydrogen phosphate $Zr(HPO_4)_2$, Al_2O_3 to form aluminum triphosphate and lanthanum phosphate have been incorporated into the catalyst layer (Fig. 20d) [296–300]. ZrO_x and Ni(0) introduced into the PGM electrode interact with PA to create more active sites [305]. Carbon nanofiber (CNF) composites doped with Zr/Ni/Gd have been proposed to create phosphate metal species on which the electrode material (Pt) is then deposited [306]. These proton-conducting fillers improve the catalyst layer proton conductivity and hinder acid (PA) leaching. Similarly, covalent organic frameworks (COFs) have high PA retention capability and good proton transfer ability [307]. Overall, approaches combining all the improvements achieved in the literature should be explored to optimize the triple-phase boundary (Fig. 20e), while accurate pore control can improve gas diffusion.

Binderless catalyst layer: interestingly, acceptable performance has been reported by using catalyst layers without any binder or filler, creating a PA interface between the membrane and catalyst layer using the capillary force within the catalyst layer [283, 295, 308, 309]. Promising durability was achieved at 0.2 A cm^{-2} in HT-PEMFCs [295], with 900 h stability at 0.2 A cm^{-2}, and the high loading used (0.96 mg_{Pt} cm^{-2}) may have created a barrier to PA leaching. This method was further refined, achieving impressive performance over 3,000 h at 0.2 A cm^{-2}, with a performance loss of 4% and a voltage decay of 5 μV h^{-1} in the last 1 500 h. This study used 0.1 mg_{Pt} cm^{-2} loading via electrospraying, which created a uniform catalyst layer with low porosity [309]. Therefore, within binderless electrodes, a triple-phase boundary in the catalyst layer can be established by acid transfer from the acid-doped membrane to the electrodes and can therefore be tailored by using catalysts with varied Pt/C, achieving impressive performance with low-loading

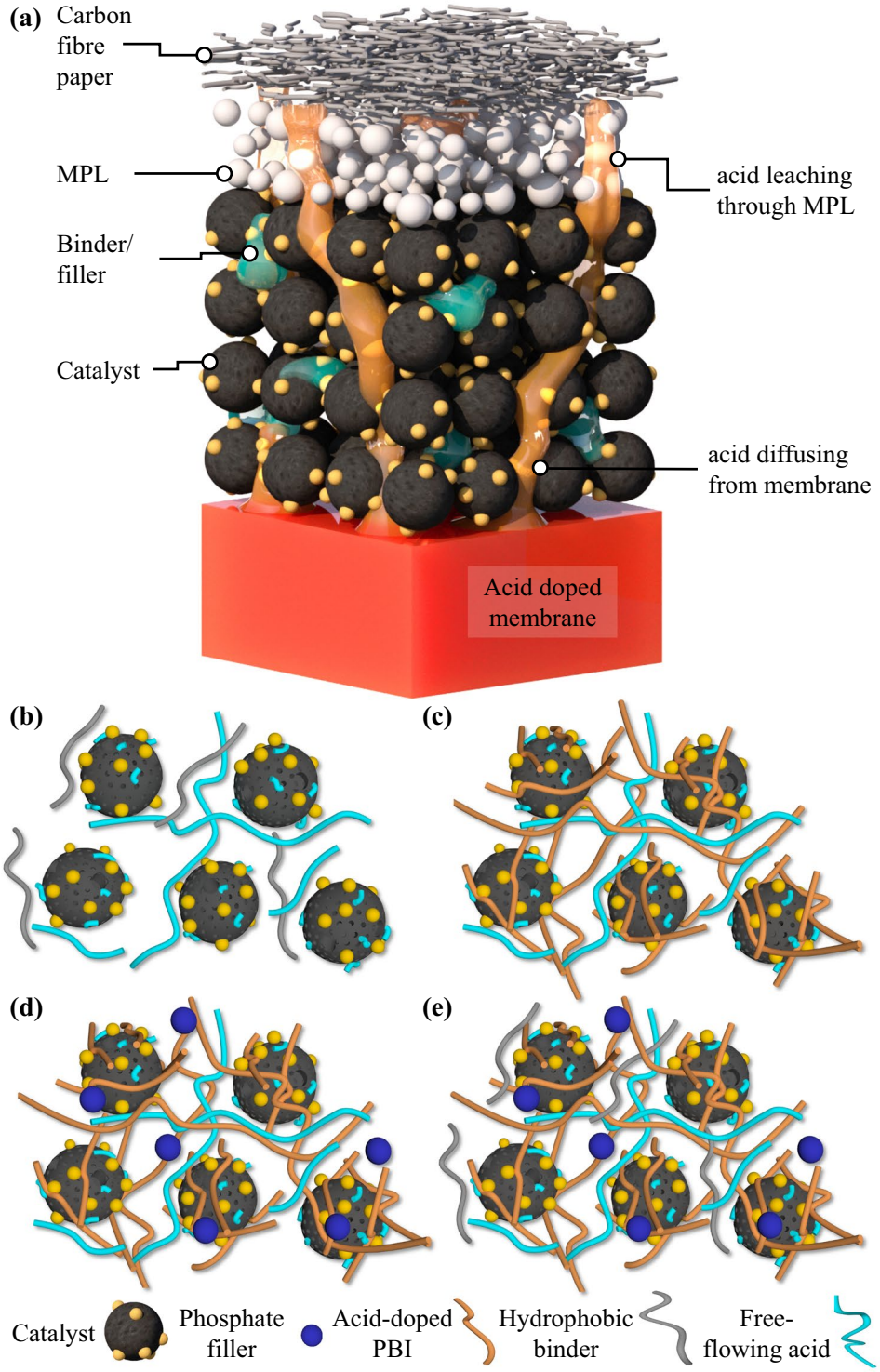

Fig. 20 **a** Schematic of the HT-PEMFC electrode with the viscous acid diffusing and leaching from the acid-doped membrane. **b** to **e** Catalyst ink binder and filler. **b** Hydrophobic binder and free-flowing acid. **c** Acid-doped PBI and free-flowing acid. **d** Phosphate filler, PBI and free-flowing acid. **e** Combination of the binder and filler from (**b**) to (**d**). The relative sizes and distances are not to scale, and the catalyst layer, binder, filler, MPL, and GDL possess significantly different porosities and sizes

cathodes (0.095 mg_{Pt} cm^{-2}) in HT-PEMFCs [310]. Therefore, this promising approach should be investigated in more detail by the research community at lower loadings.

4.2.2 Hindering Acid Leaching

Even with the addition of hydrophobic binders, polymer ionomers, and phosphate fillers, a portion of free-flowing liquid acid remains within the membrane electrode assembly, which cannot be contained/stabilized. Its leaching from

the catalyst layer will eventually reduce the number of triple-phase boundaries and reduce the HT-PEMFC performance and durability. Physically containing this acid within the catalyst layer by reducing both the catalyst layer and MPL porosities and the MPL hydrophobicity has been proposed.

Catalyst layer: aside from the efforts summarized previously regarding PA stabilization within the catalyst layer, other studies have focused on suppressing the formation of macropores within the catalyst layer, as these lead to acid build-up and breakthrough from the catalyst layer. As investigated by Halter, build-up of pressure with the catalyst layer pores and cracks as low as 40 mbar (1 bar = 1×10^5 Pa) is sufficient for PA breakthrough from the membrane to the flow fields [311]. This was achieved by blending CNTs into the ink and using advanced deposition techniques, such as ultrasonic spraying, to achieve uniform deposition [312–314]. However, excessive reduction in the catalyst layer porosity would reduce the active site utilization by hindering PA diffusion into the depths of the catalyst layer.

MPL: the MPL (the top layer of the GDL, deposited on the carbon fibers) is composed of densely packed carbon black NPs with a hydrophobic binder. While MPLs with wide cracks enhance water management in LT-PEMFCs, these are unsuitable for HT-PEMFCs because they accelerate acid leaching [315, 316]. In contrast, highly hydrophobic, crack-free MPLs with coarse graphitized carbon particles function as a barrier to PA and are widely used for HT-PEMFCs [252, 317–319]. Replacing the carbon black NPs of the MPL with materials better suited for the harsh PA environment has been explored [287, 320–322]. For instance, carbon nanospheres are resistant to carbon corrosion in the PA environment and increase the thermal and electrochemical stability [287, 320]. Silicon carbide has higher electrochemical and thermal resistance than carbon black, but as its conductivity is lower, it may not be the best candidate [321]. Finally, reticulated polyaniline nanowires, with a fine porous structure and densely packed carbon NPs, improved the performance by 36% by enhancing oxygen diffusion and reducing the resistance [322]. Altogether, improvement in the catalyst layer and GDEs is necessary to sustain sufficient triple-phase boundaries and avoid acid flooding and leaching.

4.2.3 Operando Monitoring of the Acid Distribution

While designing HT-PEMFCs with optimal acid distribution is a challenge, this is worsened by the difficulty in monitoring acid diffusion in real devices. The performance after a long-term stability test (polarization, electrochemical impedance spectroscopy (EIS)) is typically used to evaluate the long-term stability of the new catalyst layer configuration toward enhancing acid diffusion and hindering acid leaching [296–300]. However, performance losses could be caused by catalyst degradation at elevated temperatures [323]. Therefore, while valuable knowledge is obtained using electrochemical techniques, more localized techniques are necessary to elucidate the electrolyte distribution within the electrode. While operando monitoring of LT-PEMFCs has been extensively studied, it has remained somewhat limited for HT-PEMFCs [12]. A few studies have investigated acid doping, diffusion, and leaching in situ and operando, with the main findings summarized below.

Monitoring the acid content in the membrane and electrode: the PA content within the PBI membrane is typically determined by titration or weighing, but these methods lack spatial resolution. Confocal Raman microscopy can evaluate the microscale PA distribution within a PA-doped PBI membrane using the 1572 and 1611 cm^{-1} peaks as an indicator of the interaction between the AB-PBI host and PA dopant within the membrane [253, 324]. However, PA redistribution occurs under load and is challenging to observe. To date, it has been captured by using a bespoke three-layered membrane embedded with microreference electrodes to measure the PA redistribution in a PBI-based membrane [325]. The transformation of PA into phosphorus acid has been observed by using scanning photoelectron microscopy (SPEM) by simultaneously probing the morphology, surface composition, and chemical state of the catalyst/electrolyte interface [326]. PA anion adsorption on the cathode has been captured by using operando X-ray absorption spectroscopy (XAS) [176]. Furthermore, neutron scattering can monitor the proton mobility within the electrode from atomic to mesoscopic length scales [327]. While these techniques supply valuable insights, more knowledge could be obtained from operando dynamics over time.

Acid diffusion and leaching in HT-PEMFCs: the acid distribution and leaching after operation for thousands of hours have been captured ex operando by using scanning electron microscopy with elemental mapping by identifying the phosphorus distribution [315]. Furthermore, Bevilacqua and Yezerska elucidated the role of the MPL in hindering PA diffusion and the collapse of the catalyst layer following hydrogen starvation using ex operando computed tomography [269, 328]. More advanced operando monitoring requires bespoke systems and new methodologies. For instance, Han detected PA leaching from fuel and oxidant exhausts via spectrophotometric analysis using a color reagent solution (such as molybdenum blue and ascorbic acid) [329]. While this method is insightful and could be broadly applicable for rapid evaluation and monitoring, it lacks localized information. Proton diffusion within operating HT-PEMFCs has been monitored by using quasielastic neutron scattering (QENS) [330]. Boillat and Lin successfully monitored the hydrogen and proton distribution within a large HT-PEMFC using neutron imaging [331, 332]. Furthermore, large heterogeneous current density and heat distributions

have been observed by using heat, voltage and current mapping in HT-PEMFCs, which could be attributed to uneven PA distributions over large areas [333, 334]. While acid leaching from bespoke microsized HT-PEMFCs has been observed by using X-ray computed tomography, large-scale information may need to be obtained as well [335, 336]. Lee and coworkers proposed a multipurpose sensor capable of locally monitoring the current density, temperature, pressure, voltage, and flow rate simultaneously for HT-PEMFCs and inserted it at different locations within individual cells (inlet and exhaust) and within stacks [337, 338]. Overall, these large-scale studies highlight that the design and assembly of the cell highly impact PA diffusion and highlight the necessity for further PA monitoring within HT-PEMFC cells and stacks [339].

5 Conclusions and Future Developments

Operating PEMFCs at elevated temperatures is particularly promising because it enables the use of less expensive and more readily available hydrogen fuels, such as reformate hydrogen, syngas, and methanol, faster ORR and HOR kinetics, easier heat and water management, and much higher tolerance for contaminants. The latest advances in PEMs have brought HT-PEMFCs into the spotlight. However, before HT-PEMFCs can truly become commercially viable, key challenges spanning from the HT-PEM to the catalysts, catalyst layer, and membrane electrode assembly properties need to be resolved, with the main findings and most promising research directions thoroughly reviewed here.

HT-PEMs: HT-PEMs with improved acid doping and retention capabilities and conductivities are essential for operations at higher temperature, current density, and gas stoichiometry, all of which demand a better understanding of polymer–acid interactions [340]. New membranes should be developed with high proton conductivity networks, with, for instance, ionic clusters on the membrane surface [341]. In addition, a trade-off may need to be reached between a membrane with intrinsically high proton conductivity and high doping and retention capabilities, as these drive different membrane synthesis approaches [342]. Recently developed cross-linked membranes synthesized based on poly(ethylene imine) (PEI) and poly(ether ketone cardo) should be explored further, as the abundant PEI amino groups provide superior PA absorption capability and conductivity for these membranes [343]. Promising new materials have also emerged that can perform within PEMFCs from − 20 to 200 °C using ultra-microporous Trager's base (TB)-based membranes or from 80 to 220 °C using QA-bisphosphate ion pairs. These breakthroughs not only open new avenues to operate PEMFCs from lower temperatures but also blur the line between LT- and HT-PEMFCs [98, 344]. Finally, to fully elucidate the HT-PEM performance and durability, long-term stability tests, along with accelerated stress tests, need to be extensively carried out [345]. Efforts to accurately monitor the changes in membrane properties during and after operation should be pursued by, for instance, continuously monitoring the acid leaching rate and membrane thickness loss [346–348].

PGM catalysts: PGM catalysts are currently the most broadly investigated and only commercially available catalysts for practical application in HT-PEMFCs. However, PGM catalysts suffer from severe PA poisoning and thermal instabilities in HT-PEMFCs. Efforts should be dedicated to using the proton carrier (PA) in HT-PEMFCs to aid the 4-proton-electron-coupled process by locally supplying protons rather than poisoning the active sites. Therefore, developing PA-promoted PGM catalysts by fine tuning both the PGM NP structures and the local environment at the nanometre scale around the NPs is of great significance. In addition, the high operating temperature and strongly acidic environment catalyze the degradation of carbon-supported PGM catalysts in HT-PEMFCs. To address these challenges in HT-PEMFCs, a combination of multiple strategies to improve the PA resistance and durability should be envisioned. Overall, the development of corrosion-resistant alloy particles and supports as well as spatial nanoconfinement and enhanced phosphate poisoning resistance will offer new opportunities to improve the performance and durability of PGM catalysts in HT-PEMFCs.

PGM-free catalysts: PGM-free catalysts are particularly attractive for replacing PGM catalysts in HT-PEMFCs. In HT-PEMFCs, PGM-free catalysts have increased ORR kinetics, are free of water flooding, and enable easier decomposition of hydrogen peroxide [31, 33, 174, 218]. In addition, PGM-free catalysts are phosphate resistant. Nevertheless, several bottlenecks remain for M–N–C single-atom catalysts in HT-PEMFCs. Strategies to reach a trade-off between the stability and active site density by reducing the thickness of the single-atom cathode catalyst layers without compromising the activity and stability and therefore enhancing the active site utilization are outlined from the findings of this review. To meet the activity and durability challenges of M-N_x single-atom catalysts for the ORR in HT-PEMFCs, novel concepts of designing high-density atomic centers with controlled configurations and coordination environments will bring about new single-atom catalysts with high intrinsic activity. Researchers should focus on single-layer or double-layer high-density bimetallic or multimetallic atomically dispersed catalysts on conductive and corrosion-resistant carbon supports to improve the intrinsic

activity and stability and increase the active site density and utilization in HT-PEMFCs.

Catalyst layer: beyond the inherent challenges of the catalyst, an efficient membrane electrode assembly in HT-PEMFCs requires a catalyst layer designed to achieve high utilization of the catalyst active sites, with an optimized structure to build efficient triple-phase boundaries and easy pathways for ion and reactant transport. In HT-PEMFCs, regarding the viscous acid, such as PA or protic ionic liquid, distribution critically influences the HT-PEMFC performance. An uneven distribution leads to PA poisoning and PA flooding, causing poor expression of catalytic sites, while an optimized distribution via in situ triple-phase boundary engineering can enhance the HT-PEMFC performance [178, 349]. Thus, optimizing the catalyst layer structures via innovative design and fabrication by controlling the local environment at the meso-, micro- and nanoscale and constructing pathways at the microscale to realize the full potential of the catalyst materials are of great significance [350]. Innovative techniques should be applied to monitor the electrode configurations and structures to understand the triple-phase boundaries. Altogether, a combination of hydrophobicity and high proton conductivity is necessary for high proton diffusivity and active site utilization within HT-PEMFC catalyst layers and for a highly efficient triple-phase boundary. Finally, while operando characterization of HT-PEMFCs has thus far received limited attention, this area needs to be continuously developed to further the understanding of the complex underlying processes [335]. Inspiration could be drawn from the extensive operando studies conducted on LT-PEMFCs while focusing on the unique HT-PEMFC environment to develop more PA monitoring methodologies [12, 335]. The authors anticipate that operando monitoring of HT-PEMFCs will help drive the development of new catalysts, catalyst layers, electrodes, and membranes and become as prevalent as it currently is for LT-PEMFCs [12]. The enhanced knowledge of the proton transport, catalyst/ionomer distribution, and oxygen transfer will further drive the fabrication of novel electrodes with dedicated channels for proton, gas, and vapor water transport in HT-PEMFCs. For instance, electrodes composed solely of electrospun CNF structures with catalytic sites, acting as both the GDL and catalyst layer, have reached impressive performance and outstanding durability (130 to 1,400 h). Overall, the next breakthrough in HT-PEMFCs will be driven by the combination of advanced operando monitoring techniques with innovative catalysts and catalyst layers [4, 305, 318].

HT-PEMFCs beyond 200 °C: while most studies have focused on increasing the operating temperature of PEMFCs from 80 °C to 120–200 °C, operating PEMFCs above 200 °C will be in principle even more attractive, as it allows utilization of in situ reformed hydrogen without cooling, significantly increased carbon monoxide tolerance, and even faster electrode kinetics. A handful of pioneering studies have ventured into this new direction, facing new challenges. While outstanding PEMFC performance has been reached at 240 °C using poly(2,3,5,6-tetrafluorostyrene-4-phosphonic acid) membranes with a peak power density approaching 1.8 W cm^{-2} at 240 °C, their durability is far from satisfactory (10–20 h) [95]. In contrast, new PA/PBI/SiO_2 membranes from Cheng's group using a phosphate silicate proton conductor operate between 200 and 250 °C for hundreds of hours with a high carbon monoxide content (10%) and achieve 0.237 W cm^{-2} at 260 °C in HT-PEMFCs. Considering these outstanding developments, efforts to improve the membrane, catalyst, and catalyst layer need to occur in unison to fulfilling the full potential of PEMFCs at even higher temperatures.

Acknowledgements C. Zhao thanks the Australian Research Council (LP200100255, DP229103294, IC200100023). Y. Cheng thanks the National Natural Science Foundation of China (U19A2017 and 22272206) and Natural Science Foundation of Hunan Province (S2021JJMSXM3153). Q. Meyer acknowledges T. Budd for the preparation of Fig. 20 and K. Dastafkan and K. Ching for proofreading the manuscript.

Funding Open Access funding enabled and organized by CAUL and its Member Institutions.

References

1. Meinshausen, M., Meinshausen, N., Hare, W., et al.: Greenhouse-gas emission targets for limiting global warming to 2 °C. Nature **458**, 1158–1162 (2009). https://doi.org/10.1038/nature08017
2. Barbir, F. (ed.): PEM fuel cells: theory and practice. Academic Press, Burlington, MA (2005)
3. Cano, Z.P., Banham, D., Ye, S.Y., et al.: Batteries and fuel cells for emerging electric vehicle markets. Nat. Energy **3**, 279–289 (2018). https://doi.org/10.1038/s41560-018-0108-1
4. Jiao, K., Xuan, J., Du, Q., et al.: Designing the next generation of proton-exchange membrane fuel cells. Nature **595**, 361–369 (2021). https://doi.org/10.1038/s41586-021-03482-7
5. Ramaswamy, N., Mukerjee, S.: Alkaline anion-exchange membrane fuel cells: challenges in electrocatalysis and interfacial charge transfer. Chem. Rev. **119**, 11945–11979 (2019). https://doi.org/10.1021/acs.chemrev.9b00157
6. Boldrin, P., Brandon, N.P.: Progress and outlook for solid oxide fuel cells for transportation applications. Nat. Catal. **2**, 571–577 (2019). https://doi.org/10.1038/s41929-019-0310-y

7. Hoogers, G.: Fuel cell technology handbook. CRC Press, Boca Raton (2002). https://doi.org/10.1201/9781420041552
8. Stamenkovic, V.R., Strmcnik, D., Lopes, P.P., et al.: Energy and fuels from electrochemical interfaces. Nat. Mater. **16**, 57–69 (2016). https://doi.org/10.1038/nmat4738
9. E4tech: The fuel cell industry review 2021. (2021). https://fuelcellindustryreview.com/
10. Ajanovic, A., Haas, R.: Economic and environmental prospects for battery electric- and fuel cell vehicles: a review. Fuel Cells **19**, 515–529 (2019). https://doi.org/10.1002/fuce.201800171
11. Wu, D., Peng, C., Yin, C., et al.: Review of system integration and control of proton exchange membrane fuel cells. Electrochem. Energy Rev. **3**, 466–505 (2020). https://doi.org/10.1007/s41918-020-00068-1
12. Meyer, Q., Zeng, Y., Zhao, C.: In situ and operando characterization of proton exchange membrane fuel cells. Adv. Mater. **31**, e1901900 (2019). https://doi.org/10.1002/adma.201901900
13. Staffell, I., Scamman, D., Velazquez Abad, A., et al.: The role of hydrogen and fuel cells in the global energy system. Energy Environ. Sci. **12**, 463–491 (2019). https://doi.org/10.1039/c8ee01157e
14. Kayfeci, M., Keçebaş, A., Bayat, M.: Hydrogen Production. Academic Press, Cambridge, MA (2019)
15. Bristowe, G., Smallbone, A.: The key techno-economic and manufacturing drivers for reducing the cost of power-to-gas and a hydrogen-enabled energy system. Hydrogen **2**, 273–300 (2021). https://doi.org/10.3390/hydrogen2030015
16. Wanniarachchi, S., Hewage, K., Wirasinghe, C., et al.: Transforming road freight transportation from fossils to hydrogen: opportunities and challenges. Int. J. Sustain. Transp. (2022). https://doi.org/10.1080/15568318.2022.2068389
17. Wang, Y., Pang, Y.H., Xu, H., et al.: PEM Fuel cell and electrolysis cell technologies and hydrogen infrastructure development–a review. Energy Environ. Sci. **15**, 2288–2328 (2022). https://doi.org/10.1039/d2ee00790h
18. Jiao, K., Alaefour, I.E., Li, X.: Three-dimensional non-isothermal modeling of carbon monoxide poisoning in high temperature proton exchange membrane fuel cells with phosphoric acid doped polybenzimidazole membranes. Fuel **90**, 568–582 (2011). https://doi.org/10.1016/j.fuel.2010.10.018
19. Lopes, P.P., Freitas, K.S., Ticianelli, E.A.: CO tolerance of PEMFC anodes: mechanisms and electrode designs. Electrocatalysis **1**, 200–212 (2010). https://doi.org/10.1007/s12678-010-0025-y
20. Nachiappan, N., Kalaignan, G.P., Sasikumar, G.: Influence of methanol impurity in hydrogen on PEMFC performance. Ionics **19**, 517–522 (2013). https://doi.org/10.1007/s11581-012-0770-4
21. Simon Araya, S., Liso, V., Cui, X.T., et al.: A review of the methanol economy: the fuel cell route. Energies **13**, 596 (2020). https://doi.org/10.3390/en13030596
22. Profatilova, I., Jacques, P.A., Escribano, S.: Evaluation of parameters accelerating the aging of PEMFCs operating under reformate containing carbon monoxide. J. Electrochem. Soc. **165**, F3251–F3260 (2018). https://doi.org/10.1149/2.0281806jes
23. Dias, V., Pochet, M., Contino, F., et al.: Energy and economic costs of chemical storage. Front. Mech. Eng. **6**, 21 (2020). https://doi.org/10.3389/fmech.2020.00021
24. Authayanun, S., Im-Orb, K., Arpornwichanop, A.: A review of the development of high temperature proton exchange membrane fuel cells. Chin. J. Catal. **36**, 473–483 (2015). https://doi.org/10.1016/S1872-2067(14)60272-2
25. Reshetenko, T.V., Bethune, K., Rubio, M.A., et al.: Study of low concentration CO poisoning of Pt anode in a proton exchange membrane fuel cell using spatial electrochemical impedance spectroscopy. J. Power Sour. **269**, 344–362 (2014). https://doi.org/10.1016/j.jpowsour.2014.06.146
26. St-Pierre, J.: PEMFC contaminant tolerance limit-CO in H_2. Electrochim. Acta **55**, 4208–4211 (2010). https://doi.org/10.1016/j.electacta.2010.02.061
27. Wang, Y.C., Wu, Q., Mei, D., et al.: Development of highly efficient methanol steam reforming system for hydrogen production and supply for a low temperature proton exchange membrane fuel cell. Int. J. Hydrog. Energy **45**, 25317–25327 (2020). https://doi.org/10.1016/j.ijhydene.2020.06.285
28. Subianto, S.: Recent advances in polybenzimidazole/phosphoric acid membranes for high-temperature fuel cells. Polym. Int. **63**, 1134–1144 (2014). https://doi.org/10.1002/pi.4708
29. Chandan, A., Hattenberger, M., El-Kharouf, A., et al.: High temperature (HT) polymer electrolyte membrane fuel cells (PEMFC): a review. J. Power Sour. **231**, 264–278 (2013). https://doi.org/10.1016/j.jpowsour.2012.11.126
30. Shabani, B., Hafttananian, M., Khamani, S., et al.: Poisoning of proton exchange membrane fuel cells by contaminants and impurities: review of mechanisms, effects, and mitigation strategies. J. Power Sour. **427**, 21–48 (2019). https://doi.org/10.1016/j.jpowsour.2019.03.097
31. Lin, C.C., Smith, F.R., Ichikawa, N., et al.: Decomposition of hydrogen peroxide in aqueous solutions at elevated temperatures. Int. J. Chem. Kinet. **23**, 971–987 (1991). https://doi.org/10.1002/kin.550231103
32. Oono, Y., Fukuda, T., Sounai, A., et al.: Influence of operating temperature on cell performance and endurance of high temperature proton exchange membrane fuel cells. J. Power Sour. **195**, 1007–1014 (2010). https://doi.org/10.1016/j.jpowsour.2009.08.097
33. Tse, E.C.M., Gewirth, A.A.: Effect of temperature and pressure on the kinetics of the oxygen reduction reaction. J. Phys. Chem. A **119**, 1246–1255 (2015). https://doi.org/10.1021/acs.jpca.5b00572
34. Zhang, J., Aili, D., Lu, S., et al.: Advancement toward polymer electrolyte membrane fuel cells at elevated temperatures. Research **2020**, 9089405 (2020). https://doi.org/10.34133/2020/9089405
35. Belgacem, N., Pauchet, J., Prat, M.: On the current distribution at the channel-rib scale in polymer-electrolyte fuel cells. Int. J. Hydrog. Energy **43**, 5112–5123 (2018). https://doi.org/10.1016/j.ijhydene.2018.01.097
36. Araya, S.S., Zhou, F., Liso, V., et al.: A comprehensive review of PBI-based high temperature PEM fuel cells. Int. J. Hydrog. Energy **41**, 21310–21344 (2016). https://doi.org/10.1016/j.ijhydene.2016.09.024
37. Haider, R., Wen, Y., Ma, Z.F., et al.: High temperature proton exchange membrane fuel cells: progress in advanced materials and key technologies. Chem. Soc. Rev. **50**, 1138–1187 (2021). https://doi.org/10.1039/d0cs00296h
38. Aili, D., Henkensmeier, D., Martin, S., et al.: Polybenzimidazole-based high-temperature polymer electrolyte membrane fuel cells: new insights and recent progress. Electrochem. Energy Rev. **3**, 793–845 (2020). https://doi.org/10.1007/s41918-020-00080-5
39. Li, G.Q., Kujawski, W., Rynkowska, E.: Advancements in proton exchange membranes for high-performance high-temperature proton exchange membrane fuel cells (HT-PEMFC). Rev. Chem. Eng. **38**, 327–346 (2022). https://doi.org/10.1515/revce-2019-0079
40. Liu, G.: Progress of high temperature polybenzimidazole proton exchange membrane: a systematic review. J. Phys. Conf. Ser. **2076**, 012032 (2021). https://doi.org/10.1088/1742-6596/2076/1/012032
41. Zhang, J., Xiang, Y., Lu, S.F., et al.: High temperature polymer electrolyte membrane fuel cells for integrated fuel cell–methanol

reformer power systems: a critical review. Adv. Sustain. Syst. **2**, 1700184 (2018). https://doi.org/10.1002/adsu.201700184
42. Qu, E.L., Hao, X., Xiao, M., et al.: Proton exchange membranes for high temperature proton exchange membrane fuel cells: challenges and perspectives. J. Power Sour. **533**, 231386 (2022). https://doi.org/10.1016/j.jpowsour.2022.231386
43. Khoo, K.S., Chia, W.Y., Wang, K., et al.: Development of proton-exchange membrane fuel cell with ionic liquid technology. Sci. Total. Environ. **793**, 148705 (2021). https://doi.org/10.1016/j.scitotenv.2021.148705
44. Ebrahimi, M., Kujawski, W., Fatyeyeva, K., et al.: A review on ionic liquids-based membranes for middle and high temperature polymer electrolyte membrane fuel cells (PEM FCs). Int. J. Mol. Sci. **22**, 5430 (2021). https://doi.org/10.3390/ijms22115430
45. Jothi, P.R., Dharmalingam, S.: An efficient proton conducting electrolyte membrane for high temperature fuel cell in aqueous-free medium. J. Membr. Sci. **450**, 389–396 (2014). https://doi.org/10.1016/j.memsci.2013.09.034
46. Rajabalizadeh Mojarrad, N., Sadeghi, S., Yarar Kaplan, B., et al.: Metal-salt enhanced grafting of vinylpyridine and vinylimidazole monomer combinations in radiation grafted membranes for high-temperature PEM fuel cells. ACS Appl. Energy Mater. **3**, 532–540 (2020). https://doi.org/10.1021/acsaem.9b01777
47. Sanlı, L.I., Tas, S., Yürüm, Y., et al.: Water free operated phosphoric acid doped radiation-grafted proton conducting membranes for high temperature polymer electrolyte membrane fuel cells. Fuel Cells **14**, 914–925 (2014). https://doi.org/10.1002/fuce.201300110
48. Saidi, H., Uthman, H.: Phosphoric acid doped polymer electrolyte membrane based on radiation grafted poly(1-vinylimidazole-co-1-vinyl-2-pyrrolidone)-g-poly(ethylene/tetrafluoroethylene) copolymer and investigation of grafting kinetics. Int. J. Hydrog. Energy **42**, 9315–9332 (2017). https://doi.org/10.1016/j.ijhydene.2016.06.187
49. Haile, S.M., Boysen, D.A., Chisholm, C.R.I., et al.: Solid acids as fuel cell electrolytes. Nature **410**, 910–913 (2001). https://doi.org/10.1038/35073536
50. Boysen, D.A., Uda, T., Chisholm, C.R., et al.: High-performance solid Acid fuel cells through humidity stabilization. Science **303**, 68–70 (2004). https://doi.org/10.1126/science.1090920
51. Jin, Y., Shen, Y., Hibino, T.: Proton conduction in metal pyrophosphates (MP_2O_7) at intermediate temperatures. J. Mater. Chem. **20**, 6214–6217 (2010). https://doi.org/10.1039/b924188d
52. Beck, N.K., de Jonghe, L.C.: Proton conduction in SnP_2O_7-LaP_3O_9 composite electrolytes. Electrochem. Solid-State Lett. **12**, B11 (2009). https://doi.org/10.1149/1.3039093
53. Jin, Y.C., Fujiwara, K., Hibino, T.: High temperature, low humidity proton exchange membrane based on an inorganic–organic hybrid structure. Electrochem. Solid-State Lett. **13**, B8 (2010). https://doi.org/10.1149/1.3267848
54. Singh, B., Devi, N., Srivastava, A.K., et al.: High temperature polymer electrolyte membrane fuel cells with polybenzimidazole-$Ce_{0.9}Gd_{0.1}P_2O_7$ and polybenzimidazole-$Ce_{0.9}Gd_{0.1}P_2O_7$-graphite oxide composite electrolytes. J. Power Sour. **401**, 149–157 (2018). https://doi.org/10.1016/j.jpowsour.2018.08.076
55. Yasuda, T., Watanabe, M.: Protic ionic liquids: fuel cell applications. MRS Bull. **38**, 560–566 (2013). https://doi.org/10.1557/mrs.2013.153
56. Paul, T., Banerjee, D., Kargupta, K.: Conductivity of phosphoric acid: an in situ comparative study of proton in phosphoric acid fuel cell. Ionics **21**, 2583–2590 (2015). https://doi.org/10.1007/s11581-015-1426-y
57. Ma, Y.L., Wainright, J.S., Litt, M.H., et al.: Conductivity of PBI membranes for high-temperature polymer electrolyte fuel cells. J. Electrochem. Soc. **151**, A8 (2004). https://doi.org/10.1149/1.1630037
58. Krishnan, N.N., Lee, S., Ghorpade, R.V., et al.: Polybenzimidazole (PBI-OO) based composite membranes using sulfophenylated TiO_2 as both filler and crosslinker, and their use in the HT-PEM fuel cell. J. Membr. Sci. **560**, 11–20 (2018). https://doi.org/10.1016/j.memsci.2018.05.006
59. Hink, S., Elsøe, K., Cleemann, L.N., et al.: Phosphoric acid doped polysulfone membranes with aminopyridine pendant groups and imidazole cross-links. Eur. Polym. J. **72**, 102–113 (2015). https://doi.org/10.1016/j.eurpolymj.2015.08.026
60. Singh, B., Duong, N.M.H., Henkensmeier, D., et al.: Influence of different side-groups and cross-links on phosphoric acid doped radel-based polysulfone membranes for high temperature polymer electrolyte fuel cells. Electrochim. Acta **224**, 306–313 (2017). https://doi.org/10.1016/j.electacta.2016.12.088
61. Li, Y., Zhang, J., Yang, H., et al.: Boosting the performance of an anion exchange membrane by the formation of well-connected ion conducting channels. Polym. Chem. **10**, 2822–2831 (2019). https://doi.org/10.1039/c9py00011a
62. Jiang, S.P.: Functionalized mesoporous structured inorganic materials as high temperature proton exchange membranes for fuel cells. J. Mater. Chem. A **2**, 7637–7655 (2014). https://doi.org/10.1039/c4ta00121d
63. Bozkurt, A., Meyer, W.H.: Proton-conducting poly(vinylpyrrolidon)-polyphosphoric acid blends. J. Polym. Sci. B Polym. Phys. **39**, 1987–1994 (2001). https://doi.org/10.1002/polb.1174
64. Lu, S.F., Xiu, R., Xu, X., et al.: Polytetrafluoroethylene (PTFE) reinforced poly(ethersulphone)-poly(vinyl pyrrolidone) composite membrane for high temperature proton exchange membrane fuel cells. J. Membr. Sci. **464**, 1–7 (2014). https://doi.org/10.1016/j.memsci.2014.03.053
65. Vogel, H., Marvel, C.S.: Polybenzimidazoles, new thermally stable polymers. J. Polym. Sci. **50**, 511–539 (1961). https://doi.org/10.1002/pol.1961.1205015419
66. Li, Q.F., Jensen, J.O., Savinell, R.F., et al.: High temperature proton exchange membranes based on polybenzimidazoles for fuel cells. Prog. Polym. Sci. **34**, 449–477 (2009). https://doi.org/10.1016/j.progpolymsci.2008.12.003
67. Asensio, J.A., Sánchez, E.M., Gómez-Romero, P.: Proton-conducting membranes based on benzimidazole polymers for high-temperature PEM fuel cells. A chemical quest. Chem. Soc. Rev. **39**, 3210–3239 (2010). https://doi.org/10.1039/b922650h
68. Pingitore, A.T., Huang, F., Qian, G.Q., et al.: Durable high polymer content *m/p*-polybenzimidazole membranes for extended lifetime electrochemical devices. ACS Appl. Energy Mater. **2**, 1720–1726 (2019). https://doi.org/10.1021/acsaem.8b01820
69. He, R., Li, Q., Bach, A., et al.: Physicochemical properties of phosphoric acid doped polybenzimidazole membranes for fuel cells. J. Membr. Sci. **277**, 38–45 (2006). https://doi.org/10.1016/j.memsci.2005.10.005
70. Xiao, L., Zhang, H., Scanlon, E., et al.: High-temperature polybenzimidazole fuel cell membranes via a sol-gel process. Chem. Mater. **17**, 5328–5333 (2005). https://doi.org/10.1021/cm050831
71. Lobato, J., Cañizares, P., Rodrigo, M.A., et al.: Improved polybenzimidazole films for H_3PO_4-doped PBI-based high temperature PEMFC. J. Membr. Sci. **306**, 47–55 (2007). https://doi.org/10.1016/j.memsci.2007.08.028
72. Tahrim, A.A., Amin, I.N.H.M.: Advancement in phosphoric acid doped polybenzimidazole membrane for high temperature PEM fuel cells: a review. J. Adv. Manuf. Sci. Technol. **23**, 37–62 (2018). https://doi.org/10.11113/amst.v23n1.136
73. Joseph, D., Krishnan, N.N., Henkensmeier, D., et al.: Thermal crosslinking of PBI/sulfonated polysulfone based blend membranes. J. Mater. Chem. A **5**, 409–417 (2017). https://doi.org/10.1039/c6ta07653j

74. Li, Q., Jensen, J.O., Pan, C., et al.: Partially fluorinated aarylene polyethers and their ternary blends with PBI and H_3PO_4. Part II. Characterisation and fuel cell tests of the ternary membranes. Fuel Cells **8**, 188–199 (2008). https://doi.org/10.1002/fuce.200800007
75. Xiao, L., Zhang, H., Jana, T., et al.: Synthesis and characterization of pyridine-based polybenzimidazoles for high temperature polymer electrolyte membrane fuel cell applications. Fuel Cells **5**, 287–295 (2005). https://doi.org/10.1002/fuce.200400067
76. Jin, Y.P., Wang, T., Che, X., et al.: Poly(arylene pyridine)s: new alternative materials for high temperature polymer electrolyte fuel cells. J. Power Sour. **526**, 231131 (2022). https://doi.org/10.1016/j.jpowsour.2022.231131
77. Gourdoupi, N., Andreopoulou, A., Deimede, V., et al.: Novel proton-conducting polyelectrolyte composed of an aromatic polyether containing main-chain pyridine units for fuel cell applications. Chem. Mater. **15**, 5044–5050 (2003). https://doi.org/10.1021/cm0347382
78. Georgezi, M., Chochos, C.L., Gourdoupi, N., et al.: High performance polymer electrolytes based on main and side chain pyridine aromatic polyethers for high and medium temperature proton exchange membrane fuel cells. J. Power Sour. **196**, 9382–9390 (2011). https://doi.org/10.1016/j.jpowsour.2011.06.031
79. Elumalai, V., Rathinavel, S., Annapooranan, R., et al.: Phosphonated mesoporous silica based composite membranes for high temperature proton exchange membrane fuel cells. J. Solid State Electrochem. **23**, 1837–1850 (2019). https://doi.org/10.1007/s10008-019-04290-w
80. Zhang, J., Chen, S., Bai, H., et al.: Effects of phosphotungstic acid on performance of phosphoric acid doped polyethersulfone-polyvinylpyrrolidone membranes for high temperature fuel cells. Int. J. Hydrog. Energy **46**, 11104–11114 (2021). https://doi.org/10.1016/j.ijhydene.2020.07.082
81. Üregen, N., Pehlivanoğlu, K., Özdemir, Y., et al.: Development of polybenzimidazole/graphene oxide composite membranes for high temperature PEM fuel cells. Int. J. Hydrog. Energy **42**, 2636–2647 (2017). https://doi.org/10.1016/j.ijhydene.2016.07.009
82. Daud, N.A.B., Abouzari Lotf, E., Sophia Sha'Rani, S., et al.: Efforts to improve PBI/acid membrane system for high temperature polymer electrolyte membrane fuel cell (HT-PEMFC). E3S Web Conf. **90**, 1002 (2019). https://doi.org/10.1051/e3sconf/20199001002
83. Ghosh, S., Maity, S., Jana, T.: Polybenzimidazole/silica nanocomposites: organic-inorganic hybrid membranes for PEM fuel cell. J. Mater. Chem. **21**, 14897 (2011). https://doi.org/10.1039/c1jm12169c
84. Rajabi, Z., Javanbakht, M., Hooshyari, K., et al.: High temperature composite membranes based on polybenzimidazole and dendrimer amine functionalized SBA-15 mesoporous silica for fuel cells. New J. Chem. **44**, 5001–5018 (2020). https://doi.org/10.1039/c9nj05369g
85. Seo, K., Nam, K.H., Han, H.: Proton transport in aluminum-substituted mesoporous silica channel-embedded high-temperature anhydrous proton-exchange membrane fuel cells. Sci. Rep. **10**, 10352 (2020). https://doi.org/10.1038/s41598-020-66935-5
86. Li, X., Ma, H., Wang, P., et al.: Construction of high-performance, high-temperature proton exchange membranes through incorporating SiO_2 nanoparticles into novel cross-linked polybenzimidazole networks. ACS Appl. Mater. Interfaces **11**, 30735–30746 (2019). https://doi.org/10.1021/acsami.9b06808
87. Zhou, Y., Yang, J., Su, H., et al.: Insight into proton transfer in phosphotungstic acid functionalized mesoporous silica-based proton exchange membrane fuel cells. J. Am. Chem. Soc. **136**, 4954–4964 (2014). https://doi.org/10.1021/ja411268q
88. Aili, D., Zhang, J., Dalsgaard Jakobsen, M.T., et al.: Exceptional durability enhancement of PA/PBI based polymer electrolyte membrane fuel cells for high temperature operation at 200 °C. J. Mater. Chem. A **4**, 4019–4024 (2016). https://doi.org/10.1039/c6ta01562j
89. Pinar, F.J., Cañizares, P., Rodrigo, M.A., et al.: Titanium composite PBI-based membranes for high temperature polymer electrolyte membrane fuel cells. Effect on titanium dioxide amount. RSC Adv. **2**, 1547–1556 (2012). https://doi.org/10.1039/c1ra01084k
90. Yang, J.Y., Li, X., Shi, C., et al.: Fabrication of PBI/SPOSS hybrid high-temperature proton exchange membranes using SPAEK as compatibilizer. J. Membr. Sci. **620**, 118855 (2021). https://doi.org/10.1016/j.memsci.2020.118855
91. Tian, X., Wang, S., Li, J., et al.: Composite membranes based on polybenzimidazole and ionic liquid functional Si–O–Si network for HT-PEMFC applications. Int. J. Hydrog. Energy **42**, 21913–21921 (2017). https://doi.org/10.1016/j.ijhydene.2017.07.071
92. Morfopoulou, C.I., Andreopoulou, A.K., Daletou, M.K., et al.: Cross-linked high temperature polymer electrolytes through oxadiazole bond formation and their applications in HT PEMfuel cells. J. Mater. Chem. A **1**, 1613–1622 (2013). https://doi.org/10.1039/c2ta00610c
93. Shen, Y.B., Nishida, M., Kanematsu, W., et al.: Synthesis and characterization of dense SnP_2O_7–SnO_2 composite ceramics as intermediate-temperature proton conductors. J. Mater. Chem. **21**, 663–670 (2011). https://doi.org/10.1039/c0jm02596h
94. Lee, K.S., Maurya, S., Kim, Y.S., et al.: Intermediate temperature fuel cells via an ion-pair coordinated polymer electrolyte. Energy Environ. Sci. **11**, 979–987 (2018). https://doi.org/10.1039/c7ee03595k
95. Atanasov, V., Lee, A.S., Park, E.J., et al.: Synergistically integrated phosphonated poly(pentafluorostyrene) for fuel cells. Nat. Mater. **20**, 370–377 (2021). https://doi.org/10.1038/s41563-020-00841-z
96. Atanasov, V., Oleynikov, A., Xia, J., et al.: Phosphonic acid functionalized poly(pentafluorostyrene) as polyelectrolyte membrane for fuel cell application. J. Power Sources **343**, 364–372 (2017). https://doi.org/10.1016/j.jpowsour.2017.01.085
97. Ramaiyan, K.P., Herrera, S., Workman, M.J., et al.: Role of phosphate source in improving the proton conductivity of tin pyrophosphate and its composite electrolytes. J. Mater. Chem. A **8**, 16345–16354 (2020). https://doi.org/10.1039/d0ta04327c
98. Lee, K.S., Spendelow, J.S., Choe, Y.K., et al.: An operationally flexible fuel cell based on quaternary ammonium-biphosphate ion pairs. Nat. Energy **1**, 16120 (2016). https://doi.org/10.1038/nenergy.2016.120
99. Cheng, Y., Zhang, J., Lu, S., et al.: Significantly enhanced performance of direct methanol fuel cells at elevated temperatures. J. Power Sour. **450**, 227620 (2020). https://doi.org/10.1016/j.jpowsour.2019.227620
100. Cheng, Y., Zhang, J., Lu, S., et al.: High CO tolerance of new SiO_2 doped phosphoric acid/polybenzimidazole polymer electrolyte membrane fuel cells at high temperatures of 200–250 °C. Int. J. Hydrog. Energy **43**, 22487–22499 (2018). https://doi.org/10.1016/j.ijhydene.2018.10.036
101. Scott, K., Xu, C.X., Wu, X.: Intermediate temperature proton-conducting membrane electrolytes for fuel cells. Wiley Interdiscip. Rev. Energy Environ. **3**, 24–41 (2014). https://doi.org/10.1002/wene.64
102. Molleo, M.A., Chen, X., Ploehn, H.J., et al.: High polymer content 3,5-pyridine-polybenzimidazole copolymer membranes with improved compressive properties. Fuel Cells **14**, 16–25 (2014). https://doi.org/10.1002/fuce.201300202

103. Maity, S., Singha, S., Jana, T.: Low acid leaching PEM for fuel cell based on polybenzimidazole nanocomposites with protic ionic liquid modified silica. Polymer **66**, 76–85 (2015). https://doi.org/10.1016/j.polymer.2015.03.040
104. Haque, M.A., Sulong, A.B., Loh, K.S., et al.: Acid doped polybenzimidazoles based membrane electrode assembly for high temperature proton exchange membrane fuel cell: a review. Int. J. Hydrog. Energy **42**, 9156–9179 (2017). https://doi.org/10.1016/j.ijhydene.2016.03.086
105. Li, M.Q., Scott, K.: A polymer electrolyte membrane for high temperature fuel cells to fit vehicle applications. Electrochim. Acta **55**, 2123–2128 (2010). https://doi.org/10.1016/j.electacta.2009.11.044
106. Li, X., Ma, H., Wang, P., et al.: Highly conductive and mechanically stable imidazole-rich cross-linked networks for high-temperature proton exchange membrane fuel cells. Chem. Mater. **32**, 1182–1191 (2020). https://doi.org/10.1021/acs.chemmater.9b04321
107. Zhang, H., Yang, D.J., Tao, K., et al.: Investigation of PEMFC stack operating at elevated temperature. World Electr. Veh. J. **4**, 481–486 (2010). https://doi.org/10.3390/wevj4030481
108. Nguyen, H., Lombeck, F., Schwarz, C., et al.: Hydrocarbon-based Pemion™ proton exchange membrane fuel cells with state-of-the-art performance. Sustain. Energy Fuels **5**, 3687–3699 (2021). https://doi.org/10.1039/d1se00556a
109. Gasteiger, H.A., Kocha, S.S., Sompalli, B., et al.: Activity benchmarks and requirements for Pt, Pt-alloy, and non-Pt oxygen reduction catalysts for PEMFCs. Appl. Catal. B Environ. **56**, 9–35 (2005). https://doi.org/10.1016/j.apcatb.2004.06.021
110. Liu, M., Zhao, Z., Duan, X., et al.: Nanoscale structure design for high-performance Pt-based ORR catalysts. Adv. Mater. **31**, e1802234 (2019). https://doi.org/10.1002/adma.201802234
111. Nesselberger, M., Ashton, S., Meier, J.C., et al.: The particle size effect on the oxygen reduction reaction activity of Pt catalysts: influence of electrolyte and relation to single crystal models. J. Am. Chem. Soc. **133**, 17428–17433 (2011). https://doi.org/10.1021/ja207016u
112. Kongkanand, A., Gu, W., Mathias, M.F.: Proton-exchange membrane fuel cells with low-Pt content. In: Lipman, T., Weber, A. (eds.) Fuel Cells and Hydrogen Production. Encyclopedia of Sustainability Science and Technology Series. Springer, New York, NY (2019). https://doi.org/10.1007/978-1-4939-7789-5_1022
113. Shao, M., Peles, A., Shoemaker, K.: Electrocatalysis on platinum nanoparticles: particle size effect on oxygen reduction reaction activity. Nano Lett **11**, 3714–3719 (2011). https://doi.org/10.1021/nl2017459
114. Imaoka, T., Kitazawa, H., Chun, W.J., et al.: Finding the most catalytically active platinum clusters with low atomicity. Angew. Chem. Int. Ed. **54**, 9810–9815 (2015). https://doi.org/10.1002/anie.201504473
115. Liu, J., Jiao, M.G., Lu, L.L., et al.: High performance platinum single atom electrocatalyst for oxygen reduction reaction. Nat. Commun. **8**, 15938 (2017). https://doi.org/10.1038/ncomms15938
116. Fang, S., Zhu, X.R., Liu, X.K., et al.: Uncovering near-free platinum single-atom dynamics during electrochemical hydrogen evolution reaction. Nat. Commun. **11**, 1029 (2020). https://doi.org/10.1038/s41467-020-14848-2
117. Mayrhofer, K.J.J., Arenz, M.: Log on for new catalysts. Nat. Chem. **1**, 518–519 (2009). https://doi.org/10.1038/nchem.380
118. Greeley, J., Stephens, I.E.L., Bondarenko, A.S., et al.: Alloys of platinum and early transition metals as oxygen reduction electrocatalysts. Nat. Chem. **1**, 552–556 (2009). https://doi.org/10.1038/nchem.367
119. Ren, X.F., Wang, Y.R., Liu, A.M., et al.: Current progress and performance improvement of Pt/C catalysts for fuel cells. J. Mater. Chem. A **8**, 24284–24306 (2020). https://doi.org/10.1039/d0ta08312g
120. Devrim, Y., Arıca, E.D.: Multi-walled carbon nanotubes decorated by platinum catalyst for high temperature PEM fuel cell. Int. J. Hydrog. Energy **44**, 18951–18966 (2019). https://doi.org/10.1016/j.ijhydene.2019.01.051
121. Yang, Z.H., Yu, X.X., Zhang, Y.F., et al.: Remarkably durable platinum cluster supported on multi-walled carbon nanotubes with high performance in an anhydrous polymer electrolyte fuel cell. RSC Adv. **6**, 108158–108163 (2016). https://doi.org/10.1039/c6ra19487g
122. Yang, Z.H., Nakashima, N.: Poly(vinylpyrrolidone)-wrapped carbon nanotube-based fuel cell electrocatalyst shows high durability and performance under non-humidified operation. J. Mater. Chem. A **3**, 23316–23322 (2015). https://doi.org/10.1039/c5ta06735a
123. Zhang, Q., Ling, Y., Cai, W., et al.: High performance and durability of polymer-coated Pt electrocatalyst supported on oxidized multi-walled in high-temperature polymer electrolyte fuel cells. Int. J. Hydrog. Energy **42**, 16714–16721 (2017). https://doi.org/10.1016/j.ijhydene.2017.05.070
124. Orfanidi, A., Daletou, M.K., Neophytides, S.G.: Preparation and characterization of Pt on modified multi-wall carbon nanotubes to be used as electrocatalysts for high temperature fuel cell applications. Appl. Catal. B Environ. **106**, 379–389 (2011). https://doi.org/10.1016/j.apcatb.2011.05.043
125. Ignaszak, A., Teo, C., Ye, S.Y., et al.: Pt-SnO_2-Pd/C electrocatalyst with enhanced activity and durability for the oxygen reduction reaction at low Pt loading: the effect of carbon support type and activation. J. Phys. Chem. C **114**, 16488–16504 (2010). https://doi.org/10.1021/jp104456j
126. Su, F.B., Tian, Z.Q., Poh, C.K., et al.: Pt nanoparticles supported on nitrogen-doped porous carbon nanospheres as an electrocatalyst for fuel cells. Chem. Mater. **22**, 832–839 (2010). https://doi.org/10.1021/cm901542w
127. Kim, M., Lim, J., Bak, J., et al.: Fe and N codoped mesoporous carbon nanofiber as a nonprecious metal catalyst for oxygen reduction reaction and a durable support for Pt nanoparticles. ACS Sustain. Chem. Eng. **7**, 17544–17552 (2019). https://doi.org/10.1021/acssuschemeng.9b05118
128. Zhang, S.Z., Fu, T., Li, J.Y., et al.: Platinum nanoparticles dispersed on high-surface-area roelike nitrogen-doped mesoporous carbon for oxygen reduction reaction. ACS Appl. Energy Mater. **1**, 6198–6207 (2018). https://doi.org/10.1021/acsaem.8b01242
129. Kim, D.S., Zeid, E.F.A., Kim, Y.T.: Additive treatment effect of TiO_2 as supports for Pt-based electrocatalysts on oxygen reduction reaction activity. Electrochim. Acta **55**, 3628–3633 (2010). https://doi.org/10.1016/j.electacta.2010.01.055
130. Hornberger, E., Bergmann, A., Schmies, H., et al.: In situ stability studies of platinum nanoparticles supported on ruthenium–titanium mixed oxide (RTO) for fuel cell cathodes. ACS Catal. **8**, 9675–9683 (2018). https://doi.org/10.1021/acscatal.8b02498
131. Gao, W., Zhang, Z., Dou, M., et al.: Highly dispersed and crystalline Ta_2O_5 anchored Pt electrocatalyst with improved activity and durability toward oxygen reduction: promotion by atomic-scale Pt-Ta_2O_5 interactions. ACS Catal. **9**, 3278–3288 (2019). https://doi.org/10.1021/acscatal.8b04505
132. Liu, Y., Mustain, W.E.: Structural and electrochemical studies of Pt clusters supported on high-surface-area tungsten carbide for oxygen reduction. ACS Catal. **1**, 212–220 (2011). https://doi.org/10.1021/cs100140s
133. Pang, M., Li, C., Ding, L., et al.: Microwave-assisted preparation of Mo_2C/CNTs nanocomposites as efficient electrocatalyst supports for oxygen reduction reaction. Ind. Eng. Chem. Res. **49**, 4169–4174 (2010). https://doi.org/10.1021/ie901741c

134. Hu, Z.F., Chen, C., Meng, H., et al.: Oxygen reduction electrocatalysis enhanced by nanosized cubic vanadium carbide. Electrochem. Commun. **13**, 763–765 (2011). https://doi.org/10.1016/j.elecom.2011.03.004
135. Ramirez-Caballero, G.E., Hirunsit, P., Balbuena, P.B.: Shell-anchor-core structures for enhanced stability and catalytic oxygen reduction activity. J. Chem. Phys. **133**, 134705 (2010). https://doi.org/10.1063/1.3481482
136. Ma, X., Meng, H., Cai, M., et al.: Bimetallic carbide nanocomposite enhanced Pt catalyst with high activity and stability for the oxygen reduction reaction. J. Am. Chem. Soc. **134**, 1954–1957 (2012). https://doi.org/10.1021/ja2093053
137. Ishihara, A., Tamura, M., Ohgi, Y., et al.: Emergence of oxygen reduction activity in partially oxidized tantalum carbonitrides: roles of deposited carbon for oxygen-reduction-reaction-site creation and surface electron conduction. J. Phys. Chem. C **117**, 18837–18844 (2013). https://doi.org/10.1021/jp405247m
138. Lori, O., Gonen, S., Kapon, O., et al.: Durable tungsten carbide support for Pt-based fuel cells cathodes. ACS Appl. Mater. Interfaces **13**, 8315–8323 (2021). https://doi.org/10.1021/acsami.0c20089
139. Vellacheri, R., Unni, S.M., Nahire, S., et al.: Pt-MoO_x-carbon nanotube redox couple based electrocatalyst as a potential partner with polybenzimidazole membrane for high temperature polymer electrolyte membrane fuel cell applications. Electrochim. Acta **55**, 2878–2887 (2010). https://doi.org/10.1016/j.electacta.2010.01.012
140. Liu, Z.M., Ma, L.L., Zhang, J., et al.: Pt alloy electrocatalysts for proton exchange membrane fuel cells: a review. Catal. Rev. **55**, 255–288 (2013). https://doi.org/10.1080/01614940.2013.795455
141. Čolić, V., Bandarenka, A.S.: Pt alloy electrocatalysts for the oxygen reduction reaction: from model surfaces to nanostructured systems. ACS Catal. **6**, 5378–5385 (2016). https://doi.org/10.1021/acscatal.6b00997
142. Stamenkovic, V.R., Fowler, B., Mun, B.S., et al.: Improved oxygen reduction activity on $Pt_3Ni(111)$ via increased surface site availability. Science **315**, 493–497 (2007). https://doi.org/10.1126/science.1135941
143. Wang, D., Xin, H.L., Hovden, R., et al.: Structurally ordered intermetallic platinum-cobalt core-shell nanoparticles with enhanced activity and stability as oxygen reduction electrocatalysts. Nat. Mater. **12**, 81–87 (2013). https://doi.org/10.1038/nmat3458
144. Wu, J.F., Shan, S.Y., Cronk, H., et al.: Understanding composition-dependent synergy of PtPd alloy nanoparticles in electrocatalytic oxygen reduction reaction. J. Phys. Chem. C **121**, 14128–14136 (2017). https://doi.org/10.1021/acs.jpcc.7b03043
145. Jia, Y., Jiang, Y., Zhang, J., et al.: Unique excavated rhombic dodecahedral $PtCu_3$ alloy nanocrystals constructed with ultrathin nanosheets of high-energy{110}facets. J. Am. Chem. Soc. **136**, 3748–3751 (2014). https://doi.org/10.1021/ja413209q
146. Zhou, M., Li, C., Fang, J.: Noble-metal based random alloy and intermetallic nanocrystals: syntheses and applications. Chem. Rev. **121**, 736–795 (2021). https://doi.org/10.1021/acs.chemrev.0c00436
147. Yoo, T.Y., Yoo, J.M., Sinha, A.K., et al.: Direct synthesis of intermetallic platinum-alloy nanoparticles highly loaded on carbon supports for efficient electrocatalysis. J. Am. Chem. Soc. **142**, 14190–14200 (2020). https://doi.org/10.1021/jacs.0c05140
148. Xie, M., Lyu, Z., Chen, R., et al.: Pt-Co@Pt octahedral nanocrystals: enhancing their activity and durability toward oxygen reduction with an intermetallic core and an ultrathin shell. J. Am. Chem. Soc. **143**, 8509–8518 (2021). https://doi.org/10.1021/jacs.1c04160
149. Zhao, X., Chen, S., Fang, Z.C., et al.: Octahedral $Pd@Pt_{1.8}Ni$ core-shell nanocrystals with ultrathin PtNi alloy shells as active catalysts for oxygen reduction reaction. J. Am. Chem. Soc. **137**, 2804–2807 (2015). https://doi.org/10.1021/ja511596c
150. Shao, M., Shoemaker, K., Peles, A., et al.: Pt monolayer on porous Pd-Cu alloys as oxygen reduction electrocatalysts. J. Am. Chem. Soc. **132**, 9253–9255 (2010). https://doi.org/10.1021/ja101966a
151. Rizo, R., Arán-Ais, R.M., Padgett, E., et al.: Pt-$rich_{core}$/Sn-$rich_{subsurface}$/Pt_{skin} nanocubes as highly active and stable electrocatalysts for the ethanol oxidation reaction. J. Am. Chem. Soc. **140**, 3791–3797 (2018). https://doi.org/10.1021/jacs.8b00588
152. Wang, C., Chi, M., Li, D., et al.: Design and synthesis of bimetallic electrocatalyst with multilayered Pt-skin surfaces. J. Am. Chem. Soc. **133**, 14396–14403 (2011). https://doi.org/10.1021/ja2047655
153. Cui, C.H., Gan, L., Heggen, M., et al.: Compositional segregation in shaped Pt alloy nanoparticles and their structural behaviour during electrocatalysis. Nat. Mater. **12**, 765–771 (2013). https://doi.org/10.1038/nmat3668
154. Li, J., Yin, H.M., Li, X.B., et al.: Surface evolution of a Pt-Pd-Au electrocatalyst for stable oxygen reduction. Nat. Energy **2**, 17111 (2017). https://doi.org/10.1038/nenergy.2017.111
155. Sasaki, K., Naohara, H., Choi, Y., et al.: Highly stable Pt monolayer on PdAu nanoparticle electrocatalysts for the oxygen reduction reaction. Nat. Commun. **3**, 1115 (2012). https://doi.org/10.1038/ncomms2124
156. He, S.Q., Liu, Y., Zhan, H.B., et al.: Direct thermal annealing synthesis of ordered Pt alloy nanoparticles coated with a thin N-doped carbon shell for the oxygen reduction reaction. ACS Catal. **11**, 9355–9365 (2021). https://doi.org/10.1021/acscatal.1c02434
157. Hu, Y., Shen, T., Zhao, X., et al.: Combining structurally ordered intermetallics with N-doped carbon confinement for efficient and anti-poisoning electrocatalysis. Appl. Catal. B Environ. **279**, 119370 (2020). https://doi.org/10.1016/j.apcatb.2020.119370
158. You, D.J., Kim, D.H., de Lile, J.R., et al.: Pd core-shell alloy catalysts for high-temperature polymer electrolyte membrane fuel cells: effect of the core composition on the activity towards oxygen reduction reactions. Appl. Catal. A Gen. **562**, 250–257 (2018). https://doi.org/10.1016/j.apcata.2018.06.018
159. Cetinbas, F.C., Ahluwalia, R.K., Kariuki, N.N., et al.: Effects of porous carbon morphology, agglomerate structure and relative humidity on local oxygen transport resistance. J. Electrochem. Soc. **167**, 013508 (2020)
160. Gao, L., Li, X., Yao, Z., et al.: Unconventional p–d hybridization interaction in PtGa ultrathin nanowires boosts oxygen reduction electrocatalysis. J. Am. Chem. Soc. **141**, 18083–18090 (2019). https://doi.org/10.1021/jacs.9b07238
161. Li, K., Li, X., Huang, H., et al.: One-nanometer-thick PtNiRh trimetallic nanowires with enhanced oxygen reduction electrocatalysis in acid media: integrating multiple advantages into one catalyst. J. Am. Chem. Soc. **140**, 16159–16167 (2018). https://doi.org/10.1021/jacs.8b08836
162. Koenigsmann, C., Santulli, A.C., Gong, K., et al.: Enhanced electrocatalytic performance of processed, ultrathin, supported Pd-Pt core-shell nanowire catalysts for the oxygen reduction reaction. J. Am. Chem. Soc. **133**, 9783–9795 (2011). https://doi.org/10.1021/ja111130t
163. Xia, B.Y., Wu, H.B., Yan, Y., et al.: Ultrathin and ultralong single-crystal platinum nanowire assemblies with highly stable electrocatalytic activity. J. Am. Chem. Soc. **135**, 9480–9485 (2013). https://doi.org/10.1021/ja402955t
164. Nair, A.S., Mahata, A., Pathak, B.: Multilayered platinum nanotube for oxygen reduction in a fuel cell cathode: origin of activity and product selectivity. ACS Appl. Energy Mater. **1**, 3890–3899 (2018). https://doi.org/10.1021/acsaem.8b00641

165. Zhu, E., Yan, X., Wang, S., et al.: Peptide-assisted 2-D assembly toward free-floating ultrathin platinum nanoplates as effective electrocatalysts. Nano Lett. **19**, 3730–3736 (2019). https://doi.org/10.1021/acs.nanolett.9b00867
166. Qin, Y., Luo, M., Sun, Y., et al.: Intermetallic hcp-PtBi/fcc-Pt core/shell nanoplates enable efficient bifunctional oxygen reduction and methanol oxidation electrocatalysis. ACS Catal. **8**, 5581–5590 (2018). https://doi.org/10.1021/acscatal.7b04406
167. Saleem, F., Zhang, Z.C., Xu, B., et al.: Ultrathin Pt-Cu nanosheets and nanocones. J. Am. Chem. Soc. **135**, 18304–18307 (2013). https://doi.org/10.1021/ja4101968
168. Becknell, N., Son, Y., Kim, D., et al.: Control of architecture in rhombic dodecahedral Pt-Ni nanoframe electrocatalysts. J. Am. Chem. Soc. **139**, 11678–11681 (2017). https://doi.org/10.1021/jacs.7b05584
169. Sievers, G.W., Jensen, A.W., Quinson, J., et al.: Self-supported Pt-CoO networks combining high specific activity with high surface area for oxygen reduction. Nat. Mater. **20**, 208–213 (2021). https://doi.org/10.1038/s41563-020-0775-8
170. Geboes, B., Ustarroz, J., Sentosun, K., et al.: Electrochemical behavior of electrodeposited nanoporous Pt catalysts for the oxygen reduction reaction. ACS Catal. **6**, 5856–5864 (2016). https://doi.org/10.1021/acscatal.6b00668
171. Chen, C., Kang, Y., Huo, Z., et al.: Highly crystalline multimetallic nanoframes with three-dimensional electrocatalytic surfaces. Science **343**, 1339–1343 (2014). https://doi.org/10.1126/science.1249061
172. Fan, J.T., Chen, M., Zhao, Z.L., et al.: Bridging the gap between highly active oxygen reduction reaction catalysts and effective catalyst layers for proton exchange membrane fuel cells. Nat. Energy **6**, 475–486 (2021). https://doi.org/10.1038/s41560-021-00824-7
173. He, Q., Yang, X., Chen, W., et al.: Influence of phosphate anion adsorption on the kinetics of oxygen electroreduction on low index Pt(*hkl*) single crystals. Phys. Chem. Chem. Phys. **12**, 12544–12555 (2010). https://doi.org/10.1039/c0cp00433b
174. Li, Q., Wu, G., Cullen, D.A., et al.: Phosphate-tolerant oxygen reduction catalysts. ACS Catal. **4**, 3193–3200 (2014). https://doi.org/10.1021/cs500807v
175. Liu, Z.Y., Wainright, J.S., Litt, M.H., et al.: Study of the oxygen reduction reaction (ORR) at Pt interfaced with phosphoric acid doped polybenzimidazole at elevated temperature and low relative humidity. Electrochim. Acta **51**, 3914–3923 (2006). https://doi.org/10.1016/j.electacta.2005.11.019
176. Kaserer, S., Caldwell, K., Ramaker, D., et al.: Analyzing the influence of H_3PO_4 as catalyst poison in high temperature PEM fuel cells using in-operando X-ray absorption spectroscopy. J. Phys. Chem. C **117**, 6210–6217 (2013). https://doi.org/10.1021/jp311924q
177. Chung, Y.H., Chung, D.Y., Jung, N., et al.: Tailoring the electronic structure of nanoelectrocatalysts induced by a surface-capping organic molecule for the oxygen reduction reaction. Clin. Cancer Res. **4**, 1304–1309 (2013). https://doi.org/10.1021/jz400574f
178. Luo, F., Zhang, Q., Yang, Z.H., et al.: Fabrication of stable and well-connected proton path in catalyst layer for high temperature polymer electrolyte fuel cells. ChemCatChem **10**, 5314–5322 (2018). https://doi.org/10.1002/cctc.201801256
179. Li, Y.P., Jiang, L., Wang, S., et al.: Influence of phosphoric anions on oxygen reduction reaction activity of platinum, and strategies to inhibit phosphoric anion adsorption. Chin. J. Catal. **37**, 1134–1141 (2016). https://doi.org/10.1016/S1872-2067(16)62472-5
180. Chung, Y.H., Kim, S.J., Chung, D.Y., et al.: Tuning the oxygen reduction activity of the Pt-Ni nanoparticles upon specific anion adsorption by varying heat treatment atmospheres. Phys. Chem. Chem. Phys. **16**, 13726–13732 (2014). https://doi.org/10.1039/c4cp00187g
181. Huang, G., Li, Y., Du, S., et al.: Silica-facilitated proton transfer for high-temperature proton-exchange membrane fuel cells. Sci. China Chem. **64**, 2203–2211 (2021). https://doi.org/10.1007/s11426-021-1142-x
182. Meyer, Q., Zeng, Y., Zhao, C.: Electrochemical impedance spectroscopy of catalyst and carbon degradations in proton exchange membrane fuel cells. J. Power Sour. **437**, 226922 (2019). https://doi.org/10.1016/j.jpowsour.2019.226922
183. Cheng, H., Gui, R., Yu, H., et al.: Subsize Pt-based intermetallic compound enables long-term cyclic mass activity for fuel-cell oxygen reduction. Proc. Natl. Acad. Sci. U. S. A. **118**, e2104026118 (2021). https://doi.org/10.1073/pnas.2104026118
184. He, Y., Liu, S., Priest, C., et al.: Atomically dispersed metal-nitrogen-carbon catalysts for fuel cells: advances in catalyst design, electrode performance, and durability improvement. Chem. Soc. Rev. **49**, 3484–3524 (2020). https://doi.org/10.1039/c9cs00903e
185. Wang, X.Q., Li, Z., Qu, Y., et al.: Review of metal catalysts for oxygen reduction reaction: from nanoscale engineering to atomic design. Chem **5**, 1486–1511 (2019). https://doi.org/10.1016/j.chempr.2019.03.002
186. Choi, C.H., Baldizzone, C., Grote, J.P., et al.: Stability of Fe–N–C catalysts in acidic medium studied by operando spectroscopy. Angew. Chem. Int. Ed. **54**, 12753–12757 (2015). https://doi.org/10.1002/anie.201504903
187. Lefèvre, M., Proietti, E., Jaouen, F., et al.: Iron-based catalysts with improved oxygen reduction activity in polymer electrolyte fuel cells. Science **324**, 71–74 (2009). https://doi.org/10.1126/science.1170051
188. Wu, G., More, K.L., Johnston, C.M., et al.: High-performance electrocatalysts for oxygen reduction derived from polyaniline, iron, and cobalt. Science **332**, 443–447 (2011). https://doi.org/10.1126/science.1200832
189. Wang, X.X., Prabhakaran, V., He, Y., et al.: Iron-free cathode catalysts for proton-exchange-membrane fuel cells: cobalt catalysts and the peroxide mitigation approach. Adv. Mater. **31**, e1805126 (2019). https://doi.org/10.1002/adma.201805126
190. Luo, F., Roy, A., Silvioli, L., et al.: P-block single-metal-site tin/nitrogen-doped carbon fuel cell cathode catalyst for oxygen reduction reaction. Nat. Mater. **19**, 1215–1223 (2020). https://doi.org/10.1038/s41563-020-0717-5
191. Barkholtz, H.M., Liu, D.J.: Advancements in rationally designed PGM-free fuel cell catalysts derived from metal-organic frameworks. Mater. Horiz. **4**, 20–37 (2017). https://doi.org/10.1039/c6mh00344c
192. Shao, Y.Y., Dodelet, J.P., Wu, G., et al.: PGM-free cathode catalysts for PEM fuel cells: a mini-review on stability challenges. Adv. Mater. **31**, 1807615 (2019). https://doi.org/10.1002/adma.201807615
193. Chung, H.T., Cullen, D.A., Higgins, D., et al.: Direct atomic-level insight into the active sites of a high-performance PGM-free ORR catalyst. Science **357**, 479–484 (2017). https://doi.org/10.1126/science.aan2255
194. Zitolo, A., Goellner, V., Armel, V., et al.: Identification of catalytic sites for oxygen reduction in iron- and nitrogen-doped graphene materials. Nat. Mater. **14**, 937–942 (2015). https://doi.org/10.1038/nmat4367
195. Li, J.Z., Chen, M.J., Cullen, D.A., et al.: Atomically dispersed manganese catalysts for oxygen reduction in proton-exchange membrane fuel cells. Nat. Catal. **1**, 935–945 (2018). https://doi.org/10.1038/s41929-018-0164-8
196. Wang, X.X., Swihart, M.T., Wu, G.: Achievements, challenges and perspectives on cathode catalysts in proton exchange

membrane fuel cells for transportation. Nat. Catal. **2**, 578–589 (2019). https://doi.org/10.1038/s41929-019-0304-9
197. Wang, X.X., Cullen, D.A., Pan, Y.T., et al.: Nitrogen-coordinated single cobalt atom catalysts for oxygen reduction in proton exchange membrane fuel cells. Adv. Mater. **30**, 1706758 (2018). https://doi.org/10.1002/adma.201706758
198. Zhang, H., Hwang, S., Wang, M., et al.: Single atomic iron catalysts for oxygen reduction in acidic media: particle size control and thermal activation. J. Am. Chem. Soc. **139**, 14143–14149 (2017). https://doi.org/10.1021/jacs.7b06514
199. Wan, X., Liu, X.F., Li, Y.C., et al.: Fe–N–C electrocatalyst with dense active sites and efficient mass transport for high-performance proton exchange membrane fuel cells. Nat. Catal. **2**, 259–268 (2019). https://doi.org/10.1038/s41929-019-0237-3
200. Banham, D., Choi, J.Y., Kishimoto, T., et al.: Integrating PGM-free catalysts into catalyst layers and proton exchange membrane fuel cell devices. Adv. Mater. **31**, e1804846 (2019). https://doi.org/10.1002/adma.201804846
201. Wang, J., Huang, Z., Liu, W., et al.: Design of N-coordinated dual-metal sites: a stable and active Pt-free catalyst for acidic oxygen reduction reaction. J. Am. Chem. Soc. **139**, 17281–17284 (2017). https://doi.org/10.1021/jacs.7b10385
202. Cheng, Q.Q., Han, S., Mao, K., et al.: Co nanoparticle embedded in atomically-dispersed Co–N–C nanofibers for oxygen reduction with high activity and remarkable durability. Nano Energy **52**, 485–493 (2018). https://doi.org/10.1016/j.nanoen.2018.08.005
203. Chen, Y.J., Ji, S.F., Zhao, S., et al.: Enhanced oxygen reduction with single-atomic-site iron catalysts for a zinc-air battery and hydrogen-air fuel cell. Nat. Commun. **9**, 5422 (2018). https://doi.org/10.1038/s41467-018-07850-2
204. Chen, L.Y., Liu, X., Zheng, L., et al.: Insights into the role of active site density in the fuel cell performance of Co–N–C catalysts. Appl. Catal. B Environ. **256**, 117849 (2019). https://doi.org/10.1016/j.apcatb.2019.117849
205. Yang, Z., Wang, Y., Zhu, M., et al.: Boosting oxygen reduction catalysis with Fe–N_4 sites decorated porous carbons toward fuel cells. ACS Catal. **9**, 2158–2163 (2019). https://doi.org/10.1021/acscatal.8b04381
206. Deng, Y.J., Chi, B., Tian, X.L., et al.: G-C_3N_4 promoted MOF derived hollow carbon nanopolyhedra doped with high density/fraction of single Fe atoms as an ultra-high performance non-precious catalyst towards acidic ORR and PEM fuel cells. J. Mater. Chem. A **7**, 5020–5030 (2019). https://doi.org/10.1039/c8ta11785c
207. Boldrin, P., Malko, D., Mehmood, A., et al.: Deactivation, reactivation and super-activation of Fe–N/C oxygen reduction electrocatalysts: gas sorption, physical and electrochemical investigation using NO and O_2. Appl. Catal. B Environ. **292**, 120169 (2021). https://doi.org/10.1016/j.apcatb.2021.120169
208. Zhang, H.G., Chung, H.T., Cullen, D.A., et al.: High-performance fuel cell cathodes exclusively containing atomically dispersed iron active sites. Energy Environ. Sci. **12**, 2548–2558 (2019). https://doi.org/10.1039/c9ee00877b
209. Al-Zoubi, T., Zhou, Y., Yin, X., et al.: Preparation of nonprecious metal electrocatalysts for the reduction of oxygen using a low-temperature sacrificial metal. J. Am. Chem. Soc. **142**, 5477–5481 (2020). https://doi.org/10.1021/jacs.9b11061
210. Qiao, M., Wang, Y., Wang, Q., et al.: Hierarchically ordered porous carbon with atomically dispersed FeN_4 for ultraefficient oxygen reduction reaction in proton-exchange membrane fuel cells. Angew. Chem. Int. Ed. **59**, 2688–2694 (2020). https://doi.org/10.1002/anie.201914123
211. Li, Y.C., Liu, X.F., Zheng, L.R., et al.: Preparation of Fe–N–C catalysts with FeN_x (x = 1, 3, 4) active sites and comparison of their activities for the oxygen reduction reaction and performances in proton exchange membrane fuel cells. J. Mater. Chem. A **7**, 26147–26153 (2019). https://doi.org/10.1039/c9ta08532g
212. Fu, X.G., Zamani, P., Choi, J.Y., et al.: In situ polymer graphenization ingrained with nanoporosity in a nitrogenous electrocatalyst boosting the performance of polymer-electrolyte-membrane fuel cells. Adv. Mater. **29**, 1604456 (2017). https://doi.org/10.1002/adma.201604456
213. Liu, Q., Liu, X., Zheng, L., et al.: The solid-phase synthesis of an Fe–N–C electrocatalyst for high-power proton-exchange membrane fuel cells. Angew. Chem. Int. Ed. **57**, 1204–1208 (2018). https://doi.org/10.1002/anie.201709597
214. Li, Y.Y., Zhang, P.Y., Wan, L.Y., et al.: A general carboxylate-assisted approach to boost the ORR performance of ZIF-derived Fe/N/C catalysts for proton exchange membrane fuel cells. Adv. Funct. Mater. **31**, 2009645 (2021). https://doi.org/10.1002/adfm.202009645
215. Hu, Y., Jensen, J.O., Zhang, W., et al.: Fe_3C-based oxygen reduction catalysts: synthesis, hollow spherical structures and applications in fuel cells. J. Mater. Chem. A **3**, 1752–1760 (2015). https://doi.org/10.1039/c4ta03986f
216. Byeon, A., Lee, K.J., Lee, M.J., et al.: Effect of catalyst pore size on the performance of non-precious Fe/N/C-based electrocatalysts for high-temperature polymer electrolyte membrane fuel cells. ChemElectroChem **5**, 1805–1810 (2018). https://doi.org/10.1002/celc.201800093
217. Ren, H., Wang, Y., Yang, Y., et al.: Fe/N/C nanotubes with atomic Fe sites: a highly active cathode catalyst for alkaline polymer electrolyte fuel cells. ACS Catal. **7**, 6485–6492 (2017). https://doi.org/10.1021/acscatal.7b02340
218. Hu, Y., Jensen, J.O., Pan, C., et al.: Immunity of the Fe–N–C catalysts to electrolyte adsorption: phosphate but not perchloric anions. Appl. Catal. B Environ. **234**, 357–364 (2018). https://doi.org/10.1016/j.apcatb.2018.03.056
219. Gokhale, R., Asset, T., Qian, G., et al.: Implementing PGM-free electrocatalysts in high-temperature polymer electrolyte membrane fuel cells. Electrochem. Commun. **93**, 91–94 (2018). https://doi.org/10.1016/j.elecom.2018.06.019
220. Strickland, K., Pavlicek, R., Miner, E., et al.: Anion resistant oxygen reduction electrocatalyst in phosphoric acid fuel cell. ACS Catal. **8**, 3833–3843 (2018). https://doi.org/10.1021/acscatal.8b00390
221. Cheng, Y., He, S., Lu, S., et al.: Iron single atoms on graphene as nonprecious metal catalysts for high-temperature polymer electrolyte membrane fuel cells. Adv. Sci. **6**, 1802066 (2019). https://doi.org/10.1002/advs.201802066
222. Razmjooei, F., Yu, J.H., Lee, H.Y., et al.: Single-atom iron-based electrocatalysts for high-temperature polymer electrolyte membrane fuel cell: organometallic precursor and pore texture tailoring. ACS Appl. Energy Mater. **3**, 11164–11176 (2020). https://doi.org/10.1021/acsaem.0c02111
223. Cheng, Y., Wang, M., Lu, S., et al.: First demonstration of phosphate enhanced atomically dispersed bimetallic FeCu catalysts as Pt-free cathodes for high temperature phosphoric acid doped polybenzimidazole fuel cells. Appl. Catal. B Environ. **284**, 119717 (2021). https://doi.org/10.1016/j.apcatb.2020.119717
224. Bevilacqua, N., Asset, T., Schmid, M.A., et al.: Impact of catalyst layer morphology on the operation of high temperature PEM fuel cells. J. Power Sour. Adv. **7**, 100042 (2021). https://doi.org/10.1016/j.powera.2020.100042
225. Cheng, Y., Zhang, J., Wu, X., et al.: A template-free method to synthesis high density iron single atoms anchored on carbon nanotubes for high temperature polymer electrolyte membrane fuel cells. Nano Energy **80**, 105534 (2021). https://doi.org/10.1016/j.nanoen.2020.105534

226. Wang, W., Chen, W., Miao, P., et al.: NaCl Crystallites as dual-functional and water-removable templates to synthesize a three-dimensional graphene-like macroporous Fe–N–C catalyst. ACS Catal. **7**, 6144–6149 (2017). https://doi.org/10.1021/acscatal.7b01695
227. Jiao, L., Li, J.K., Richard, L.L., et al.: Chemical vapour deposition of Fe–N–C oxygen reduction catalysts with full utilization of dense Fe–N_4 sites. Nat. Mater. **20**, 1385–1391 (2021). https://doi.org/10.1038/s41563-021-01030-2
228. Jin, Z.Y., Li, P.P., Meng, Y., et al.: Understanding the inter-site distance effect in single-atom catalysts for oxygen electroreduction. Nat. Catal. **4**, 615–622 (2021). https://doi.org/10.1038/s41929-021-00650-w
229. Mehmood, A., Gong, M.J., Jaouen, F., et al.: High loading of single atomic iron sites in Fe–NC oxygen reduction catalysts for proton exchange membrane fuel cells. Nat. Catal. **5**, 311–323 (2022). https://doi.org/10.1038/s41929-022-00772-9
230. Ebbesen, T.W., Lezec, H.J., Hiura, H., et al.: Electrical conductivity of individual carbon nanotubes. Nature **382**, 54–56 (1996). https://doi.org/10.1038/382054a0
231. Yuan, W.Y., Lu, S.F., Xiang, Y., et al.: Pt-based nanoparticles on non-covalent functionalized carbon nanotubes as effective electrocatalysts for proton exchange membrane fuel cells. RSC Adv. **4**, 46265–46284 (2014). https://doi.org/10.1039/c4ra05120c
232. Cheng, Y., Zhang, J., Jiang, S.P.: Are metal-free pristine carbon nanotubes electrocatalytically active? Chem. Commun. **51**, 13764–13767 (2015). https://doi.org/10.1039/c5cc02218e
233. Cheng, Y., Xu, C., Jia, L., et al.: Pristine carbon nanotubes as non-metal electrocatalysts for oxygen evolution reaction of water splitting. Appl. Catal. B Environ. **163**, 96–104 (2015). https://doi.org/10.1016/j.apcatb.2014.07.049
234. Cheng, Y., Memar, A., Saunders, M., et al.: Dye functionalized carbon nanotubes for photoelectrochemical water splitting-role of inner tubes. J. Mater. Chem. A **4**, 2473–2483 (2016). https://doi.org/10.1039/c6ta00143b
235. Sa, Y.J., Seo, D.J., Woo, J., et al.: A general approach to preferential formation of active Fe–N_x sites in Fe–N/C electrocatalysts for efficient oxygen reduction reaction. J. Am. Chem. Soc. **138**, 15046–15056 (2016). https://doi.org/10.1021/jacs.6b09470
236. Woo, J., Yang, S.Y., Sa, Y.J., et al.: Promoting oxygen reduction reaction activity of Fe–N/C electrocatalysts by silica-coating-mediated synthesis for anion-exchange membrane fuel cells. Chem. Mater. **30**, 6684–6701 (2018). https://doi.org/10.1021/acs.chemmater.8b02117
237. Wu, X., Wang, Q.C., Yang, S.Z., et al.: Sublayer-enhanced atomic sites of single atom catalysts through in situ atomization of metal oxide nanoparticles. Energy Environ. Sci. **15**, 1183–1191 (2022). https://doi.org/10.1039/d1ee03311e
238. Engl, T., Gubler, L., Schmidt, T.J.: Think different! Carbon corrosion mitigation strategy in high temperature PEFC: a rapid aging study. J. Electrochem. Soc. **162**, F291–F297 (2015). https://doi.org/10.1149/2.0681503jes
239. Kannan, A., Kaczerowski, J., Kabza, A., et al.: Operation strategies based on carbon corrosion and lifetime investigations for high temperature polymer electrolyte membrane fuel cell stacks. Fuel Cells **18**, 287–298 (2018). https://doi.org/10.1002/fuce.201700096
240. Rosenthal, J., Nocera, D.G.: Role of proton-coupled electron transfer in O–O bond activation. Acc. Chem. Res. **40**, 543–553 (2007). https://doi.org/10.1021/ar7000638
241. Gautam, R.P., Lee, Y.T., Herman, G.L., et al.: Controlling proton and electron transfer rates to enhance the activity of an oxygen reduction electrocatalyst. Angew. Chem. Int. Ed. **57**, 13480–13483 (2018). https://doi.org/10.1002/anie.201806795
242. Tse, E.C.M., Barile, C.J., Kirchschlager, N.A., et al.: Proton transfer dynamics control the mechanism of O_2 reduction by a non-precious metal electrocatalyst. Nat. Mater. **15**, 754–759 (2016). https://doi.org/10.1038/nmat4636
243. Meyer, Q., Ashton, S., Jervis, R., et al.: The hydro-electro-thermal performance of air-cooled, open-cathode polymer electrolyte fuel cells: combined localised current density, temperature and water mapping. Electrochim. Acta **180**, 307–315 (2015). https://doi.org/10.1016/j.electacta.2015.08.106
244. Suter, T.A.M., Smith, K., Hack, J., et al.: Engineering catalyst layers for next-generation polymer electrolyte fuel cells: a review of design, materials, and methods. Adv. Energy Mater. **11**, 2101025 (2021). https://doi.org/10.1002/aenm.202101025
245. Zhu, W.K., Pei, Y., Douglin, J.C., et al.: Multi-scale study on bifunctional Co/Fe–N–C cathode catalyst layers with high active site density for the oxygen reduction reaction. Appl. Catal. B Environ. **299**, 120656 (2021). https://doi.org/10.1016/j.apcatb.2021.120656
246. Ehelebe, K., Seeberger, D., Paul, M.T.Y., et al.: Evaluating electrocatalysts at relevant currents in a half-cell: the impact of Pt loading on oxygen reduction reaction. J. Electrochem. Soc. **166**, F1259–F1268 (2019). https://doi.org/10.1149/2.0911915jes
247. Pinaud, B.A., Bonakdarpour, A., Daniel, L., et al.: Key considerations for high current fuel cell catalyst testing in an electrochemical half-cell. J. Electrochem. Soc. **164**, F321–F327 (2017). https://doi.org/10.1149/2.0891704jes
248. Wiberg, G.K., Fleige, M.J., Arenz, M.: Design and test of a flexible electrochemical setup for measurements in aqueous electrolyte solutions at elevated temperature and pressure. Rev. Sci. Instrum. **85**, 085105 (2014). https://doi.org/10.1063/1.4890826
249. Wiberg, G.K.H., Fleige, M., Arenz, M.: Gas diffusion electrode setup for catalyst testing in concentrated phosphoric acid at elevated temperatures. Rev. Sci. Instrum. **86**, 024102 (2015). https://doi.org/10.1063/1.4908169
250. Hu, Y., Jiang, Y., Jensen, J.O., et al.: Catalyst evaluation for oxygen reduction reaction in concentrated phosphoric acid at elevated temperatures. J. Power Sour. **375**, 77–81 (2018). https://doi.org/10.1016/j.jpowsour.2017.11.054
251. Zalitis, C.M., Kramer, D., Kucernak, A.R.: Electrocatalytic performance of fuel cell reactions at low catalyst loading and high mass transport. Phys. Chem. Chem. Phys. **15**, 4329–4340 (2013). https://doi.org/10.1039/c3cp44431g
252. Mack, F., Heissler, S., Laukenmann, R., et al.: Phosphoric acid distribution and its impact on the performance of polybenzimidazole membranes. J. Power Sour. **270**, 627–633 (2014). https://doi.org/10.1016/j.jpowsour.2014.06.171
253. Arslan, F., Böhm, T., Kerres, J., et al.: Spatially and temporally resolved monitoring of doping polybenzimidazole membranes with phosphoric acid. J. Membr. Sci. **625**, 119145 (2021). https://doi.org/10.1016/j.memsci.2021.119145
254. Liang, H.G., Su, H., Pollet, B.G., et al.: Development of membrane electrode assembly for high temperature proton exchange membrane fuel cell by catalyst coating membrane method. J. Power Sour. **288**, 121–127 (2015). https://doi.org/10.1016/j.jpowsour.2015.04.123
255. Liang, H.G., Su, H., Pollet, B.G., et al.: Membrane electrode assembly with enhanced platinum utilization for high temperature proton exchange membrane fuel cell prepared by catalyst coating membrane method. J. Power Sour. **266**, 107–113 (2014). https://doi.org/10.1016/j.jpowsour.2014.05.014
256. Matar, S., Higier, A., Liu, H.: The effects of excess phosphoric acid in a polybenzimidazole-based high temperature proton exchange membrane fuel cell. J. Power Sour. **195**, 181–184 (2010). https://doi.org/10.1016/j.jpowsour.2009.06.084
257. Meyer, Q., Mansor, N., Iacoviello, F., et al.: Investigation of hot pressed polymer electrolyte fuel cell assemblies via X-ray

computed tomography. Electrochim. Acta **242**, 125–136 (2017). https://doi.org/10.1016/j.electacta.2017.05.028
258. Hack, J., Heenan, T.M.M., Iacoviello, F., et al.: A structure and durability comparison of membrane electrode assembly fabrication methods: self-assembled versus hot-pressed. J. Electrochem. Soc. **165**, F3045–F3052 (2018). https://doi.org/10.1149/2.0051806jes
259. Jean-Fulcrand, A., Masen, M.A., Bremner, T., et al.: High temperature tribological properties of polybenzimidazole (PBI). Polymer **128**, 159–168 (2017). https://doi.org/10.1016/j.polymer.2017.09.026
260. Mack, F., Morawietz, T., Hiesgen, R., et al.: Influence of the polytetrafluoroethylene content on the performance of high-temperature polymer electrolyte membrane fuel cell electrodes. Int. J. Hydrog. Energy **41**, 7475–7483 (2016). https://doi.org/10.1016/j.ijhydene.2016.02.156
261. Yu, S., Xiao, L., Benicewicz, B.C.: Durability studies of PBI-based high temperature PEMFCs. Fuel Cells **8**, 165–174 (2008). https://doi.org/10.1002/fuce.200800024
262. Søndergaard, T., Cleemann, L.N., Becker, H., et al.: Long-term durability of HT-PEM fuel cells based on thermally cross-linked polybenzimidazole. J. Power Sour. **342**, 570–578 (2017). https://doi.org/10.1016/j.jpowsour.2016.12.075
263. Yuk, S., Lee, D.H., Choi, S., et al.: An electrode-supported fabrication of thin polybenzimidazole membrane-based polymer electrolyte membrane fuel cell. Electrochim. Acta **270**, 402–408 (2018). https://doi.org/10.1016/j.electacta.2018.03.052
264. Ganesan, A., Narayanasamy, M.: Ultra-low loading of platinum in proton exchange membrane-based fuel cells: a brief review. Mater. Renew. Sustain. Energy **8**, 1–14 (2019). https://doi.org/10.1007/s40243-019-0156-x
265. Su, H.N., Jao, T.C., Barron, O., et al.: Low platinum loading for high temperature proton exchange membrane fuel cell developed by ultrasonic spray coating technique. J. Power Sour. **267**, 155–159 (2014). https://doi.org/10.1016/j.jpowsour.2014.05.086
266. Yusof, M.S.M., Jalil, A.A., Ahmad, A., et al.: Effect of Pt-Pd/C coupled catalyst loading and polybenzimidazole ionomer binder on oxygen reduction reaction in high-temperature PEMFC. Int. J. Hydrog. Energy **44**, 20760–20769 (2019). https://doi.org/10.1016/j.ijhydene.2018.07.192
267. Martin, S., Jensen, J.O., Li, Q., et al.: Feasibility of ultra-low Pt loading electrodes for high temperature proton exchange membrane fuel cells based in phosphoric acid-doped membrane. Int. J. Hydrog. Energy **44**, 28273–28282 (2019). https://doi.org/10.1016/j.ijhydene.2019.09.073
268. Yu, H., Roller, J.M., Kim, S., et al.: One-step deposition of catalyst layers for high temperature proton exchange membrane fuel cells (PEMFC). J. Electrochem. Soc. **161**, F622–F627 (2014). https://doi.org/10.1149/2.045405jes
269. Bevilacqua, N., George, M.G., Galbiati, S., et al.: Phosphoric acid invasion in high temperature PEM fuel cell gas diffusion layers. Electrochim. Acta **257**, 89–98 (2017). https://doi.org/10.1016/j.electacta.2017.10.054
270. Wu, Q.X., Li, H., Yuan, W., et al.: Performance evaluation of an air-breathing high-temperature proton exchange membrane fuel cell. Appl. Energy **160**, 146–152 (2015). https://doi.org/10.1016/j.apenergy.2015.09.042
271. Galbiati, S., Baricci, A., Casalegno, A., et al.: Experimental study of water transport in a polybenzimidazole-based high temperature PEMFC. Int. J. Hydrog. Energy **37**, 2462–2469 (2012). https://doi.org/10.1016/j.ijhydene.2011.09.159
272. Galbiati, S., Baricci, A., Casalegno, A., et al.: On the activation of polybenzimidazole-based membrane electrode assemblies doped with phosphoric acid. Int. J. Hydrog. Energy **37**, 14475–14481 (2012). https://doi.org/10.1016/j.ijhydene.2012.07.032
273. Søndergaard, T., Cleemann, L.N., Becker, H., et al.: Long-term durability of PBI-based HT-PEM fuel cells: effect of operating parameters. J. Electrochem. Soc. **165**, F3053–F3062 (2018). https://doi.org/10.1149/2.0081806jes
274. Fleige, M., Holst-Olesen, K., Wiberg, G.K.H., et al.: Evaluation of temperature and electrolyte concentration dependent oxygen solubility and diffusivity in phosphoric acid. Electrochim. Acta **209**, 399–406 (2016). https://doi.org/10.1016/j.electacta.2016.05.048
275. Wang, Z.Q., Yang, L., Wang, S., et al.: Measurement and separation of cathodic mass transport resistance in high temperature proton exchange membrane fuel cell. Prog. Nat. Sci. Mater. Int. **30**, 868–875 (2020). https://doi.org/10.1016/j.pnsc.2020.10.002
276. Myles, T., Bonville, L., Maric, R.: Catalyst, membrane, free electrolyte challenges, and pathways to resolutions in high temperature polymer electrolyte membrane fuel cells. Catalysts **7**, 16 (2017). https://doi.org/10.3390/catal7010016
277. Kazdal, T.J., Lang, S., Kühl, F., et al.: Modelling of the vapour-liquid equilibrium of water and the in situ concentration of H_3PO_4 in a high temperature proton exchange membrane fuel cell. J. Power Sour. **249**, 446–456 (2014). https://doi.org/10.1016/j.jpowsour.2013.10.098
278. Su, H.N., Pasupathi, S., Bladergroen, B., et al.: Optimization of gas diffusion electrode for polybenzimidazole-based high temperature proton exchange membrane fuel cell: evaluation of polymer binders in catalyst layer. Int. J. Hydrog. Energy **38**, 11370–11378 (2013). https://doi.org/10.1016/j.ijhydene.2013.06.107
279. Liu, G., Zhang, H., Hu, J., et al.: Studies of performance degradation of a high temperature PEMFC based on H_3PO_4-doped PBI. J. Power Sour. **162**, 547–552 (2006). https://doi.org/10.1016/j.jpowsour.2006.07.008
280. Kim, S., Myles, T.D., Kunz, H.R., et al.: The effect of binder content on the performance of a high temperature polymer electrolyte membrane fuel cell produced with reactive spray deposition technology. Electrochim. Acta **177**, 190–200 (2015). https://doi.org/10.1016/j.electacta.2015.02.025
281. Kim, D.H., Min, C.M., Lee, E., et al.: Effect of vinylphosphonic acid and polymer binders with phosphate groups on performance of high-temperature polymer electrolyte membrane fuel cell. Catal. Today **358**, 333–337 (2020). https://doi.org/10.1016/j.cattod.2019.07.046
282. Mack, F., Morawietz, T., Hiesgen, R., et al.: PTFE distribution in high-temperature PEM electrodes and its effect on the cell performance. ECS Trans. **58**, 881–888 (2013). https://doi.org/10.1149/05801.0881ecst
283. Liu, S., Wippermann, K., Lehnert, W.: Mechanism of action of polytetrafluoroethylene binder on the performance and durability of high-temperature polymer electrolyte fuel cells. Int. J. Hydrog. Energy **46**, 14687–14698 (2021). https://doi.org/10.1016/j.ijhydene.2021.01.192
284. Lee, W.J., Lee, J.S., Park, H.Y., et al.: Improvement of fuel cell performances through the enhanced dispersion of the PTFE binder in electrodes for use in high temperature polymer electrolyte membrane fuel cells. Int. J. Hydrog. Energy **45**, 32825–32833 (2020). https://doi.org/10.1016/j.ijhydene.2020.03.095
285. Jeong, G., Kim, M., Han, J., et al.: High-performance membrane-electrode assembly with an optimal polytetrafluoroethylene content for high-temperature polymer electrolyte membrane fuel cells. J. Power Sour. **323**, 142–146 (2016). https://doi.org/10.1016/j.jpowsour.2016.05.042
286. Yao, D.M., Zhang, W., Ma, Q., et al.: Achieving high Pt utilization and superior performance of high temperature polymer electrolyte membrane fuel cell by employing low-Pt-content catalyst and microporous layer free electrode design. J. Power Sour. **426**, 124–133 (2019). https://doi.org/10.1016/j.jpowsour.2019.04.045

287. Zamora, H., Plaza, J., Cañizares, P., et al.: Improved electrodes for high temperature proton exchange membrane fuel cells using carbon nanospheres. Chemsuschem **9**, 1187–1193 (2016). https://doi.org/10.1002/cssc.201600050
288. Mamlouk, M., Scott, K.: Phosphoric acid-doped electrodes for a PBI polymer membrane fuel cell. Int. J. Energy Res. **35**, 507–519 (2011). https://doi.org/10.1002/er.1708
289. Su, H.N., Jao, T.C., Pasupathi, S., et al.: A novel dual catalyst layer structured gas diffusion electrode for enhanced performance of high temperature proton exchange membrane fuel cell. J. Power Sour. **246**, 63–67 (2014). https://doi.org/10.1016/j.jpowsour.2013.07.062
290. Su, H.N., Liang, H.G., Bladergroen, B.J., et al.: Effect of platinum distribution in dual catalyst layer structured gas diffusion electrode on the performance of high temperature PEMFC. J. Electrochem. Soc. **161**, F506–F512 (2014). https://doi.org/10.1149/2.077404jes
291. Zhang, W.Q., Yao, D., Tian, L., et al.: Enhanced performance of high temperature polymer electrolyte membrane fuel cell using a novel dual catalyst layer structured cathode. J. Taiwan Inst. Chem. Eng. **125**, 285–290 (2021). https://doi.org/10.1016/j.jtice.2021.06.037
292. Lee, E., Kim, D.H., Pak, C.: Effect of inner catalyst layer with PTFE binder on performance of high temperature polymer electrolyte membrane fuel cells. ECS Trans. **92**, 741–748 (2019). https://doi.org/10.1149/09208.0741ecst
293. Galbiati, S., Coulon, P.E., Rizza, G., et al.: Poly(vinylimidazole) radiografted PVDF nanospheres as alternative binder for high temperature PEMFC electrodes. J. Power Sour. **296**, 117–121 (2015). https://doi.org/10.1016/j.jpowsour.2015.06.105
294. Kim, D.K., Kim, H., Park, H., et al.: Performance enhancement of high-temperature polymer electrolyte membrane fuel cells using Pt pulse electrodeposition. J. Power Sour. **438**, 227022 (2019). https://doi.org/10.1016/j.jpowsour.2019.227022
295. Martin, S., Li, Q., Steenberg, T., et al.: Binderless electrodes for high-temperature polymer electrolyte membrane fuel cells. J. Power Sour. **272**, 559–566 (2014). https://doi.org/10.1016/j.jpowsour.2014.08.112
296. Barron, O., Su, H.N., Linkov, V., et al.: $CsHSO_4$ as proton conductor for high-temperature polymer electrolyte membrane fuel cells. J. Appl. Electrochem. **44**, 1037–1045 (2014). https://doi.org/10.1007/s10800-014-0715-x
297. Oh, H.S., Cho, Y., Lee, W.H., et al.: Modification of electrodes using Al_2O_3 to reduce phosphoric acid loss and increase the performance of high-temperature proton exchange membrane fuel cells. J. Mater. Chem. A **1**, 2578 (2013). https://doi.org/10.1039/c2ta00492e
298. Barron, O., Su, H., Linkov, V., et al.: Enhanced performance and stability of high temperature proton exchange membrane fuel cell by incorporating zirconium hydrogen phosphate in catalyst layer. J. Power Sour. **278**, 718–724 (2015). https://doi.org/10.1016/j.jpowsour.2014.12.139
299. Chai, Z.L., Suo, Q.Y., Wang, H., et al.: Mesoporous lanthanum phosphate nanostructures containing H_3PO_4 as superior electrolyte for PEM fuel cells. RSC Adv. **3**, 21928 (2013). https://doi.org/10.1039/c3ra42094a
300. Gatto, I., Carbone, A., Pedicini, R., et al.: Comparative study on composite electrodes for medium temperature PEFC. Int. J. Membrane Sci. Techno. **4**, 37–44 (2017). https://doi.org/10.15379/2410-1869.2017.04.02.01
301. Lobato, J., Cañizares, P., Rodrigo, M.A., et al.: Study of the catalytic layer in polybenzimidazole-based high temperature PEMFC: effect of platinum content on the carbon support. Fuel Cells **10**, 312–319 (2010). https://doi.org/10.1002/fuce.200900088
302. Lobato, J., Cañizares, P., Rodrigo, M.A., et al.: Study of the influence of the amount of PBI-H_3PO_4 in the catalytic layer of a high temperature PEMFC. Int. J. Hydrog. Energy **35**, 1347–1355 (2010). https://doi.org/10.1016/j.ijhydene.2009.11.091
303. Kongstein, O.E., Berning, T., Børresen, B., et al.: Polymer electrolyte fuel cells based on phosphoric acid doped polybenzimidazole (PBI) membranes. Energy **32**, 418–422 (2007). https://doi.org/10.1016/j.energy.2006.07.009
304. Berber, M.R., Fujigaya, T., Sasaki, K., et al.: Remarkably durable high temperature polymer electrolyte fuel cell based on poly(vinylphosphonic acid)-doped polybenzimidazole. Sci. Rep. **3**, 1764 (2013). https://doi.org/10.1038/srep01764
305. Ponomarev, I.I., Skupov, K.M., Naumkin, A.V., et al.: Probing of complex carbon nanofiber paper as gas-diffusion electrode for high temperature polymer electrolyte membrane fuel cell. RSC Adv. **9**, 257–267 (2018). https://doi.org/10.1039/c8ra07177b
306. Ponomarev, I.I., Skupov, K.M., Zhigalina, O.M., et al.: New carbon nanofiber composite materials containing lanthanides and transition metals based on electrospun polyacrylonitrile for high temperature polymer electrolyte membrane fuel cell cathodes. Polymers **12**, 1340 (2020). https://doi.org/10.3390/polym12061340
307. Tian, L.L., Zhang, W.Q., Xie, Z., et al.: Enhanced performance and durability of high-temperature polymer electrolyte membrane fuel cell by incorporating covalent organic framework into catalyst layer. Acta Phys. Chimica Sin. (2020). https://doi.org/10.3866/pku.whxb202009049
308. Jabbari, Z., Nassernejad, B., Fallah, N., et al.: Fabrication of novel binderless anode via electrophoretic deposition for HT-PEMFC. Surf. Eng. **35**, 1013–1020 (2019). https://doi.org/10.1080/02670844.2019.1597426
309. Martin, S., Garcia-Ybarra, P.L., Castillo, J.L.: Ten-fold reduction from the state-of-the-art platinum loading of electrodes prepared by electrospraying for high temperature proton exchange membrane fuel cells. Electrochem. Commun. **93**, 57–61 (2018). https://doi.org/10.1016/j.elecom.2018.06.007
310. Martin, S., Li, Q., Jensen, J.O.: Lowering the platinum loading of high temperature polymer electrolyte membrane fuel cells with acid doped polybenzimidazole membranes. J. Power Sour. **293**, 51–56 (2015). https://doi.org/10.1016/j.jpowsour.2015.05.031
311. Halter, J., Gloor, T., Amoroso, B., et al.: Wetting properties of porous high temperature polymer electrolyte fuel cells materials with phosphoric acid. Phys. Chem. Chem. Phys. **21**, 13126–13134 (2019). https://doi.org/10.1039/c9cp02149c
312. Satjaritanun, P., Zenyuk, I.V.: Water management strategies for PGM-free catalyst layers for polymer electrolyte fuel cells. Curr. Opin. Electrochem. **25**, 100622 (2021). https://doi.org/10.1016/j.coelec.2020.08.004
313. Zhang, J.J., Wang, H., Li, W., et al.: Effect of catalyst layer microstructures on performance and stability for high temperature polymer electrolyte membrane fuel cells. J. Power Sour. **505**, 230059 (2021). https://doi.org/10.1016/j.jpowsour.2021.230059
314. Zhang, J.J., Bai, H.J., Yan, W.R., et al.: Enhancing cell performance and durability of high temperature polymer electrolyte membrane fuel cells by inhibiting the formation of cracks in catalyst layers. J. Electrochem. Soc. **167**, 114501 (2020). https://doi.org/10.1149/1945-7111/ab9fe0
315. Kannan, A., Li, Q., Cleemann, L.N., et al.: Acid distribution and durability of HT-PEM fuel cells with different electrode supports. Fuel Cells **18**, 103–112 (2018). https://doi.org/10.1002/fuce.201700181
316. Meyer, Q., Ashton, S., Boillat, P., et al.: Effect of gas diffusion layer properties on water distribution across air-cooled, open-cathode polymer electrolyte fuel cells: a combined ex-situ X-ray

tomography and in-operando neutron imaging study. Electrochim. Acta **211**, 478–487 (2016). https://doi.org/10.1016/j.electacta.2016.06.068
317. Chevalier, S., Fazeli, M., Mack, F., et al.: Role of the microporous layer in the redistribution of phosphoric acid in high temperature PEM fuel cell gas diffusion electrodes. Electrochim. Acta **212**, 187–194 (2016). https://doi.org/10.1016/j.electacta.2016.06.121
318. Delikaya, Ö., Bevilacqua, N., Eifert, L., et al.: Porous electrospun carbon nanofibers network as an integrated electrode@gas diffusion layer for high temperature polymer electrolyte membrane fuel cells. Electrochim. Acta **345**, 136192 (2020). https://doi.org/10.1016/j.electacta.2020.136192
319. Mack, F., Galbiati, S., Gogel, V., et al.: Evaluation of electrolyte additives for high-temperature polymer electrolyte fuel cells. ChemElectroChem **3**, 770–773 (2016). https://doi.org/10.1002/celc.201500561
320. Zamora, H., Cañizares, P., Rodrigo, M.A., et al.: Improving of micro porous layer based on advanced carbon materials for high temperature proton exchange membrane fuel cell electrodes. Fuel Cells **15**, 375–383 (2015). https://doi.org/10.1002/fuce.201400139
321. Lobato, J., Zamora, H., Cañizares, P., et al.: Microporous layer based on SiC for high temperature proton exchange membrane fuel cells. J. Power Sour. **288**, 288–295 (2015). https://doi.org/10.1016/j.jpowsour.2015.04.102
322. Fu, X.D., Li, T., Tang, L., et al.: Reticulated polyaniline nanowires as a cathode microporous layer for high-temperature PEMFCs. Int. J. Hydrog. Energy **46**, 8802–8809 (2021). https://doi.org/10.1016/j.ijhydene.2020.12.033
323. Yao, D.M., Jao, T.C., Zhang, W., et al.: In-situ diagnosis on performance degradation of high temperature polymer electrolyte membrane fuel cell by examining its electrochemical properties under operation. Int. J. Hydrog. Energy **43**, 21006–21016 (2018). https://doi.org/10.1016/j.ijhydene.2018.09.103
324. Mack, F., Klages, M., Scholta, J., et al.: Morphology studies on high-temperature polymer electrolyte membrane fuel cell electrodes. J. Power Sources **255**, 431–438 (2014). https://doi.org/10.1016/j.jpowsour.2014.01.032
325. Becker, H., Reimer, U., Aili, D., et al.: Determination of anion transference number and phosphoric acid diffusion coefficient in high temperature polymer electrolyte membranes. J. Electrochem. Soc. **165**, F863–F869 (2018). https://doi.org/10.1149/2.1201810jes
326. Doh, W.H., Gregoratti, L., Amati, M., et al.: Scanning photoelectron microscopy study of the Pt/phosphoric-acid-imbibed membrane interface under polarization. ChemElectroChem **1**, 180–186 (2014). https://doi.org/10.1002/celc.201300134
327. Holderer, O., Carmo, M., Shviro, M., et al.: Fuel cell electrode characterization using neutron scattering. Mater. Basel Switz. **13**, E1474 (2020). https://doi.org/10.3390/ma13061474
328. Yezerska, K., Liu, F., Dushina, A., et al.: Analysis of the regeneration behavior of high temperature polymer electrolyte membrane fuel cells after hydrogen starvation. J. Power Sour. **449**, 227562 (2020). https://doi.org/10.1016/j.jpowsour.2019.227562
329. Han, S., Jeong, Y.H., Jung, J.H., et al.: Spectrophotometric analysis of phosphoric acid leakage in high-temperature phosphoric acid-doped polybenzimidazole membrane fuel cell application. J. Sens. **2016**, 1–8 (2016). https://doi.org/10.1155/2016/5290510
330. Khaneft, M., Shuai, L., Lin, Y., et al.: Proton dynamics of phosphoric acid in HT-PEFCs: towards "operando" experiments. AIP Conf. Proc. **1969**, 030003 (2018). https://doi.org/10.1063/1.5039295
331. Boillat, P., Biesdorf, J., Oberholzer, P., et al.: Evaluation of neutron imaging for measuring phosphoric acid distribution in high temperature PEFCs. J. Electrochem. Soc. **161**, F192–F198 (2014). https://doi.org/10.1149/2.023403jes
332. Lin, Y., Arlt, T., Kardjilov, N., et al.: In operando neutron radiography analysis of a high-temperature polymer electrolyte fuel cell based on a phosphoric acid-doped polybenzimidazole membrane using the hydrogen-deuterium contrast method. Energies **11**, 2214 (2018). https://doi.org/10.3390/en11092214
333. Úbeda, D., Lobato, J., Cañizares, P., et al.: Using current distribution measurements to characterize the behavior of HTPEMFCs. Chem. Eng. Trans. **41**, 229 (2014). https://doi.org/10.3303/CET1441039
334. Yu, M.F., Sun, H., Zhang, T., et al.: Current density distribution in an HT-PEM fuel cell with a poly (2, 5-benzimidazole) membrane. Int. J. Hydrog. Energy **46**, 3022–3031 (2021). https://doi.org/10.1016/j.ijhydene.2020.04.117
335. Bailey, J.J., Chen, J., Hack, J., et al.: Lab-based X-ray microcomputed tomography coupled with machine-learning segmentation to investigate phosphoric acid leaching in high-temperature polymer electrolyte fuel cells. J. Power Sources **509**, 230347 (2021). https://doi.org/10.1016/j.jpowsour.2021.230347
336. Eberhardt, S.H., Toulec, M., Marone, F., et al.: Dynamic operation of HT-PEFC: in-operando imaging of phosphoric acid profiles and (re)distribution. J. Electrochem. Soc. **162**, F310–F316 (2015). https://doi.org/10.1149/2.0751503jes
337. Lee, C.Y., Weng, F.B., Kuo, Y.W., et al.: In-situ measurement of high-temperature proton exchange membrane fuel cell stack using flexible five-in-one micro-sensor. Sens. Basel Switz. **16**, E1731 (2016). https://doi.org/10.3390/s16101731
338. Chen, C.H., Lee, C.Y., Weng, F.B., et al.: In-situ monitoring of internal temperature, flow rate and pressure in the high-temperature proton exchange membrane fuel cell stack using flexible integrated micro sensor. Int. J. Electrochem. Sci. **10**, 1731 (2015). https://doi.org/10.3390/s16101731
339. Bandlamudi, G., Siegel, C., Heßke, C., et al.: Fluid flow and current density distribution in large-area HT PEMFCs. In: Proceeding 2011 COMSOL Conference, (2011)
340. Lee, A.S., Choe, Y.K., Matanovic, I., et al.: The energetics of phosphoric acid interactions reveals a new acid loss mechanism. J. Mater. Chem. A **7**, 9867–9876 (2019). https://doi.org/10.1039/c9ta01756a
341. Sun, L., Gu, Q., Wang, H., et al.: Anhydrous proton conductivity of electrospun phosphoric acid-doped PVP-PVDF nanofibers and composite membranes containing MOF fillers. RSC Adv. **11**, 29527–29536 (2021). https://doi.org/10.1039/d1ra04307b
342. Li, S., Peng, C., Shen, Q., et al.: Impact of membrane phosphoric acid doping level on transport phenomena and performance in high temperature PEM fuel cells. Membranes **11**, 817 (2021). https://doi.org/10.3390/membranes11110817
343. Jin, Y.P., Liu, R.H., Che, X.F., et al.: New high temperature polymer electrolyte membranes based on poly(ethylene imine) crosslinked poly(ether ketone cardo). J. Electrochem. Soc. **168**, 054524 (2021). https://doi.org/10.1149/1945-7111/ac009c
344. Tang, H.Y., Geng, K., Wu, L., et al.: Fuel cells with an operational range of –20 °C to 200 °C enabled by phosphoric acid-doped intrinsically ultramicroporous membranes. Nat. Energy **7**, 153–162 (2022). https://doi.org/10.1038/s41560-021-00956-w
345. Büsselmann, J., Rastedt, M., Klicpera, T., et al.: Analysis of HT-PEM MEAs' long-term stabilities. Energies **13**, 567 (2020). https://doi.org/10.3390/en13030567
346. Schonvogel, D., Rastedt, M., Wagner, P., et al.: Impact of accelerated stress tests on high temperature PEMFC degradation. Fuel Cells **16**, 480–489 (2016). https://doi.org/10.1002/fuce.201500160
347. Lee, C.Y., Weng, F.B., Yang, C.Y., et al.: Real-time monitoring of HT-PEMFC. Membranes **12**, 94 (2022). https://doi.org/10.3390/membranes12010094

348. Li, J.J., Yang, L., Wang, Z., et al.: Degradation study of high temperature proton exchange membrane fuel cell under start/stop and load cycling conditions. Int. J. Hydrog. Energy **46**, 24353–24365 (2021). https://doi.org/10.1016/j.ijhydene.2021.05.010
349. Gangadharan, P.K., Vijayakumar, V., Nediyirakkal, S.A., et al.: In situ preparation of ionomer as a tool for triple-phase boundary enhancement in 3D graphene supported Pt catalyst. Adv. Sustainable Syst. **5**, 2000125 (2021). https://doi.org/10.1002/adsu.202000125
350. Müller-Hülstede, J., et al.: Implementation of different Fe–N–C catalysts in high temperature proton exchange membrane fuel cells-Effect of catalyst and catalyst layer on performance. J. Power Sour. **537**, 231529 (2022). https://doi.org/10.1016/j.jpowsour.2022.231529

Quentin Meyer received his Ph.D. degree from University College London (UCL) (2015). He joined Prof. Zhao's group at UNSW (Sydney, Australia) in 2018 working on hydrogen fuel cells. His research interests include low-temperature proton exchange membrane fuel cell, from non-precious metal catalysts and catalyst layer challenges to systems design and prototyping. He is also an expert on electrochemical impedance spectroscopy for energy devices. He was awarded the Young Electrochemist Award in Australia New Zealand in 2021.

Chujie Yang received his BS degree in Environmental Engineering and Technology from the Yangzhou University in 2020. He is pursuing a master degree under the supervision of Prof. Yi Cheng at Central South University. His scientific interests focus on the design and synthesis of intermetallic electrocatalysts with high activity and long-term stability for oxygen reduction reaction as well as PEMFCs.

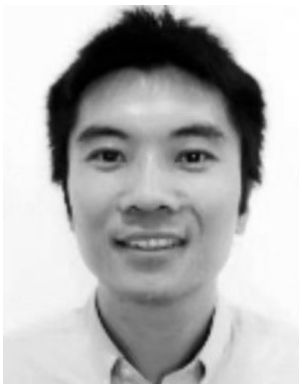

Yi Cheng is a professor at Central South University. He received his Ph.D. degree from Curtin University, Australia, in 2015. Following his graduate studies, he began working as a postdoctoral fellow at Curtin University, Australia, from 2015 to 2018. He then worked as a professor at School of Metallurgy and Environment of Central South University. His research interests include developing novel materials for low-temperature and high-temperature proton exchange membrane fuel cells, chemical energy storage by water electrolysis and carbon dioxide reduction.

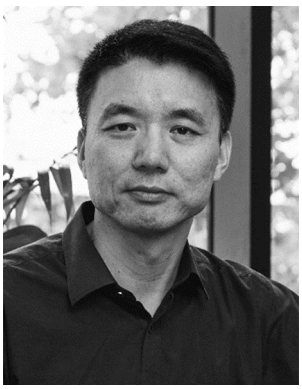

Chuan Zhao received his Ph.D. degree from Northwest University (2002). He completed postdoctoral research at the University of Oldenburg and Monash University before starting his independent career at UNSW in 2010. He was awarded an Australian Research Fellow in 2011 and a Future Fellowship in 2017. He chairs the Electrochemistry Division of the Royal Australian Chemical Institute (RACI) and is elected Fellow of the RACI and Royal Society of Chemistry. His research focuses on developing electrochemical technologies for energy storage and conversion.